EURADOS
European Radiation Dosimetry Group e. V.

EURADOS Report 2019-02

Neuherberg, July 2019

Patient maximum skin dose in interventional procedures in radiology and cardiology: summary of WG 12 activities

Olivera Ciraj Bjelac, Jérémie Dabin, Jad Farah, Hannu Järvinen, Francoise Malchair, Teemu Siiskonen, Željka Knežević

ISSN 2226-8057

ISBN 978-3-943701-19-7

European Radiation Dosimetry Group e.V.

EURADOS Report 2019-02

Neuherberg, July 2019

Patient maximum skin dose in interventional procedures in radiology and cardiology: summary of WG 12 activities

Authors:

Olivera Ciraj Bjelac[1], Jérémie Dabin[2], Jad Farah[3], Hannu Järvinen[4], Francoise Malchair[5], Teemu Siiskonen[4], Željka Knežević[6]

[1]VINČA Institute of Nuclear Sciences, Belgrade, Serbia

[2]SCK-CEN, Belgian Nuclear Research Centre, Mol, Belgium

[3] Paris Sud University Hospitals, Radiology and Nuclear Medicine Division, Le Kremlin-Bicêtre, France

[4] STUK, Radiation and Nuclear Safety Authority Helsinki, Finland

[5]CHULG, Centre Hospitalier Universitaire de Liège Liège, Belgium

[6]RBI, Ruđer Bošković Institute Zagreb, Croatia

ISSN 2226-8057

ISBN 978-3-943701-19-7

Imprint

Issued by:
European Radiation Dosimetry e.V.
Postfach 1129
D-85758 Neuherberg
Germany
office@eurados.org
www.eurados.org

The European Radiation Dosimetry e.V. is a non-profit organization promoting research and development and European cooperation in the field of the dosimetry of ionizing radiation. Itis registered in the Register of Associations (Amtsgericht Braunschweig, registry number VR 200387) and certified to be of non-profit character (Finanzamt Braunschweig-Altewiekring, notification from 2008-03-03).

Liability Disclaimer

Contributors

Contributing members of Working Group 12 during the preparation of this report:

Elefteria Carinou, (GAEC), Greek Atomic Energy Commission, Athens, Greece

Isabelle Clairand, IRSN, Institut de Radioprotection et de Sûreté Nucléaire (IRSN), Fontenay-aux-Roses, France

Hannan Datz, Soreq Nuclear Research Centre, Yavne, Israel

Cinzia De Angelis, ISS Istituto Superiore di Sanità, Rome; Italy

Joanna Domienik-Andrzejewska, NIOM, Nofer Institute of Occupational Medicine Łódź, Poland

Aoife Gallagher, University Hospital Limerick, Limeric, Ireland

Sigalit Haruz Waschitz, Assaf Harofeh Medical Center, Israel

Christelle Huet, IRSN, Institut de Radioprotection et de Sûreté Nucléaire Fontenay-aux-Roses, France

Renata Kopec, IFJ-PAN, Institute of Nuclear Physics Polish Academy of Sciences, Kraków, Poland

Marija Majer, RBI, Ruđer Bošković Institute Zagreb, Croatia

Anna Negri, Oncology and Radiotherapy Department, Fakultní nemocnice Královské Vinohrady,Prague, Czech Republic

Leos Novák, NRPI, National Radiation Protection Institute, Prague, Czech Republic

Piotr Pankowski, National Centre for Radiation Protection in Health Care, Lodz, Poland

Marta Sans Merce, HUG, Hôpitaux Universitaires de Genève, Genève, Switzerland

Sandra Sarmento, (IPO Porto), Portuguese Oncology Institute of Porto Porto, Portugal

Agnieszka Szumska, IFJ PAN, Institute of Nuclear Physics Polish Academy of Sciences Kraków, Poland

Filip Vanhavere, SCK-CEN, Belgian Nuclear Research Centre, Mol, Belgium

Annalisa Trianni, Udine University Hospital (AOUD), Udine, Italy

Acknowledgement

The authors gratefully acknowledge the invaluable contributions of staff in Institutes and hospitals where experimental work was carried out.

Content:

Abstract

Fluoroscopically guided interventional procedures in radiology (IR) and cardiology (IC) are techniques that have had wide diffusion in the last decades. Scarcely invasive, they reduce most of the risks to patients and the expenses of operating theatres. Nevertheless, prolonged exposures due, for instance, to complicated interventional procedures or inappropriate equipment may result in high doses to both patients and staff members, in particular, with potentially high radiation doses to the skin of a patient.

Working group 12 of EURADOS is dealing with various aspects of dosimetry in medical imaging. In line with most recent developments in radiation protection in medicine, a lot of effort has been made in the area of patient dosimetry in medical imaging. As the number and complexity of interventional procedures have been steadily growing, it becomes crucial to provide patient-specific, skin dose estimate during these procedures. To tackle this issue, EURADOS Working group 12 has initiated a number of activities to estimate the maximum skin dose in various procedures in radiology and cardiology.

This report presents Working group 12 activities in the area of dosimetry for interventional procedures in cardiology and radiology. The document is dealing with characterization of different dosimetric methods for skin dose assessment in interventional procedures, their application for skin doses measurement in clinical practice and establishment of trigger levels in order to evaluate the feasibility of identifying a common dosimetric indicator that correlates with the maximum skin dose. In order to determine the suitability of XR-TypeR Gafchromic™ films and of detectors based on thermolumiescent materials: pellets, chips and foils to measure skin dose, an intercomparison exercise has been organized within EURADOS Working Group 12. Furthermore, an assessment of the uncertainty associated with the sampling process of point detector grids used for maximum skin dose measurements was performed. Among all possible solutions, film dosimetry represents the most convenient method to determine skin dose. Hence, EURADOS Working Group 12 performed a comprehensive evaluation in order to investigate the optimal use of films in the interventional environment while addressing the means to reduce uncertainties in the quantitative assessment of patient skin dose. Finally, patient skin dose measurements, along with assessment of other dose indices as dose area product and cumulative dose at interventional reference point was performed at different European hospitals for selected high dose interventional procedures in radiology and cardiology. The inter-center variability of online dose indicators and their correlation with the maximum skin dose were examined along with feasibility to establish the generic alert levels for skin injuries.

1. Introduction

Fluoroscopically guided interventional procedures in radiology (IR) and cardiology (IC) are techniques that have had wide diffusion in the last decades (Picano *et al.* 2014, Jaschke *et al.* 2017). Scarcely invasive, they reduce most of the risks to patients and the expenses of operating theatres. Nevertheless, prolonged exposures due, for instance, to complicated interventional procedures or inappropriate equipment may result in high doses to both patients and staff members (Jaschke *et al.* 2017, Shope 1996, Balter *et al.* 2010, Bolderston *et al.* 2006, ICRP 2000, Ciraj-Bjelac *et al.* 2016).

In particular, interventional procedures in radiology and cardiology are associated with potentially high radiation doses to the skin. Numerous cases of radiation-induced deterministic tissue reactions following exposure in interventional procedures, such as erythema and hair loss, have been reported in the literature (Jaschke *et al.* 2017, Shope 1996, Balter *et al.* 2010, Bolderston *et al.* 2006, ICRP 2000). As early as 1998, recommendations for operators performing interventional procedures were published and the need for measuring patient dose was expressed (Vano *et al.* 1998) and since then, tremendous effort has been done to identify practical and easy-to-use methods to monitor and reduce patient skin doses in interventional procedures (Jaschke *et al.* 2017, Domienik *et al.* 2008, Bogaert *et al.* 2009).

Working group 12 (WG12) of EURADOS is dealing with various aspects of dosimetry in medical imaging. The aim of the WG12 is focused on dosimetry harmonization, evaluation and development of dosimetry methods, intercomparisons, literature reviews and measurement campaigns to assess occupational and patient exposure (Carionou *et al.* 2015, Ciraj-Bjelac *et al.* 2016, Kopec *et al.* 2014, Farah *et al.* 2015, Dabin *et al.* 2015). In line with most recent developments in radiation protection in medicine, a lot of effort has been made in the area of patient dosimetry in medical imaging (Kopec *et al.* 2014, Farah *et al.* 2015, Dabin *et al.* 2015). Following vision 4 of EURADOS's Strategic Research Agenda: "Towards integrated personalized dosimetry in medical applications", WG12 is currently focusing on the development and evaluation of dosimetric basis for organ dose and risk estimation in different imaging modalities, in particular in interventional radiology (EURADOS 2014).

This report presents WG12 activities in the area of dosimetry for interventional procedures in cardiology and radiology. The document is dealing with characterization of different dosimetric methods for skin dose assessment in interventional procedures, their application for skin doses measurement in clinical practice and establishment of trigger levels in order to evaluate the feasibility of identifying a common dosimetric indicator that correlates with the maximum skin dose.

References

Balter S., Hopewell JW., Miller DL., Wagner LK., Zelefsky MJ., 2010. Fluoroscopically Guided Interventional Procedures: A Review of Radiation Effects on Patients' Skin and Hair, Radiology, 254(2), 326-341.

Bolderston A., Lloyd NS., Wong RK., Holden L., Robb-Blenderman L., 2006. The prevention and management of acute skin reactions related to radiation therapy: a systematic review and practice guideline, Support Care Cancer,14, 802 – 817.

Bogaert E., Bacher K., Lemmens K., Carlier M., Desmet W., De Wagter X., Djian D., Hanet C., Heyndrickx G., Legrand V., Taeymans Y., Thierens H. 2009. A large-scale mutlicentre study of patient skin doses

in interventional cardiology: dose-area product action levels and dose reference level. Br J Radiol, 82:303–312.

Carinou E., Ferrari P., Bjelac O.C., Gingaume M, Merce MS, O'Connor U., 2015.Eye lens monitoring for interventional radiology personnel: dosemeters, calibration and practical aspects of Hp (3) monitoring. A 2015 review. J Radiol Prot. 35: R17-34.

Ciraj-Bjelac O., Carinou E., Ferrari P., Gingaume M., Sans Merce M., O'Connor U., 2016. Occupational Exposure of the Eye Lens in Interventional Procedures: How to Assess and Manage Radiation Dose, Journal of Americal Colleauge of Radiology, 13(11), pp. 1347-1353.

Dabin J., Negri A., Farah J., Ciraj-Bjelac O., Clairand I., De Angelis C., Domienik J., Jarvinen H., Kopec R., Majer M., Malchair F., Novák L., Siiskonen T., Vanhavere F., Trianni A., Knežević Ž., 2015. Characterization of grids of point detectors in maximum skin dose measurement in fluoroscopically-guided interventional procedures, Phys. Med., 31(8): 1112–17.

Domienik J., Papierz S., Jankowski J., Peruga JZ., Werduch A., Religa W., 2008. Correlation of patient maximum skin doses in cardiac procedures with various dose indicators. Radiat. Prot Dosim. 132:18-24.

EURADOS 2014. Visions for Radiation Dosimetry over the Next Two Decades – Strategic Research Agenda of the European Radiation Dosimetry Group, EURADOS Report 2014-01, Braunschweig, 2014.

Farah J., Trianni A., Ciraj-Bjelac O., Clairand I., De Angelis C., Delle Canne S., Hadid L., Huet C., Jarvinen H., Negri A., Novák L., Pinto M., Siiskonen T., Waryn M.J, Knežević Ž., 2015 Characterization of XR-RV3 GafChromicTM films in standard laboratory and clinical conditions and means to estimate uncertainties and reduce errors, Med. Phys. 42(7) 4211-26.

ICRP 2000. International Commission on Radiological Protection (ICRP), Avoidance of Radiation Injuries from Medical Interventional Procedures, ICRP Publication 85, Ann. ICRP 30(2) (2000).

Jaschke W., Schmuth M., Trianni A., Bartal G., 2017. Radiation-Induced Skin Injuries to Patients: What the Interventional Radiologist Needs to Know. Cardiovasc Intervent Radiol. 40(8):1131-1140.

Kopec R., Novák L., Carinou E., Clairand I., Dabin J., Datz H., De Angelis C., Farah J., Huet C., Knežević Ž., Järvinen H., Majer M., Malchair F., Negri A., Waschitz Haruz S., Siiskonen T., Szumska A., 2014. Intercomparison of Gafchromic films, TL chips and TL foils for the measurements of skin dose in interventional radiology. Radiat. Meas. 71: 282–6.

Picano E., Vano E., Rehani MM., Cuocolo A., Mont L., Bodi V., et al. T2014. The appropriate and justified use of medical radiation in cardiovascular imaging: a position document of the ESC associations of cardiovascular imaging, percutaneous cardiovascular interventions and electrophysiology. Eur Heart J. 35(10):665–72.

Shope TB, 1996. Radiation-induced skin injuries from fluoroscopy, RadioGraphics 16, 1195–1199.

Vano E., Arranz L., Sastre J M., Moro C., Ledo A., Gárate M T. and Minguez I., 1998. Radiation protection considerations based on some cases of patient skin injuries in interventional cardiology. Br J Radiol. 71(845):510-6.

2. Methods for estimating skin dose

Skin dose in interventional radiology can be assessed by calculations based on skin dose distribution from exposure and geometrical data supplied by the X-ray equipment (tube output, field sizes, geometry of irradiation, etc.) or by direct measurements (thermoluminescent dosimeter, film, solid state detector).

2.1 Dosimetric quantities

Diagnostic imaging generally covers a diverse range of examination types, many of which are increasing in frequency and technical complexity. This has resulted in the development of new dosimetric measuring instruments, techniques and terminologies which affect the work both in the clinical environment and calibration facilities.

In examinations using fluoroscopy, irradiation geometry and time vary individually from patient to patient. In fluoroscopy guided interventional procedures, an integral dosimetric quantity as the air kerma–area product, offers a convenient quantity for monitoring patient exposure. However, such procedures may give rise to high skin absorbed doses and monitoring of the skin absorbed dose is important because of the potential for reaching the threshold for the tissue reactions. The determination of the dose to the most exposed area is not straightforward since exposure parameters and projection angle change during the procedure and the most exposed area cannot always be anticipated. In order to estimate the peak skin absorbed dose, it is therefore necessary to have a detector that registers the skin dose at many points simultaneously. To address all relevant aspects of assessment of patient exposure, multiple dosimetric quantities are used (ICRU 2006, IAEA 2007).

Dosimetric quantities used for these purposes can be divided in several categories: basic dosimetric quantities, application specific quantities and risk-related quantities. Basic dosimetric quantities are fundamental quantities based on which we define application specific quantities and risk-related quantities that are used in diagnostic radiology measurements (ICRU 2006, IAEA 2007, ICRP 2007).

2.1.1 Basic dosimetric quantities

2.1.1.1 Kerma

The kerma, *K*, is the quotient dE_{tr}/dm, where *dEtr* is the sum of the initial kinetic energies of all the charged particles liberated by uncharged particles in a mass *dm* of material. Unit: J/kg. The special name for the unit of kerma is Gray (Gy).

2.1.1.2 Energy imparted

The mean energy imparted to the matter in a given volume equals the radiant energy of all those charged and uncharged ionizing particles which enter the volume minus the radiant energy of all those charged and uncharged ionizing particles which leave the volume, plus the sum of all changes of the rest energy of nuclei and elementary particles which occur in the volume (zero for the photon energies in diagnostic radiology). Unit: Joule (J).

2.1.1.3 Absorbed dose

The absorbed dose is the mean energy imparted to matter of mass *dm*. Unit: J/kg. The special name for the unit of absorbed dose is Gray (Gy).

In diagnostic and interventional radiology energy range, the production of bremsstrahlung within low atomic number materials is negligible. For a given material and radiation field, absorbed dose and kerma are then numerically equal when secondary electron equilibrium is established. There will be important numerical differences between the two quantities wherever secondary electron equilibrium is not established (i.e. close to an interface between different materials).

2.1.2 Application specific dosimetric quantities

2.1.2.1 Incident air kerma

The incident air kerma is the kerma to air from an incident X ray beam measured on the central beam axis at the position of the patient or phantom surface. Only the radiation incident on the patient or phantom and not the backscattered radiation is included. Unit: J/kg. The name for the unit of kerma is Gray (Gy).

2.1.2.2 Entrance surface air kerma

The entrance surface air kerma is the kerma to air measured on the central beam axis at the position of the patient or phantom surface. The radiation incident on the patient or phantom and the backscattered radiation are included. Unit: J/kg. The name for the unit of kerma is Gray (Gy).

The entrance surface air kerma is related to the incident air kerma by the backscatter factor (IAEA 2007).

2.1.2.3 Air kerma–area product

The air kerma–area product is the integral of the air kerma over the area of the X ray beam in a plane perpendicular to the beam axis. The unit of air kerma–area product is $Gy \cdot m^2$.

The air kerma–area product has the useful property that it is approximately invariant with distance from the X ray tube focus (when interactions in air and extrafocal radiation can be neglected), as long as the planes of measurement and calculation are not so close to the patient or phantom that there is a significant contribution from backscattered radiation.

2.1.2.4 Local skin dose

The local skin dose is the dose absorbed by the portion of skin under the beam. Unit: J/kg. The name for the unit of local skin dose is gray (Gy).

2.2 Direct Dose Measurements

A suitable method for skin dose determination is to place a dosemeter on the patients' skin. Nevertheless, there is still no clear consensus about an ideal dosimeter for monitoring surface radiation during procedures should have a response which is linear within the measured dose range, have good angular response minimally interfere with the image (tissue equivalent or small area). Moreover, it should be practical and simple to use (Dong *et al.* 2002). Dosimeters used in interventional radiology for skin dose assessment are thermoluminescent dosimeters (TLD),

radiological and radiochromic film and semiconductor detector (high sensitivity MOSFET dosimeters and silicon diodes).

2.2.1 Thermoluminescent dosemeters

Thermoluminescence dosemeters (TLDs) are widely used in various patient dosimetry applications because they are – nearly – tissue equivalent and have good dosimetry performance. Most widespread thermoluminescence materials for radiologic application are: LiF:Mg,Ti and LiF:Mg,Cu,P. Sources of uncertainty in dose measurements are: TLD calibration, batch homogeneity, TLD reader stability, linearity, energy and angle dependence, fading and background subtraction (Dong *et al.* 2002, Duggan *et al.* 2004, Moskovitch *et al.* 2007, Bogaert *et al.* 2009, Struelens *et al.* 2014, Kopec *et al.* 2014, Dabin *et al.* 2015).

When TLDs are correctly positioned during interventional procedures, TLDs can deliver accurate information on the peak skin dose. One of the main advantages of TLDs is their small size associated with a good spatial resolution and measurements accuracy.

However, in practice it is very difficult or even impossible to predict the locations of the highest incident dose. For this reason, arrays/grids of multiple TLDs are sometimes used to provide skin dose mapping (Kopec *et al.* 2014, Dabin *et al.* 2015). Improving the spatial resolution of dose distribution by increasing the number of point detectors makes the procedure of determining peak skin dose laborious and therefore impractical to use in routine practice. Another disadvantage of TLDs is that the information about the skin dose and the possibility of exceeding the dose threshold is not available in real-time, but is delivered hours or even days after the intervention when the read out of TLDs and the estimation of doses have been completed (Balter *et al.* 2006).

2.2.2 MOSFET dosemeters

The dosemeters based on metal oxide semiconductor field effect transistor (MOSFET) technology can be an alternative tool to TLDs to measure entrance surface dose in interventional radiology. The principle of detection is the following: the irradiation induces a permanent shift in the threshold voltage of the transistor which is proportional to the absorbed dose.

Small size and radio-transparency make the MOSFET detectors a good choice for dosimetry. They were initially developed for the measurement of patient dose in radiotherapy (Soubra *et al.* 1994, Ramani *et al.* 1997) and are still frequently used for this application today for photon (Kohno *et al.* 2008, Mercié *et al.* 2005) and electron beams (Manigandan *et al.* 2009). These last years, they have been proven to be sensitive enough to be used at diagnostic energy levels (Chida *et al.* 2009) and are now more and more used in this field (Glennie *et al.* 2008, Miksys *et al.* 2010).

The main advantage of MOSFET dosemeters versus TLDs is the possibility to perform dose measurements in real-time. They can be used for *in vivo* dosimetry in interventional radiology since they can provide an alert if a dose threshold fixed by the operator has been reached during the procedure. The main drawback lies in the fact that, since the dose can be measured only for a limited number of points, as opposite to TLDs that can be placed in arrays containing a relatively large number of dosemeters, the appropriate location to place the MOSFET detectors has to be known before the procedure and this is an issue for interventional procedures.

Concerning skin dose measurements in interventional radiology, the MOSFET detectors present in general a correct reproducibility, a response linear with the dose and no dependency with the dose rate. However, uncertainties related to energy, angular and temperature dependence are more or

less important depending on the devices (Chida *et al.* 2009, Gopiraj *et al.* 2008, Cheung *et al.* 2009). The energy dependence that can be observed in the case of some devices, in particular in the energy range 50-80 keV, is the major drawback of these types of dosemeters. In addition, a dependency with the pulse duration was observed (Bassinet *et al.* 2013).

2.2.3 Slow radiographic films

Slow radiographic films (e.g. Kodak X-Omat V, Kodak EDR 2) are designed for verification in radiation therapy and therefore optimized for high energies. These films, when calibrated, can be used as a large area dosimeter (35 cm x 43 cm sheets pre-wrapped in light-proof paper). Optical density of each point of the film is converted in absorbed dose using a calibration curve. By placing a slow film on patient's back during a cardiac interventional procedure it is possible to measure patient skin dose and dose distribution. A limiting factor is the narrow useful dose range: from some to 800 mGy with the X-Omat V and to 1200 mGy with the EDR 2 (Morrel *et al.* 2006, Domienik *et al.* 2008, Balter *et al.* 2006). In very complex procedures, it is easy to reach film saturation in the area with highest doses, where skin can reach doses near or higher the deterministic effects threshold, and MSD cannot be estimated

2.2.4 Radiochromic films

Radiochromic large area films (Gafchromic XR type T, for viewing in transmitted light and R, for viewing in reflected light) are intended for the measurement of maximum skin dose in high dose procedures. They are made of nearly tissue equivalent material and are of the size 35 cm x 42 cm. When exposed to radiation, their color changes proportionally to the dose received. The sheets could be quantitatively analyzed with appropriate software after digital scanning (Farah *et al.* 2015).

Dosimetric properties of the radiochromic films are discussed extensively in this report.

2.2.5 Radiosensitive indicators

Radiosensitive indicators (RadiMap; NichiyuGiken Kogyo, Saitama, Japan) are point detectors very often used in studies concerning MSD estimation. They are of rectangular shape (1.3cm x 1.8 cm) and in the literature they are arranged in rows and columns at intervals of 5 cm for patient dose measurements. The indicators have 2 kinds of functional dye (high-dose type and low-dose type) which, when they absorb X-ray, change color from pellucid to dark green and from pellucid to red in high and low dose ranges, respectively. The color of the indicators is then analyzed with color-measuring instrument (Chroma Meters CR-300; Konika Minolta Holdings, Tokyo, Japan) and the absorbed dose is calculated from the color difference of the indicators. The absorbed dose can also be evaluated at visual observation by comparing the indicators with the color samples arranged in order of increasing dose. This method enables the operator to estimate the MSD immediately after the procedure which might be important for reducing cumulative skin dose to the same area in repeated procedures (Suzuki *et al.* 2008a, Suzuki *et al.* 2008b).

2.3 Indirect Dose Measurements

It very useful to define an indicator alerting the operator in real-time about the potential for deterministic effects on the basis of the dosimetric indicators readily available in the interventional rooms (Jarvinen *et al.* 2018).

2.3.1 Fluoroscopy time

Fluoroscopy time (FT) is the most common dosimetric indicator routinely employed in many interventional fluoroscopy units. However, it provides inadequate skin-dose estimates for several reasons (Balter *et al.* 2006). The dose can be estimated only if fluoroscopic dose rate is available. It includes only time from fluoroscopy mode and not from both fluoroscopy and cine mode. The information concerning the incidence of X-ray beam is missed.

2.3.2 Kerma-Area Product (KAP)

The kerma area product (KAP) is a dosimetric quantity defined as the integral of air-kerma over the area of the x-ray beam in a plane perpendicular to the beam axis. KAP is often referred to as dose area product (DAP). KAP can be measured by the use of a plane parallel transmission ionization chamber associated to an electrometer or it can be calculated from irradiation data (EURADOS 2015).

KAP can directly, but approximately, be related to the patient dose using appropriate conversion factors and then used for stochastic risk assessment associated with different interventional procedures (ICRU 2006, Jarvinen *et al.* 2018).

To get a reliable estimate of patient dose it is essential that the KAP-meter is properly calibrated (EURADOS 2015, IAEA 2007).

2.3.3 Cumulative dose

Cumulative dose (CD) is defined as the total dose delivered during the entire procedure and includes fluoroscopic and radiographic exposure. It is calculated in a point defined as Interventional Reference Point (IRP) at a location that is 'representative-of the patient's skin' (IEC 2010). For isocentrical C-arm units it is located on the central axis of the X-ray beam at 15 cm from the isocenter in the direction of the X-ray tube. The methods use measurements of air kerma at IRP and does not take into consideration changes of projection during the procedure. The cumulative air kerma at the interventional reference point and thus may overestimate the maximum incident air kerma at any point on the patient.

Cumulative dose could be good indicator for maximum skin dose even if it doesn't provide any information on the distribution of the entrance beam over the patient's skin and it is measured, for a given unit, in the fixed distance from the x-ray tube while the table (thus the patient) can be moved during the procedure. For this reason, the MSD is usually overestimated (IAEA 2007).

2.4 Dose Calculation Methods

There are attempts to estimate the entrance skin dose (ESD) using calculation methods (Jones and Pasciak. 2011, Jones and Pasciak 2012 Jones *et al.* 2014). This approach requires some assumptions on geometry settings and exposure factors which, however, can hardly be met in practice. For example, estimation of ESD in interventional radiology from measured values of dose – area product assuming that all procedures of one type are performed with the same nominal geometry (Mc Praland 1998). Since the assumed single nominal geometry can differ from realistic ones, significant uncertainties are expected when estimating ESD through the ESD/DAP conversion factors. The resulting uncertainties due to deviations in the focus-to-skin and focus-to-image intensifier distances from their nominal values evaluated by the author are about 30 %. In addition, the error resulting from changes in image intensifier field-of-view or the use of collimation can be as large as 40%.

The presented approach allows a quick estimation of the ESD. However, it has some limitations in the evaluation of MSD. In fact, the total ESD for a single procedure is obtained by adding up the ESD resulting from the single projections. For this reason, the final estimated patient dose can be interpreted only as the upper limit of the maximum local skin dose in situation of overlapping fields from different projections, and the MSD is therefore overestimated.

The methodology to estimate peak skin dose is also described elsewhere (Jones and Pasciak 2011, Jones and Pasciak 2012, Jones 2014). The different methods can be applied, depending on the availability of DICOM RDSR. The accuracy of the calculation depends on the availability of the different data required for the calculations. The most accurate case is when the DICOM RDSR report is available, nevertheless it has been demonstrated that it is possible to determine PSD using indirect methods with better than 50 % accuracy for most, if not all, vascular and interventional oncology procedures.

2.5 Dose Mapping

Dose mapping systems compute and display the dose distribution on the skin of the patient. Currently, most equipment vendors have implemented some form of skin dose calculations in their angiographic systems with simple solutions only providing a schematic representation of patient exposure and beam overlap (Siemens and Philips), or more advanced 2D skin dose mapping software (Dosemap from GE Healthcare and Dose Tracking System by Toshiba). Offline skin dose calculation software have also been developed in research-based institutions (Johnson *et al*. 2011, Khodadadegan *et al*. 2011) or for commercial purposes both as stand-alone products (Em.dose from Esprimed) or integrated into the Dose Archiving and Communication Systems (DACS); examples of such software include Radimetrics (Bayer), Dose (Qaelum)and Radiation Dose Monitor (Medsquare).

2.5.1 Real Time Dose Mapping Systems

2.5.1.1 Basic visual solutions

Basic software (Philips and Siemens) combine KAP data with geometrical settings of gantry and table positions, X-ray beam data (beam quality, position of the collimator shutters, etc.) and patient size (weight and height) to estimate the body-area with highest exposure. No skin dose calculation is however performed and PSD estimates are only provided in terms of KAP. These solutions also generally suffer from simplistic representations of the patient anatomy and morphology.

2.5.1.2 Advanced solutions

For the more advanced solutions (GE and Toshiba), skin doses are estimated from KAP data while accounting for backscattered radiation, mass energy absorption coefficients, table and pad attenuation, etc. The dose representation is also improved with 1 cm^2 maps projected on a set of super ellipses defined by the patient BMI (GE) or on a full 3D numerical model matching the actual patient size, based on the CASER database (Toshiba). Such software has also been thoroughly benchmarked (Bordier *et al.* 2015) and proved to provide accurate skin dose estimates with differences to measurements within 25 %. Figure 1 presents the cumulative skin dose distribution on a patient graphic as well as the real-time peak skin dose rate and cumulative skin dose values at a given beam projection.

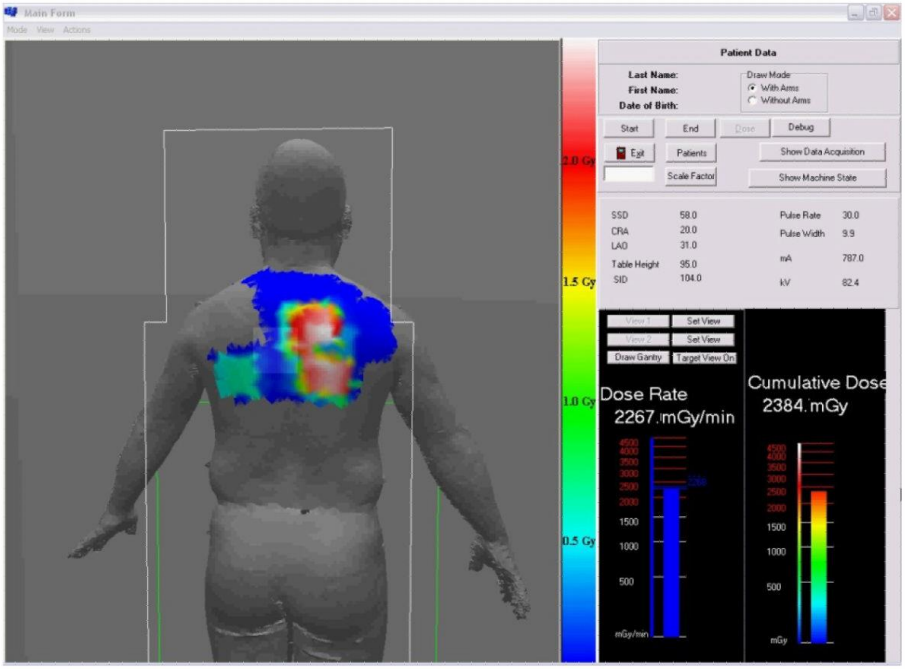

Figure 2.1. DTS display at end of a cardiac procedure showing the color-coded mapping of skin dose over the back of the patient (Bednarek et al., 2011)

2.5.2 Off-line Dose Mapping Systems

Several skin dose mapping solutions have also been commercialized independently from the manufacturer. The Em.dose (Esprimed) stand-alone software calculates skin dose using information from DICOM image headers. It has been successfully benchmarked against experimental data performed on patients receiving neuroradiology interventions (Greffier *et al.* 2017). One major limitation of such system is the extrapolation of fluoroscopy dose contribution since the latter is not registered in DICOM headers.

Meanwhile, three other DACS-integrated solutions can be found on the marked. These rely on the RDSR to compute skin dose while accounting for Backscattered radiation; they are generally of comparable performance. One major limitation of such system is

2.5.3 Non-commercial solutions

Several non-commercial solutions have been documented in the literature. These were developed at San Giovanni Battista hospital (Rampado *et al.* 2006), Mayo Clinic (Khodadadegan *et al.* 2011), the University of Florida (Johnson *et al.* 2011) and the FDA and University of Maryland (Badal *et al.* 2013). These systems are generally based on the RDSR and work by translating the reference point air kerma to the location of the patient's skin, which is represented by a computational model.

The first software (Rampado *et al.* 2006) was designed for cerebral interventions and tested on a PHILIPS INTEGRIS V 5000 angio unit with a combined uncertainty of the skin dose at each point estimated to be within 20 % (k=1). The software developed at Mayo clinic (Khodadadegan *et al.* 2011, Khodadadegan *et al.* 2013) suffers from several limitations due to simplifications on backscatter correction, phantom geometry, etc. Meanwhile, the software developed at the University of Florida features a good representation of the patient (Johnson *et al.* 2011) and proper selection of energy dependent corrections (namely, BF and μ/ρ coefficients) through the use of

effective beam energy. However, this software was not benchmarked against measurements. The last software uses Monte Carlo simulations to calculate the dose to the patient' skin and organs (Badal *et al.* 2013). At the present time, the system is still under development and only virtual simulations of idealized procedures were performed. No tests in clinical conditions were performed yet and information on the accuracy of the dose estimations is thus not available.

References

Badal A., Zafar F., Dong H., and Badano A., 2013. A real-time radiation dose monitoring system for patients and staff during interventional fluoroscopy using a GPU-accelerated Monte Carlo simulator and an automatic 3D localization system based on a depth camera", Proc. SPIE 8668, Medical Imaging 2013: Physics of Medical Imaging, 866828; doi: 10.1117/12.2008031.

Balter, S. 2006. Methods for measuring fluoroscopic skin dose. Pediatr Radiol, Vol. 36:136-44.

Bassinet C., Huet C., Baumann M., Etard C., Réhel JL., Boisserie G., Debroas J., Aubert B., Clairand I., 2013. Characterization of MOSFET detectors for in vivo dosimetry in interventional radiology and for dose reconstruction in case of overexposure. Health Phys.Vol.104(4):379-84.

Bednarek *et al.* 2011. Verification of the performance accuracy of a real-time skin-dose tracking system for interventional fluoroscopic procedures. Proc SPIE Int Soc Opt Eng. 13;7961(796127). pii: 796127_1.

Bogaert E., Bacher K., Lemmens K., Carlier M., Desmet W., De Wagter X., Djian D., Hanet C., Heyndrickx G., Legrand V., Taeymans Y., Thierens H., 2009. A large-scale mutlicentre study of patient skin doses in interventional cardiology: dose-area product action levels and dose reference level.: Br J Radiol, Vol. 82:303–312.

Bordier C., Klausz R., Desponds L., 2015. Patient dose map indications on interventional X-ray systems and validation with Gafchromic XR-RV3 film. Radiat Prot Dosimetry.;163:306-18.

Cheung T., Butson MJ., Yu PK., 2009. Energy dependence corrections to MOSFET dosimetric sensitivity. Australas Phys Eng Sci Med, Vol. 32(1):16-20.

Chida K., Inaba Y., Masuyama H., Yanagawa I., Mori I., Saito H., Maruoka S., Zuguchi M., 2009. Evaluating the performance of a MOSFET dosimeter at diagnostic X-ray energies for interventional radiology. Radiol Phys Technol, Vol. 2(1):58–61.

Dabin J., Negri A., Farah J., Ciraj-Bjelac O., Clairand I., De Angelis C., Domienik J., J arvinen H., Kopec R., Majer M., Malchair F., Novák L., Siiskonen T., Vanhavere F., Trianni A., Knežević Ž., 2015. Characterization of grids of point detectors in maximum skin dose measurement in fluoroscopically-guided interventional procedures, Phys. Med. 31(8): 1112–17.

Domienik J., Papierz S., Jankowski J., Peruga JZ., Werduch A., Religa W., 2008. Correlation of patient maximum skin doses in cardiac procedures with various dose indicators. Radiat Prot Dosim.,132:18-24.

Dong SL., Chu TC., Lan GY., Wu TH., Lin YC., Lee JS., 2002. Characterization of high-sensitivity metal oxide semiconductor field effect transistor dosimeters system and LiF:Mg,Cu,P thermoluminescence dosimeters for use in diagnostic radiology. Appl Radiat Isot, Vol. 57(6):883-891.

Duggan L., Hood C., Warren-Forward H., Haque M., Kron T., 2004. Variations in dose response with x-ray energy of LiF:Mg,Cu,P thermoluminescence dosimeters: implications for clinical dosimetry. Phys Med Biol, Vol. 49(17):3831-45.

EURADOS 2015.Järvinen H., Turak O., Ginjaume M., Daures J., Hourdakis C., Ferrar P., Mariotti. F., Technical aspects on DAP calibration and CT calibration. EURADOS Report 2015-03. Braunschweig, 2015.

Farah J., Trianni A., Ciraj-Bjelac O., Clairand I., De Angelis C., Delle Canne S., Hadid L., Huet C., Jarvinen H., Negri A., Novák L., Pinto M., Siiskonen T., Waryn MJ., Knežević Ž., 2015. Characterization of XR-RV3 GafChromicTM films in standard laboratory and clinical conditions and means to estimate uncertainties and reduce errors, Med. Phys. 42(7),4211-26.

Glennie D., Connolly BL., Gordon C., 2008. Entrance skin dose measured with MOSFETs in children undergoing interventional radiology procedures. Pediatr Radiol, 38(11): 1180-1187.

Gopiraj A., Billimagga R., Ramasubramanian B., 2008. Performance characteristics and commissioning of MOSFET as an in-vivo dosimeter for high energy photon external beam radiation therapy. Reports of Practical Oncology & Radiotherapy, Vol. 13(3):114–125.

Greffier J., Van Ngoc Ty C., Bonniaud G., Moliner G., Ledermann B., Schmutz L., Cornillet L., Cayla G., Beregi JP., Pereira F., 2017. Assessment of peak skin dose in interventional cardiology: A comparison between Gafchromic film and dosimetric software em.dose. Phys Med. Jun; 38:16-22.

IAEA 2007. International Atomic Energy Agency. Technical report series 457: Dosimetry in diagnostic radiology – an international code of practice, Vienna, 2007.

ICRP 2007. International Commission on Radiological Protection. The 2007 Recommendations of the International Commission on Radiological Protection. ICRP Publication 103, Ann. ICRP 37 (2-4), 2007.

ICRU 2006. International Commission on Radiation Units and Measurements, *Patient Dosimetry for X Rays Used in Medical Imaging*, ICRU Rep. 74, ICRU, Bethesda, MD, 2006.

IEC 2010. Medical electrical equipment - Part 2-43: Particular requirements for the basic safety and essential performance of X-ray equipment for interventional procedures. IEC 60601-2-43:2010, IEC, 2010.

Jarvinen H., Farah J., Siiskonen T., Ciraj-Bjelac O., Dabin J., Carinou E., Domienik J., Kluszczynski D., Knezevic Z., Kopec R., Majer M., Malchair F., Negri A., Pankowski P., Sarmento S., and Trianni A., 2018. Feasibility of setting up generic alert levels for maximum skin dose in fluoroscopically guided procedures, Phys Med.;46:67-74.

Johnson PB., Borrego D., Balter S., Johnson K, Siragusa D., Bolch WE., 2011 Skin dose mapping for fluoroscopically guided interventions. Med Phys.;38(10):5490-9.

Jones and Pasciak A. Calculating the peak skin dose resulting from fluoroscopically guided interventions. Part I: Methods. Journal of applied clinical medical physics, 2011, Vol. 12(4): 231-244.

Jones and Pasciak A. 2012. Calculating the peak skin dose resulting from fluoroscopically-guided interventions. Part II: Case studies. Journal of applied clinical medical physics, Vol. 13(1): 174-186.

Jones A., Ensor J., Pasciak A., 2014. How accurately can the peak skin dose in fluoroscopy be determined using indirect dose metrics? Med Phys, Vol 41: 071913-1 - 071913-9.

Khodadadegan Y., Zhang M., Pavlicek W., Paden RG., Chong B., Schueler B.A., Kenneth A., Fetterly KA., Lang SG., Wu T., 2011. Automatic monitoring of localized skin dose with fluoroscopic and interventional procedures. J Digit Imaging.;24(4):626-39.

Khodadadegan Y., Zhang M., Pavlicek W., Paden RG., Chong B., Huettl EA., Schueler BA., Fetterly KA., Langer SG., Wu T., 2013. Validation and initial clinical use of automatic peak skin dose localization with fluoroscopic and interventional procedures. Radiology;266(1):246-55.

Kohno R., Hirano E., Nishio T., Miyagishi T., Goka T., Kawashima M., Ogino T., 2008. Dosimetric evaluation of a MOSFET detector for clinical application in photon therapy. Radiol Phys Technol, Vol. 1(1):55–61.61(5):1603-1606.

Kopec R., Novák L, Carinou E., Clairand I., Dabin J., Datz H., De Angelis C., Farah J., Huet C., Knežević Z., Järvinen H., Majer M., Malchair F., Negri A., Waschitz Haruz S., Siiskonen T., Szumska A., 2014.Intercomparison of Gafchromic films, TL chips and TL foils for the measurements of skin dose in interventional radiology. Radiat. Meas. 71: 282–6.

Manigandan D., Bharanidharan G., Aruna P., Devan K., Elangovan D., Patil V., Tamilarasan R., Vasanthan S., Ganesan S., 2009. Dosimetric characteristics of a MOSFET dosimeter for clinical electron beams. Phys Med, Vol. 25(3):141-147.

Marcié S., Charpiot E., Bensadoun RJ., Ciais G., Hérault J., Costa A., Gérard JP., 2005. In vivo measurements with MOSFET detectors in oropharynx and nasopharynx intensity-modulated radiation therapy. Int J Radiat Oncol Biol Phys, 61(5):1603-6.

McParland BJ, 1998. Entrance skin dose estimates derived from dose-area product measurements in interventional radiological procedures. Br J Radiol.;71(852):1288-95.

Miksys N., Gordon CL., Thomas K., Connolly BL., 2010. Estimating Effective Dose to Pediatric Patients Undergoing Interventional Radiology procedures using anthropomorphic phantoms and MOSFET Dosimeters. Am J Roengtenol, Vol. 194(5):1315-1322.

Morrell RE., Rogers AT., 2006. Kodak EDR2 film for patient skin dose assessment in cardiac catheterization procedures. Br J Radiol, Vol. 73:504-13.

Moscovitch M and Horowitz Y. S. 2007. Moscovitch M, Horowitz Y. S. Thermoluminescent materials for medical applications: LiF:Mg,Ti and LiF:Mg,Cu,P. Radiation Measurements Vol.41 71-77.

Ramani R., Russell S., O'Brien P., 1997. Clincal dosimetry using MOSFETs. Int J Radiat Oncol Biol Phys, Vol. 37(4):959–964.

Rampado O., Garelli E., Deagostini S., Ropolo R., 2006. Dose area product evaluation with GafChromic® XR-R films and a flat bed scanner, Phys. Med. Biol. 51, 403–409.

Soubra M., Cygler J., Mackay G., 1994. Evaluation of a dual bias dual metal oxide-silicon semiconductor field effect transistor detector as radiation dosimeter. Med Phys.21(4):567-72.

Struelens L., Bacher K., Bosmans H., Bleeser F., Hoornaert MT., Malchair F., Balter S., 2014. Establishment of trigger levels to steer the follow-up of radiation effects in patients undergoing fluoroscopically-guided interventional procedures in Belgium, Physica Medica 30;934-40.

Suzuki S., Furui S., Isshiki T., Kozuma K., Koyama Y., Ochiai M., Asakura Y., 2008. Methods to reduce patient's maximum skin dose during percutaneous coronary intervention for chronic total occlusion. Catheter CardiovascInterv, Vol. 71:792-798.

Suzuki S., Furui S. Matsumaru Y., Nobuyuki S., Ebara M., Abe T., Itoh D., 2008. Patient skin dose during neuroembolization by multiple-point measurement using a radiosensitive indicator. Am J Neurorad, Vol. 29:1076-81.

3. EURADOS WG 12 activities on patient skin dose assessment in interventional procedures in radiology and cardiology

As the number and complexity of interventional procedures have been steadily growing, it becomes crucial to provide patient-specific, skin dose estimate during these procedures. In fact, EURADOS and EURAMED have identified patient-specific dose calculation in interventional procedures as a top-priority topic (EURADOS 2014, EURAMED 2017). To tackle this issue, EURADOS Working group 12 has initiated a number of activities to estimate the maximum skin dose in various procedures in radiology and cardiology.

In order to determine the suitability of XR-TypeR Gafchromic™ films and of detectors based on TL materials: pellets, chips and foils to measure skin dose, an intercomparison exercise has been organized within EURADOS Working Group 12 (Kopec *at al.* 2014). Furthermore, an assessment of the uncertainty associated with the sampling process of point detector grids used for maximum skin dose measurements was performed (Dabin *at al.* 2015).

As elaborated in Chapter 2 of this report, among all possible solutions, film dosimetry represents the most convenient method to determine skin dose. Hence, EURADOS Working Group 12 performed a comprehensive evaluation in order to investigate the optimal use of films in the interventional environment while addressing the means to reduce uncertainties in the quantitative assessment of patient skin dose (Farah *at al.* 2015a, Farah *at al.* 2015b).

Finally, patient skin dose measurements, along with assessment of other dose indices as dose area product and cumulative dose at interventional reference point was performed at different European hospitals for selected high dose interventional procedures in radiology and cardiology. The inter-center variability of online dose indicators and their correlation with the maximum skin dose were examined along with feasibility to establish the generic alert levels for skin injuries (Farah *at al.* 2015b, Jarvinen *et al.* 2018).

References

EURADOS 2014. Visions for Radiation Dosimetry over the Next Two Decades – Strategic Research Agenda of the European Radiation Dosimetry Group, EURADOS Report 2014-01, Braunschweig, 2014.

EURAMED 2017. EUROPEAN ASSOCIATION OF NUCLEAR MEDICINE (EANM), EUROPEAN FEDERATION OF ORGANIZATIONS FOR MEDICAL PHYSICS (EFOMP), EUROPEAN FEDERATION OF RADIOGRAPHER SOCIETIES (EFRS), EUROPEAN SOCIETY OF RADIOLOGY (ESR), EUROPEAN SOCIETY FOR RADIOTHERAPY AND ONCOLOGY (ESTRO). Common strategic research agenda for radiation protection in medicine. Insights into Imaging. 8(2017):183-197.

Dabin J., Negri A., Farah J., Ciraj-Bjelac O., Clairand I., De Angelis C., Domienik J., Jarvinen H., Kopec R., Majer M., Malchair F., Novák L., Siiskonen T., Vanhavere F., Trianni A., Knežević Ž., 2015. Characterization of grids of point detectors in maximum skin dose measurement in fluoroscopically-guided interventional procedures, Phys. Med., 31(8): 1112–17.

Farah J., Trianni A., Ciraj-Bjelac O., Clairand I., De Angelis C., Delle Canne S., Hadid L., Huet C., Jarvinen H., Negri A., Novák L., Pinto M., Siiskonen T., Waryn MJ., Knežević Ž., 2015a. Characterization of XR-RV3 GafChromicTM films in standard laboratory and clinical conditions and means to estimate uncertainties and reduce errors, Med. Phys. 42(7),4211-26.

Farah J., Trianni A., Carinou E., Ciraj-Bjelac O., Clairand I., Dabin J., De Angelis C., Domienik J., Jarvinen H., Kopec R., Majer M., Malchair F., Negri A., Novák L., Siiskonen T., Vanhavere F., Knežević Ž., 2015.b Measurement of maximum skin dose interventional radiology and cardiology and challenges in the set-up of European alert thresholds, Rad. Prot. Dos. 164 (1-2) 138–42.

Jarvinen H., Farah J., Siiskonen T., Ciraj-Bjelac O., Dabin J., Carinou E., Domienik J., Kluszczynski D., Knezevic Z., Kopec R., Majer M., Malchair F., Negri A., Pankowski P., Sarmento S., and Trianni A., 2018. Feasibility of setting up generic alert levels for maximum skin dose in fluoroscopically guided procedures, Phys Med. 46:67-74.

Kopec R., Novák L., Carinou E., Clairand I., Dabin J., Datz H., De Angelis C., Farah J., Huet C., Knežević Z., Järvinen H., Majer M., Malchair F., Negri A., Waschitz Haruz S., Siiskonen T., Szumska A., 2014. Intercomparison of Gafchromic films, TL chips and TL foils for the measurements of skin dose in interventional radiology. Radiat. Meas. 71: 282–6.

3.1 Comparisons of dosimetry systems used for skin dose assessment

Several passive solid state dosemeters, such as Gafchromic™ films and thermoluminescence (TL) detectors, are used to estimate and monitor patient skin doses in interventional radiology. Nowadays, Gafchromic® films are probably the most convenient and affordable solution for clinical routine, despite a need for careful calibration in beam qualities used in interventional procedures (Dabin *et al.* 2015, Farah *et al.* 2015, Kopec *et al.* 2014). Point detectors are frequently used to measure patient's maximum skin dose (MSD) in fluoroscopically-guided interventional procedures. However, their performance and ability to detect the actual MSD are rarely evaluated.

3.1.1 Intercomparison of dosimetry systems

To determine the suitability of XR-TypeR Gafchromic™ films and of detectors based on TL materials: pellets, chips and foils to measure skin dose, an intercomparison exercise has been organized within EURADOS Group 12 (WG 12–Dosimetry in Medical Imaging). A total of 8 institutions from different countries participated in the intercomprison. The following dosimetry systems that were investigated: XR-RV3 Gafchromic films routinely used in for IR dose measurements and several types of TLDs. TLDs used in the intercomparison are shown in Table 3.1.

Table 3.1 Dosimetry systems used for the intercomparison measurements (adopted from Kopec *et al.* 2014)

Detector type	*Shape*
LiF:Mg,Ti(TLD-100)	Square 3.2 mm x 3.2 mm, 0.38 mm thickness
LiF:Mg,Ti (MTS-100)	Square 3.2 mm x 3.2 mm,0.9 mm thickness
LiF:Mg,Cu,P (TLD-100H)	Square 3.2 mm x 3.2 mm, 0.38 mm thickness
LiF:Mg,Cu,P(MCP-N)	Pellets: 4.5 mm diameter, 0.9 mm thickness
LiF:Mg,Ti(MTS-N)	Pellets: 4.5 mm diameter, 0.9 mm thickness
LiF:Mg,Ti(TLD-100)	Pellets: 4.5 mm diameter, 0.9 mm thickness
2D TL foils (LiF:Mg, Cu, P powder + ETFE (Ethylene tetrafluoroethylene copolymer))	Sections 30 x 30 mm^2, 0.3 mm thickness

The dosimeters were irradiated in the Secondary Standard Dosimetry laboratory (SSDL) using different beam qualities and doses representative for the clinical routine as shown in Table 3.2. In addition, a blind test was carried with unknown dose, beam quality and modality in order to investigate the precision of the complete dosimetric systems in realistic conditions.

Table 3.2. Radiation beam qualities used for irradiation of dosemeters (adopted from Kopec *et al.* 2014)

Radiation quality	*Tube voltage (kV)*	*Filtration*	*First HVL (mm Al)*	*Effective energy (kev)*	*Mean energy (keV)*
RQR 5	70	2.835 mm Al	2.56	31.5	39.9
RQR 9	120	3.95 mm Al	5.09	42.5	56.6
A2	80	3 mm Al + 0,1 mm Cu	4.68	40.75	48.4
A4	120	3 mm Al + 0,1 mm Cu	6.64	48.5	60.2
B2	80	4.0 mm Al + 0.2 mm Cu	6	46	52.1
B4	120	4.0 mm Al + 0.2 mm Cu	8.17	55	64.4
C2	80	1.5 mm Al + 0.9 mm Cu	8.63	57	60.1
C4	120	1.5 mm Al + 0.9 mm Cu	11.2	70	74.7

To estimate the linearity of the dose response, RQR5X- ray beam was used and the irradiation doses were 0.1, 0.5, 1.3 and 5 Gy were used. For all other conditions delivered dose was 0.5 Gy. Except for the blind test irradiations which were done both on PMMA phantom and free in air, all other irradiations were done "free in air". All participating institutions used their own procedures of calibration and readout.

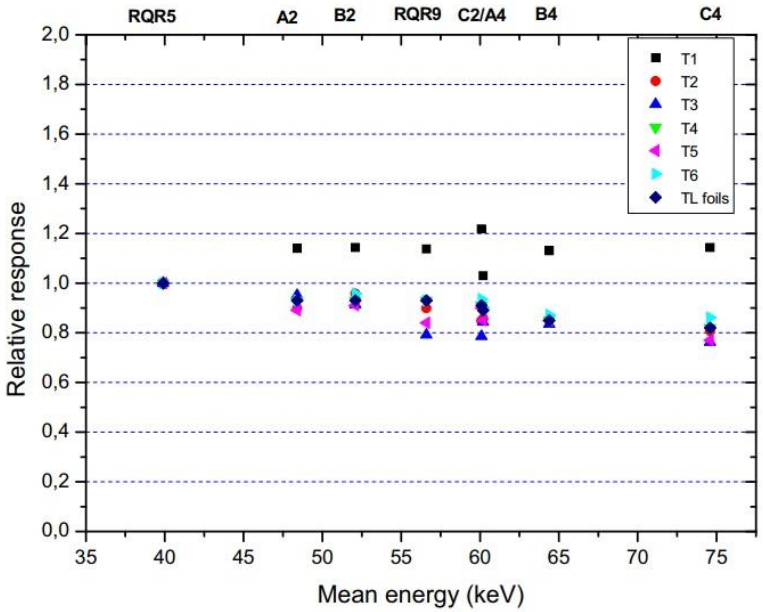

Figure 3.1. Relative energy response of TL detectors and foils normalized to the response after RQR5 X-ray beams adopted (adopted from Kopec *et al.* 2014)

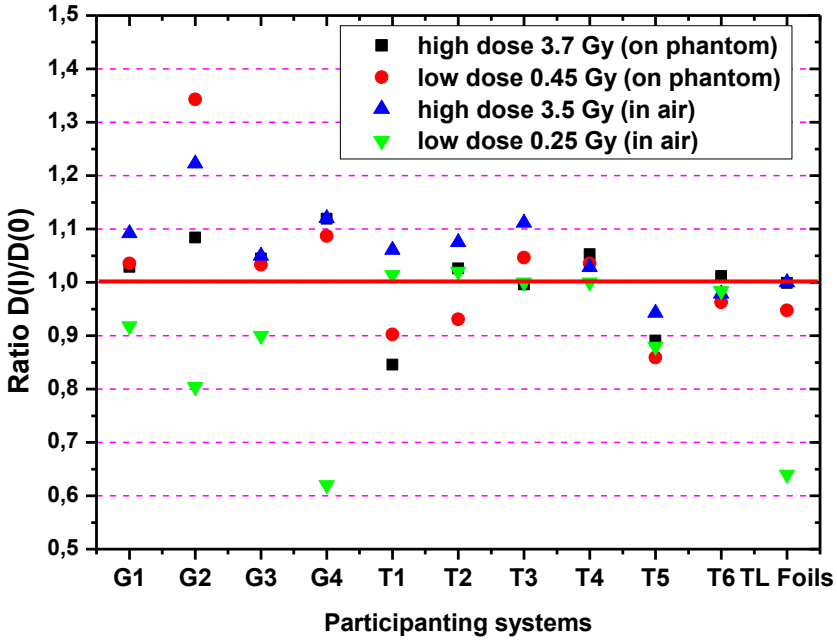

Figure 3.2. Results of the blind test used for intercomparisons of different dosimetry systems for skin dose measurements (adopted from Kopec *et al.* 2014)

Relative energy response of TL detectors and foils normalized to the response after RQR5 X-ray beams is presented in Figure 3.1. The dose response of Gafchromic films was not linear while TLDs shown linear dose response in investigated dose range. Gafchromic films showed an over response for all investigated energies an a large dependence on the calibration process and on beam energy and filtration.

TLD systems have shown lower dependence on beam energy and filtration. However, the energy dependence remained within 25 % for all beam qualities. The divergence from the reference beam quality increases with increasing filtration and becomes as high as 80 % for a 0.9 mm Cu beam quality. TL foils were among the most efficient systems, showing low uncertainties for the measurement of skin doses. In addition, they are easier to use if a large surface (patient skin) is to be monitored, however their performance deteriorates for doses below a few hundred mGy and they are still not commercially available

Blind test results are presented in Figure 3.2. refers to Gafchromic films and T to TLDs. For Gafchromic films spreads between Institutions were highest (up to 40 %), for TLDs the spreads were up to 15 % while for TL foils was the lowest.

3.1.2 Characterisation of grids of point detectors in maximum skin dose measurement

In addition to uncertainty due to dosimetric properties of detectors, it is important to take into account for uncertainty due to the spatial coverage of the dosimeters, i.e. their ability to detect the MSD. When point detectors are used, it is difficult to know whether the MSD was really measured or if it remained undetected and thus underestimated. This may be crucial in procedures with small

MSD area, when overlapping fields or multiple projections are used. With no prior knowledge of the region where the MSD is expected, it is necessary to cover a large measurement area with enough detectors to ensure sufficient sampling resolution. Even so, one cannot assure that the MSD will be measured. The probability to miss the MSD and measure a lower dose is referred to in this work as the sampling uncertainty. The total uncertainty budget in MSD assessment must include both the uncertainty arising from the intrinsic dose measurement (calibration, energy dependence…) and from the sampling process. Such uncertainty should be characterised, or at least estimated and reported along with the MSD values; but it is rarely, if ever, done in practice. Therefore, it was necessary to perform assessment of the uncertainty associated with the sampling process of point detector grids used for MSD measurements and to provide users an uncertainty estimate when it cannot be assessed in practice**.**

3.1.2.1 Gafchromic® films

Self-developing XR-RV3 Gafchromic® films (36 cm x 44 cm) were used for MSD measurements. Skin dose measurements using such films can be subject to high uncertainties due to the readout process (mainly affected by scanner uniformity and long term stability), calibration conditions (strong variability of film response with beam quality and film orientation) and data fitting (equation type and parameters) (Farah *et al.* 2015). Films were calibrated in a RQR5 beam quality (70 kV, half-value layer of 2.6 mm Al) according to IEC 61267 standard (IEC 2005) and read and analysed in a single centre using an Epson Expression 1680 Pro scanner operating in reflection mode. The centralised film reading enabled a strong reduction of scanner-related uncertainties. Third order polynomial data fitting based on reflectance ($R=\log(MPV_{unexposed}/MPV_{exposed})$) was used (Farah *et al.* 2015). Image reading and processing was done using an in-house Matlab® routine which identifies the darkest film area and determines the MSD.

3.1.2.2 Thermoluminescence detector grids

Grids of TLD (*e.g.*, LiF:Mg,Ti or LiF:Mg,Cu,P) have been used in numerous studies for dose measurement in IP (Kopec *et al.* 2014, Bogaert *et al.* 2009, Struelens *et al.* 2014). They show good energy and dose response in clinical conditions, and have been thoroughly characterised (Olko 2002). Examples of TLD grids used for MSD measurements in NE, and PCI and CE procedures are given in Figure 3.3.

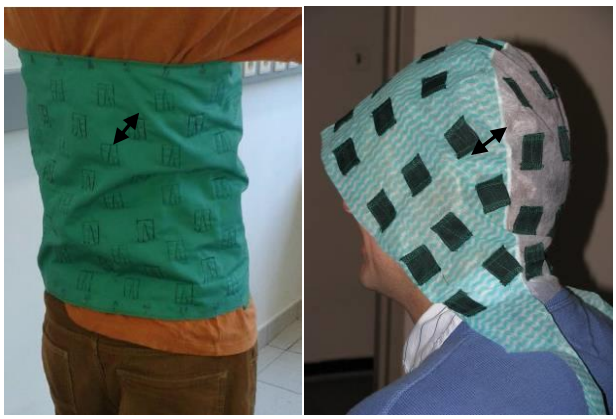

Figure 3.3. TLD grids for PCI and CE (left), and NE procedures (right). The arrow indicates the minimum spacing between two adjacent dosimeters (adopted from Dabin *et al.* 2015)

3.1.2.3 Procedures

Three types of interventional procedures usually associated with extensive use of fluoroscopy were studied: percutaneous coronary intervention (PCI), chemoembolization of the liver (CE) and neuroembolization (NE) procedures. Skin dose measurements were performed with XR-RV3 Gafchromic® films for 50 CE, 68 PCI and 58 NE procedures in four hospitals, from Czech Republic, France, Finland and Italy. All procedures were performed with under couch tube configuration; some NE procedures were performed with a biplane system.

For CE and PCI procedures, a film was placed between the couch and the patient's back at the level where the primary X-ray beam was expected to enter the skin; the orange side was set facing the X-ray tube. For NE procedures, a piece of film of 14 cm x 35 cm was placed in the head holder between the couch and the patient to intercept the primary beam from posterior-anterior and lateral projections.

3.1.2.4 Numerical simulation

A Matlab® routine was developed to simulate numerically grids of detectors superimposed on the dose maps measured with Gafchromic® films. The uncertainty in the absolute dose and in the spatial dose distribution of film measurements was not taken into account in the simulation: the films were considered as ideal dosimeters reporting the true dose and the dose distribution values at the patient's skin. The detectors were modelled as squared surfaces of 9 mm^2; the detector dose was calculated as the average dose over the 9 mm^2 film surface on which the detector was simulated. Different spacing intervals between the simulated detectors were investigated. For CE and PCI procedures, grids covering the complete film area (36 cm x 44 cm) were simulated with detector spacing of 1.4, 2.8, 4.2, 5.6 and 7cm corresponding to a total number of detectors of 792, 198, 84, 40 and 24, respectively. For NE procedures, grids covering the entire film area (14 cm x 35 cm) were simulated with detector spacing of 2, 4, 6, 8 and 10 cm corresponding to a total number of detectors of 305, 70, 27, 18 and 10, respectively. Those detector spacing was chosen based on the dimensions of TLD grids used by the authors in practice.

To simulate different position of the grid on the patient, the initial position of the grid was shifted both horizontally and vertically by 1 mm increment up to a distance equal to the detector spacing (Figure 3.4).

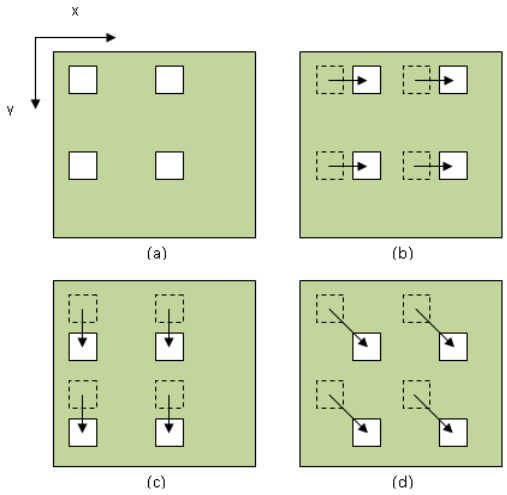

Figure 3.4. Different positioning of the detector grid was simulated by shifting the initial detector positioning (a) by 1 mm increment: horizontally (b), vertically (c), and both horizontally and vertically (d) (adopted from Dabin *et al.* 2015)

For each individual procedure *x*, the MSD which would have been measured by the grid of point detectors was estimated for each possible grid position *i* ($MSD_{x,i}$), and normalised to the corresponding MSD measured with a Gafchromic® film, which was used as the conventional true MSD value of the procedure (MSD_{TRUE}).

3.1.2.5 Statistical analysis

To evaluate the effect of the position of the detector grids on the patient, the $MSD_{x,i}$ was averaged over all simulated grid positions for each individual procedure *x* and detector spacing *D*, which is mathematically expressed as:

$$MSD_{x,D} = \frac{1}{M}\sum_{pos_i}^{M}\frac{MSD_{x,i}}{MSD_{TRUE}} \quad (3.1.)$$

Where pos_i is the position i of the detector grid on the patient, and M is the number of simulated positions. In other words, the $MSD_{x,D}$ is the average MSD which would have been measured for a procedure *x* using a detector spacing D.

In order to investigate the relationship between procedure complexity and the sampling uncertainty, the MSD_{TRUE} was used as a complexity indicator of the procedure. The difference in the $MSD_{x,D}$ between high (>2 Gy) and low dose procedures (<2 Gy) of a specific type was statistically tested by performing a Wilcoxon test.

For each type of procedure *T* and detector spacing *D*, the average simulated MSD was calculated as:

$$MSD_{T,D} = \frac{1}{N}\sum_{x}^{N} MSD_{x,D} \quad (3.2.)$$

where T is the type of procedure, and N is the number of procedures of type T. The $MSD_{T,D}$ represents the average MSD which would have been measured in procedures of type T using a detector spacing D.

For each type of procedure and detector spacing, the reverse cumulative frequency was calculated as follows:

$$F_{T,D}(a) = \frac{n}{N} \tag{3.3.}$$

where a is a $MSD_{x,D}$ value between 0 and 100% of the MSD_{TRUE}, and n is the number of procedures with $MSD_{x,D} \geq a$. For a specific procedure type and detector spacing, the reverse cumulative frequency distribution enables one to estimate the frequency of measuring a certain percentage of the MSD_{TRUE}.

The $MSD_{x,D}$ interval including 68 % (95 %) of the procedures of a specific type was calculated based on the reverse cumulative frequency, and expressed as [$a_{68\%}$; 100] ([$a_{95\%}$; 100]) % of MSD_{TRUE}, where $a_{68\%}$ ($a_{95\%}$) is a $MSD_{x,D}$ value between 0 and 100 % of the MSD_{TRUE} such as $F_{T,D}(a_{68\%})$=68 % ($F_{T,D}(a_{95\%})$=95 %) of the procedure cases. These intervals correspond to the confidence intervals associated with normally distributed variables (k=1 and 2, respectively) which are commonly used in uncertainty estimation, yet no assumptions were made on the normal character of the $MSD_{x,D}$ distribution.

3.1.2.6 Correction of TLD grid measurements

Simulated $MSD_{T,D}$ values could be used to correct for the dose underestimation occurring when MSD measurements are performed with TLD grids, as these suffer from sampling uncertainties. For TLD grids with detector spacing D and for procedure type T, the corrected MSD value could be expressed as:

$$MSD_{Corr} = \frac{MSD_{meas}}{MSD_{T,D}} \tag{3.4.}$$

where MSD_{meas} is the uncorrected MSD value measured with TLD grid. $MSD_{T,D}$ represents the average underestimation of TLD grid detector, for a specific type of procedure T and a detector spacing D. The standard deviation of the corresponding $MSD_{x,D}$ distribution ($\sigma(MSD_{x,D})$) could then be used in the assessment of the combined uncertainty as an independent factor representing the sampling uncertainty. Expressing the uncertainty according to the IAEA report 457 (IAEA 2007), the combined uncertainty in the - corrected - TLD grid measurements was:

$$\sigma_{TLD,Corr}^2 = \sqrt{\sigma\left(MSD_{x,D}\right)^2 + \sigma_{meas}^2} \tag{3.5.}$$

Where $(MSD_{x,D})$ is the standard deviation of the $MSD_{x,D}$ distribution for a specific type of procedures and σ_{meas} is the inherent uncertainty in TLD measurements.

3.1.2.7 Numerical simulation and statistical analysis

For each individual procedure, the $MSD_{x,i}$ was simulated for all possible grid positions and detector spacing, and normalised to the MSD_{TRUE}. Table 3.3. shows statistics of the simulated $MSD_{x,i}$ with

detector spacing of 5.6 cm for few examples of CE and PCI procedures, and with detector spacing of 6 cm for some NE procedures; the corresponding film images are given in Figure 3.5.

Table 3.3. Statistics of the simulated MSDx,i for all possible positions of the detector grid for examples of CE, PCI and NE procedures; 5.6 cm detector spacing was simulated for CE and PCI procedures, 6 cm for NE procedures. All values are reported in % of MSD_{TRUE} (adopted from Dabin *et al.* 2015)

	CE		*PCI*		*NE*	
	#41	*#50*	*#6*	*#13*	*#1*	*#8*
Average	92	72	82	67	81	94
Median	93	71	90	67	82	94
Minimum	79	41	48	32	44	88
Maximum	100	100	100	100	100	100
Standard deviation	5	14	17	19	11	3

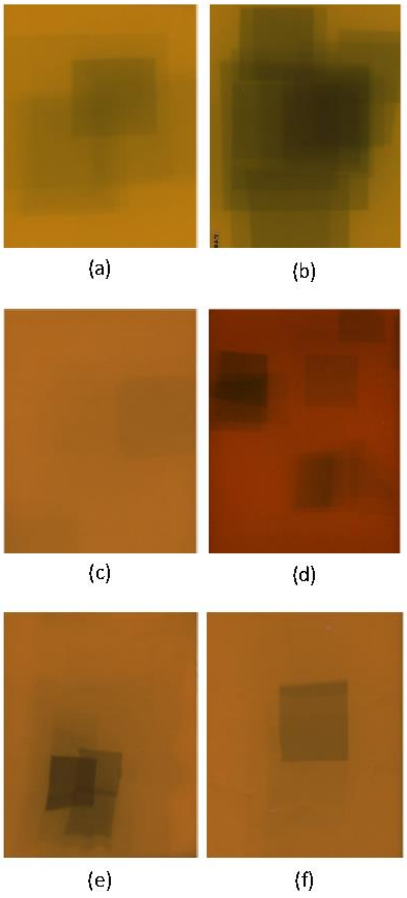

Figure 3 5. Irradiation fields of CE procedures 41 (a) and 50 (b), PCI procedures 6 (c) and 13 (d), and NE procedures 1 (e) and 8 (f) (adopted from Dabin *et al.* 2015)

The multiple positions, which are possible for a detector grid on the patient, make the sampling uncertainty difficult to assess for a single procedure. It is evident that different positions of the detector grid may in certain cases result in large differences in dose measurement for the very same procedure. For example, for the NE procedure #1, MSD values ranging from 44 % to 100 % of the

MSD_{TRUE} (81 % on average) would be measured depending on the position of the detector grid, while for the NE procedure #8 between 88 % and 100 % of the MSD_{TRUE} (94 % on average) would be measured. The reasons for this variation are clear from a visual examination of the procedure films (Figure 3.5): for NE procedure #1, multiple changes in beam orientation and field overlapping resulted in a very narrow MSD region at the field intersection, while for procedure #8 fewer changes in beam orientation resulted in a more homogenous skin dose distribution. The same observation can be made for other cases of NE, CE and PCI procedures as shown in Figure 3.5. From the complete measurement data set, PCI and NE procedures are particularly sensitive to the positioning of the grid, while CE procedures are much less sensitive to this issue. This is mainly because the beam orientation changes the least in the case of CE procedures while it is continuously adjusted during PCI and NE procedures, potentially resulting in local field overlapping and strong dose variation. However, the above mentioned general observation may also be influenced by different working practice of the different operators performing the same procedure.

$F_{T,D}$, the reverse cumulative frequencies of the simulated $MSD_{x,D}$ for the different detector spacing are given in Figure 3.6 to Figure 3.8 for CE, PCI and NE procedures, respectively. Those distributions enable one to estimate how frequently the MSD_{TRUE} is underestimated when a grid of point detectors is used, and to quantify this underestimation. For example, using a grid with 5.6 cm detector spacing for CE procedures, at least 90% of the MSD_{TRUE} would be measured in half the procedure cases, and at least 55% of the MSD_{TRUE} would be measured in all cases.

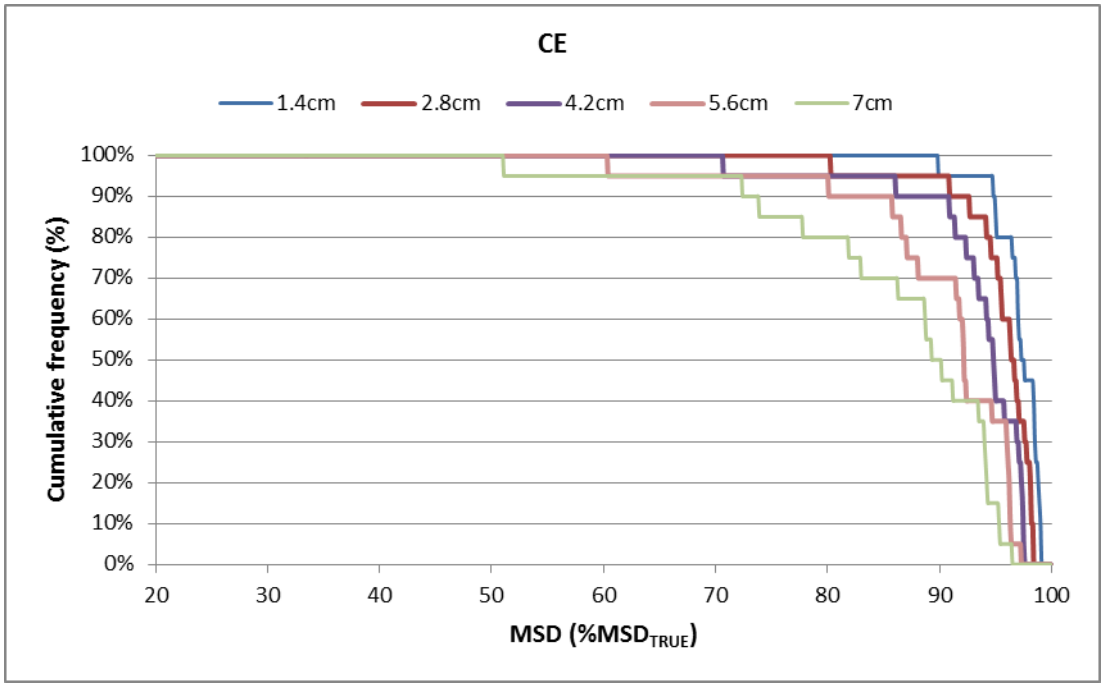

Figure 3.6. The reverse cumulative frequency of MSD measurements in CE procedures ($F_{CE, D}$) with different detector spacing (adopted from Dabin *et al.* 2015)

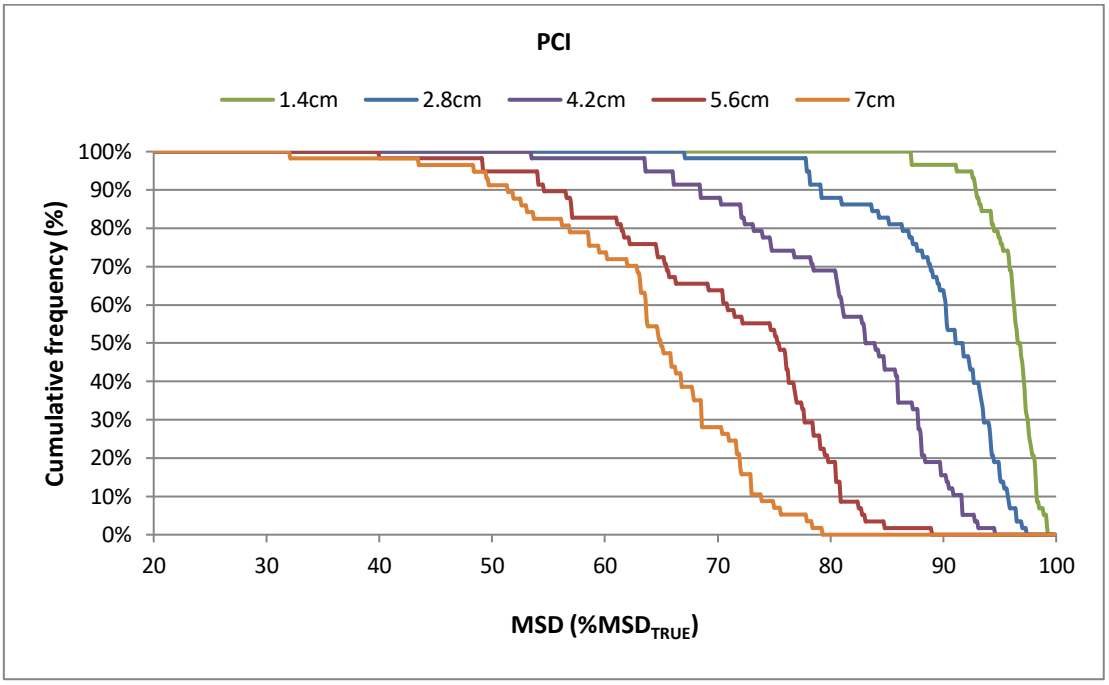

Figure 3.7. The reverse cumulative frequency of MSD measurements in PCI procedures ($F_{PCI, D}$) with different detector spacing (adopted from Dabin *et al.* 2015)

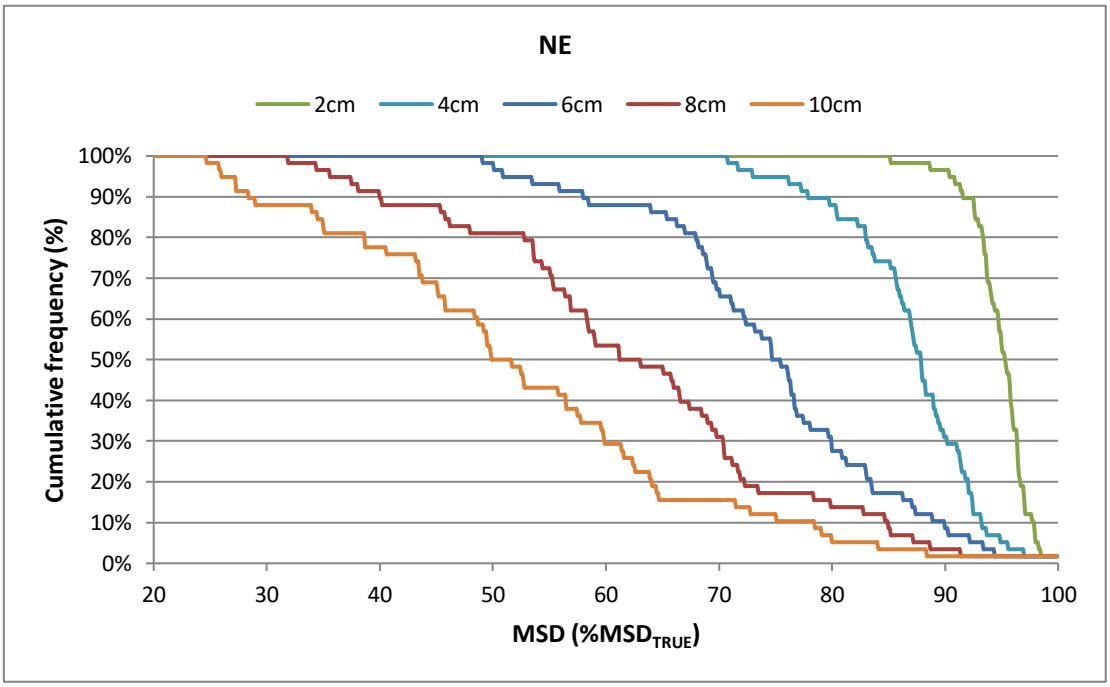

Figure 3.8. The reverse cumulative frequency of MSD measurements in NE procedures ($F_{NE, D}$) with different detector spacing (adopted from Dabin *et al.* 2015)

Similarly, the $MSD_{x,D}$ intervals including 95 % and 68 % of the procedures for the different detectors spacing were calculated from the reverse cumulative frequency distributions and are reported in Table 3.4..The average $MSD_{x,D}$ per type of procedure ($MSD_{T,D}$), and the standard deviation of the $MSD_{x,D}$ distribution (σ ($MSD_{x,D}$)) are also reported. The boundaries of those intervals are the minimum and maximum MSD values which would have been measured in 95% and68% of the procedure cases

when point detector grids are used. For instance, using a grid with 1.4 cm detector spacing at least 95 and 92 % of the MSDTRUE would have been measured in 95 % of the cases of the CE and PCI procedures, respectively. With the largest detector spacing (7 cm spacing for CE and PCI procedures), at least 52 and 29 % of the MSD_{TRUE} would have been measured in 95 % of the CE and PCI procedures, respectively. Whereas, in 68 % of the CE and PCI procedures with 7 cm detector spacing, at least 78% and 49 % of the MSD_{TRUE} would have been measured for these two procedures, respectively. Though the simulated $MSD_{x,D}$ are not normally distributed, 95 % and 68 % intervals were chosen because they correspond to the confidence intervals associated with normally distributed variables (factor of coverage of 1 and 2, respectively) which are commonly used in uncertainty analysis.

The MSD measured with gafchromic films was used as a complexity indicator of the procedure, and tested against the sampling uncertainty. Difference in the $MSD_{x,D}$ between high (>2 Gy) and low dose procedures (<2 Gy) of a same type was statistically tested by performing a Wilcoxon test. No significant difference was found ($p>0.05$) for CE and NE procedures whatever the TLD spacing. For PCI procedures, the difference was not significant ($p>0.05$), except for 7 cm TLD spacing ($p<0.01$). This suggests that the regions of high skin dose cover smaller areas in high exposure PCI procedures, and are likely to be more significantly underestimated using detector grids with low spatial resolution, than in low dose procedures. This may be because there is more variation in the projection angles in complex procedures, resulting in field overlapping and strong dose gradients.

Depending on the type of procedures, the uncertainty in MSD values measured with grids of point detectors may be high and eventually outbalance the intrinsic measurement uncertainty of such detectors (±10 % at k=2 for TLD [10, 11]). With detector spacing of 5.6 cm covering the patient's back, the MSD for CE procedures was on average 86 % of the MSD_{TRUE} and within [61 %-100 %] of the MSD_{TRUE} in 95 % of the procedure instances. Considering the same detector spacing, the MSD for PCI procedures was on average 63 % of the MSD_{TRUE} and within [42 %-100 %] of the MSD_{TRUE} in 95 % of the procedures (Table 3.4.).

When multiple point detectors are to be used for MSD measurement in interventional procedures, the sampling uncertainty of the whole dosimetric system should be estimated and reported in the uncertainty budget. To the authors' best knowledge, only a few approaches are currently available for this purpose. Radiochromic films may be conveniently used. Skin dose mapping software tools with sufficient spatial resolution are also promising (IAEA 2007, Bordier *et al.* 2015); however, they are not widely available yet and few clinical studies on software validation have been performed so far, if any. In the literature, comparison between the DAP value as displayed on the DAP-meter and as calculated from the detector grid measurements has been used (Bogaert *et al.* 2009). Though agreement between the DAP values extrapolated from the detector grid measurements and as displayed on the angiography unit may suggest that the actual MSD has been measured, this cannot solely sufficient evidence for reliable detection of MSD and further prediction of skin injuries. The results of the present study may also be used to evaluate the sampling uncertainty. It is however important to be aware of the limitations of this work: though the dose distributions were drawn from several measurements in different hospitals, they might not be fully representative of specific local practice. Besides, the dimensions of the simulated detectors do not represent all detector types. In the present work, 3 mm x 3 mm squared detectors were numerically simulated, those dimensions are close to the dimensions of standard TLD chips, but might not properly account for larger detectors such as PLD or MOSFET detectors.

Table 3.4. Characteristics of the simulated detector grids and the corresponding $MSD_{x,D}$ intervals including 95% and 68% of the procedures. The average $MSD_{x,D}$ ($MSD_{T,D}$), the minimum, the maximum and the standard deviation of the $MSD_{x,D}$ distributions (σ ($MSD_{x,D}$)) are reported. All values are reported in % of MSD_{TRUE}, unless otherwise stated (adopted from Dabin *et al.* 2015)

	Measurement area (cm^2)	*TLD spacing (cm)*	*Number of TLDs*	*$MSD_{T,D}$*	*[min:max] $MSD_{x,D}$*	*$\sigma(MSD_{x,D})$*	*95% frequency interval*	*68% frequency interval*
CE	36 x 44	1.4	792	97	[92,99]	2	[95,100]	[97,100]
		2.8	198	94	[81,98]	4	[84,100]	[94,100]
		4.2	84	91	[67,98]	8	[76,100]	[91,100]
		5.6	40	86	[55,97]	12	[61,100]	[85,100]
		7	24	80	[42,96]	15	[52,100]	[78,100]
NE	21 x 29	2	305	96	[87,100]	2	[92,100]	[96,100]
		4	70	90	[55,97]	8	[75,100]	[90,100]
		6	27	82	[42,96]	13	[52,100]	[80,100]
		8	18	74	[33,93]	16	[40,100]	[70,100]
		10	10	66	[27,90]	17	[32,100]	[60,100]
PCI	36 x 44	1.4	792	96	[91,99]	2	[92,100]	[95,100]
		2.8	198	88	[67,98]	6	[74,100]	[84,100]
		4.2	84	76	[53,95]	10	[55,100]	[71,100]
		5.6	40	63	[37,88]	12	[42,100]	[59,100]
		7	24	53	[26,80]	12	[29,100]	[49,100]

3.1.2.8 Correction of TLD grid measurements

An example of estimation of the combined uncertainty in corrected MSD measurements using different detector spacing for CE, NE and PCI procedures is given in Table 3.4. The uncertainty in TLD grid measurements was calculated as described in the material and method section "Correction of TLD grid measurements". It is composed of the inherent uncertainty in TLD measurements (5 %, k=1) and the sampling uncertainty (σ ($MSD_{X,D}$) from Table3.4. Those values can be compared with typical uncertainties in film measurement ranging from 5 % to 40 % (k=1) (Farah *et al.* 2015), depending on the calibration and reading process.

For example, considering 20 % uncertainty in film measurements and using the total uncertainty calculated for corrected TLD grid measurements as given in Table 3.5, the TLD grid show better performance than films up to a detector spacing of about 6 cm for NE procedures; for a detector spacing between 8 and 10 cm, the sampling uncertainty becomes the predominant term in the combined uncertainty of TLD grids, but the performances of TLD grids still compare with films. Though this approach is only a rough estimation, it may be used to compare measurement methods and to choose the number of TLD according to the desired precision. However, increasing the

number of detectors in the grid quickly becomes a heavy burden in routine measurements; for example, using a detector spacing of 4.2 cm rather than 5.6 cm for PCI procedures would result in a twice fold increase in the number of detectors (from 40 to 82, Table 3.4.). If there is sufficient knowledge of the procedure's characteristics and local practice to determine beforehand where the MSD is to be expected, reducing the monitored area is a good approach to balance accuracy and practicality in order to improve the spatial resolution of the detector grid and thus decrease the sampling uncertainty with no additional labour. Besides, an increased number of tissue equivalent detectors such as TLDs do not significantly affect the image quality, whereas MOSFET detectors, for instance, may degrade the image quality. Another disadvantage of MOSFET detectors in multiple grids is their cost.

Table 3.5. Estimated uncertainty (k=1) in TLD grid measurement corrected for sampling uncertainty. A 5% inherent uncertainty in TLD measurements was considered; the sampling uncertainty (standard deviation) from Table 3.4.was used (adopted from Dabin *et al.* 2015)

Procedure	*TLD spacing*	*Uncertainty (%)*
CE	1.4	5
	2.8	7
	4.2	9
	5.6	13
	7	16
NE	2	5
	4	10
	6	14
	8	17
	10	18
PCI	1.4	5
	2.8	8
	4.2	11
	5.6	13
	7	13

3.1.3 Conclusions

It was found that the response of films to be strongly dependent on beam quality and filtration (increasing by up to 80 % with respect to reference beam quality). The response of TL detectors was found to be less dependent on beam quality (less than 25 % variation), with TL foils showing less than 10 % variation with respect to reference beam quality.

Therefore, point detectors such as TLDs show good energy response in clinical conditions, are easy to calibrate and rather insensitive to environmental conditions; however their poor spatial resolution may outweigh those advantages when used for MSD measurements in presence of strong, local dose variations, such as the overlapping region of radiation fields. Among the three types of procedures studied, sampling uncertainty was the highest for NE and PCI procedures, while the uncertainty in CE procedures was lower owing to a limited variability in tube orientation during such procedures.

If grids of point detectors are to be used, the spatial resolution of the dosimetric system should be provided, along with the uncertainty associated with the sampling process of the dosimetric system. Films or skin dose mapping software can be used for this purpose if available; if not, the results presented in this report could be used.

References

Bordier C., Klausz R., Desponds L., 2015. Patient dose map indications on interventional X-ray systems and validation with Gafchromic XR-RV3 film. Radiat Prot Dosim.,163:306-18.

Bogaert E., Bacher K., Lemmens K., Carlier M., Desmet W., De Wagter X., et al. 2009. A large-scale multicentre study of patient skin doses in interventional cardiology: dose-area product action levels and dose reference levels. Br J Radiol.,82:303-12.

Dabin J., Negri A., Farah J., Ciraj-Bjelac O., Clairand I., De Angelis C., Domienik J., Jarvinen H., Kopec R., Majer M., Malchair F., Novák L., Siiskonen T., Vanhavere F., Trianni A., Knežević Ž., 2015. Characterization of grids of point detectors in maximum skin dose measurement in fluoroscopically-guided interventional procedures, Phys. Med., 31(8): 1112–17.

Farah J., Trianni A., Ciraj-Bjelac O., Clairand I., De Angelis C., Delle Canne S., Hadid L., Huet C., Jarvinen H., Negri A., Novák L., Pinto M., Siiskonen T., Waryn MJ., Knežević Ž. 2015a. Characterization of XR-RV3 GafChromicTM films in standard laboratory and clinical conditions and means to estimate uncertainties and reduce errors, Med. Phys., 42(7): 4211-26.

IAEA 2007. International Atomic Energy Agency. Technical report series 457: Dosimetry in diagnostic radiology – an international code of practice, Vienna, 2007.

IEC 2005. Medical diagnostic X-ray equipment - Radiation conditions for use in the determination of characteristics. IEC 61267:2005, Geneva, 2005.

Kopec R, Novák L, Carinou E, Clairand I, Dabin J, Datz H, De Angelis C, Farah J, Huet C, Knežević Z, Majer M, Malchair F, Negri A, HaruzWaschitz S, Siiskonen T, Szumska A, Trianni A, Vanhavere F. 2014. Intercomparison of Gafchromic films, TL chips and TL foils for the measurements of skin dose in Interventional Radiology. Radiat. Meas., 71 282-286.

Olko P. 2002. Microdosimetric modelling of physical and biological detectors. Report1914/D. Kraków: IFJ.

Struelens L., Bacher K., Bosmans H., Bleeser F., Hoornaert MT., Malchair F., Balter S., 2014. Establishment of trigger levels to steer the follow-up of radiation effects in patients undergoing fluoroscopically-guided interventional procedures in Belgium, Physica Medica 30;934-40.

3.2 Calibration of Gafchromic films and associated measurement uncertainties

To provide accurate estimates of skin doses in interventional procedures, many different dosemeter can be used, as described in Chapter 2 of this report. Among all possible solutions, film dosimetry represents the most convenient method to determine skin dose. Indeed, GafChromic films are easy to use and position on the patient, do not affect image quality, do not add patient discomfort, and allow direct qualitative (visual) or quantitative assessment of patient exposure[8]. XR-Type R GafChromic films (Ashland, Inc., Covington, KY) are self-developing, near tissue equivalent and light

insensitive and are specifically designed for interventional radiology. However, film dosimetry involves several challenges and extra care should be taken to reduce measurement uncertainties.

EURADOS Group 12 (WG 12–Dosimetry in Medical Imaging) performed hence a comprehensive evaluation in order to investigate the optimal use of films in the interventional environment while addressing the means to reduce uncertainties in the quantitative assessment of patient skin dose (Farah *et al.* 2015a, Farah *et al.* 2015b). The study involves eleven European partners from six countries. This section first reviews the current status of film dosimetry. Next, a careful investigation of film response with beams of different radiation quality was performed under both standard dosimetry laboratory and clinical conditions. Additionally, scanner-related (uniformity, short and long term stability, and scanner-to-scanner variability) and film-related (uniformity, post-exposure growth, and dose rate dependence) uncertainties are investigated, broadening the literature work with a multi-site approach. Finally, fitting-related uncertainties were carefully studied by testing multiple fit equations commonly used in the literature. This investigation is particularly novel since it takes into account the variability in film characterization between dosimetry laboratory conditions and clinical conditions when calculating the overall uncertainty in skin dose assessment. The study provides a comprehensive analysis of uncertainties associated with the use of XR-RV3 GafChromic films to assess patient skin dose in interventional radiology while identifying the multiple sources of errors and their potential impact on dosimetry.

3.2.1 State of the art and dosimetry challenges

The reliability and applicability of GafChromic films for quantitative estimates of skin dose in interventional radiology and cardiology is directly related to film properties and performance in clinical conditions. Uncertainties related to the use of such films for patient skin dose assessment in the interventional environment have been extensively addressed in the literature. Specifically, for XR-Type R GafChromic films, tremendous effort has been invested to determine their dosimetric characteristics in terms of film uniformity, dose linearity, dose fractionation, post-exposure density growth, energy dependence, dose-rate dependence, storage lighting, and UV light sensitivity (Giles *et al.* 2002, Thomas *et al.* 2003, Butson *et al.* 2005, Dini *et al.* 2005, Blair and Meyer 2009, McCabe *et al.* 2011), However, contradictory results can be found in the literature (Giles *et al.* 2002, Thomas *et al.* 2003, Butson *et al.* 2005, Dini *et al.* 2005, Blair and Meyer 2009) indicating that film dosimetry can be far more challenging than expected. In addition, to the best of our knowledge, the paper by McCabe et al. represents the only study on the characteristics of XR-RV3 films in particular (McCabe *et al.*2011). Moreover, some relevant aspects of radiochromic film dosimetry are not addressed in that paper.

Although McCabe et al. (McCabe *et al.* 2011) studied the energy dependence of XR-RV3 film covering the entire interventional energy range (from 60 to 120 kV, half value layers (HVL) ranging from 1.68 to 6.96 mm Al), the considered X-ray beam qualities are not fully close to clinical beam qualities. In addition, clinical conditions involve backscatter radiation and use high-dose rate pulsed beams while laboratory beams are typically free in- air, continuous, and of low dose rate. Since film response variation with dose rate was not studied by McCabe *et al.* (2011) and GafChromic films are expected to show different darkening with continuous or pulsed beams (Giles *et al.* 2002, McCabe *et al.* 2011) film characterization under clinical conditions is needed. In addition, the previous study only involved the characterization of XR-RV3 films of a single batch and with a single scanner model. Thus, the batch-to-batch film behavior needs to be checked and the performance of multiple and commonly used scanner models should be assessed to determine scanner-specific uncertainties, as

recommended by film manufacturer. Finally, film dosimetry is governed by the pixel-value-to-dose conversion function, i.e., the dose fitting equation, and since there is a lack of clear recommendations regarding the optimal calibration function and parameters specific for XR-RV3 films, it is thus necessary to test the different equations used in the literature (Blair and Meyer 2009, Quai *et al.* 2002, Thomas *et al.* 2005, Rampado *et al.* 2006, Lewis *et al.* 2012, Labattu *et al.* 2013).

3.2.2 XR-RV3 films, reading equipment and scanning protocol

Reflective-type XR-RV3 GafChromic films consist of five layers including a 97 µm yellow polyester layer, a 12 µm thick pressure sensitive adhesive layer, a 17 µm thick active layer, a 3 µm surface layer, and a 97 µm thick opaque white polyester backing. The five layers are composed primarily of carbon, hydrogen, and oxygen. The active layer contains small quantities (less than 2 % by mass) of lithium, nitrogen, and chlorine, while the opaque white polyester layer contains quantities of sulfur (less than 4 % by mass) and barium (less than 16 % by mass) (McCabe *et al.* 2011). As such, film response can be slightly enhanced by the barium material in the white polyester layer in the case of white side irradiations. Other key features of XRRV3 films, given by the manufacturer, include sensitivity to a high dose (0.05–15 Gy) and energy range (30 keV–30 MeV), good uniformity (<5 %), low dose rate dependence (<3 %), a quickly stable polymerization process (after 24 h), and a large commercial sheet size (36×43 cm^2). Meanwhile, reading equipment is a key element to correctly estimate dose registered by XR-RV3 films. Technically efficient and easy to use desktop scanners have provided a more economical and compact method of scanning such films when compared to regular film densitometers (Alva *et al.* 2002, Devic *et al.* 2005). However, it is well known that the response over the scan area can vary, depending on the scan region (central vs edge regions), the scanning direction (parallel vs perpendicular to the lamp), the color channel, the type of medium (overhead sheet, radiographic or radiochromic film, etc.), lamp warm-up effects, film darkness, and the scanner mode (Thomas *et al.* 2003, Alva *et al.* 2002, Devic *et al.* 2005, Alnawaf *et al.* 2012) . In addition, Thomas et al. (2003) compared five reflective flatbed scanners of different vendors (Microtek, Umax, HP, and Canon) and concluded that these scanners are efficient but should be tested before being used for dosimetry purposes. Similarly, three Epson desktop scanners (V330, V700, and 10000XL) have been quoted as devices which match the characteristics required for the evaluation of radiation dose exposure by radiochromic films (Alnawaf *et al.* 2012). In this work, different Epson and HP scanners were tested (Table 3.6.).

To reduce reading uncertainties, a common reading procedure was developed and used by all sites. It consists in carrying out film readings in reflection mode, the only possible reading mode with XR-RV3 films, with the best scan quality after a period of 48 h post exposure. During scanning, 48-bit color images (good sensitivity) were acquired without any image adjustment or post-processing options and output files were saved in tif format. In addition, all readings were done in the red light channel since it provides the maximum sensitivity as well as the best differentiation in the low-kerma region (<1 Gy air kerma) in the reflection reading mode (Thomas *et al.* 2003, Dini *et al.* 2015, Blair and Meyer 2009, McCabe *et al.* 2011). Two scans per film piece were performed and average reading was taken to reduce the scan-to-scan variability. All film pieces were scanned in the central area of scanner beds to reduce scanner non-uniformity uncertainties. The analysis was done using several wellknown and dedicated software packages, including ImageJ (National Institutes of Health), FilmQA™ (Ashland, Inc.), and Picodose (Tecnologie Avanzate, Italy).

Table 3.6. Desktop scanners used at each institution and main reading characteristics (adopted from Farah *et al.* 2015a).

Institution	*Scanner model*	*Resolution*	*Scanner bed size*	*Analyze Software*
AOUD	Epson Expression 1680 Pro	50 dpi	A4	Picodose
	Epson Perfection V750 Pro	75 dpi	A4	Picodose
IRSN	Epson Perfection V700 Photo	150 dpi	A4	FilmQA
FBF	EPSON Expression 10000XL	75 dpi	A3	Picodose Pro
STUK	EPSON Expression 1600 Pro	72 dpi	A4	ImageJ
VINCA	HP Scanjet G3110	96 dpi	A4	ImageJ

3.2.3 Calibration with standard dosimetry laboratory beams

3.2.3.1 SSDL beams and characterization setup

Three secondary standard dosimetry laboratories (SSDLs): IRSN (France), NRPI (National Radiation Protection Institute, Czech Republic), and VINCA (Serbia), and one primary standard dosimetry laboratory (PSDL): ENEA-INMRI (Italy), were involved in this project. Radiation qualities representative of clinical beams were used in each institution to carry out film characterization with a radiation environment similar to interventional clinic. These include reference ISO N and H series and IEC RQR beams (ISO 1996, IEC 2005) as well as other non-reference highly filtrated beam qualities (in text, referred to as A, B, and C series). SSDL characterizations were carried out free-in-air, where films were placed on a 0.5 cm-thick polystyrene support providing negligible backscatter and irradiated at 1 m from the focal spot (Figure 3.9). All dosimeters were placed in the central homogenous part of the beam to guarantee a uniform and identical irradiation (better than 2 % in all SSDLs). For each beam quality and kerma value, two film pieces of the same batch were used. These were cut in small pieces of 3×3 cm^2 and aligned to the central flat region of the x-ray field (Figure 3.9).

Prior to film irradiations, the dose delivery was monitored using different ionization chambers properly calibrated at the same beam qualities used for the measurement. These detectors were positioned in the central uniform region of the radiation fields at the presumed position of films. Meanwhile, during film irradiations, tube output was monitored using monitor chambers. Table 3.7. presents the list of equipment used in SSDL facilities for the characterization of XR-RV3 films including the type of x-ray tube, the type of ionization chamber, the considered radiation beam qualities, air kerma rates, and delivery-specific uncertainties. It should be noted that beam uniformity is included in the overall delivery uncertainty (2.5 % in SSDL). In fact, as small film pieces were irradiated and aligned to the center of the field, the heel effect impact is minimized and beam uniformity is expected to be within 1.7 % (k = 1). Additionally, since the characterization was done free-in-air, the dose to the skin will be slightly overestimated since these irradiations do not account for low-energy backscattered photons present in the case of on-patient film exposure (Mart *et al.* 2012). Backscatter factor converting the air kerma measured free-in-air to air kerma on the surface of

the patient is however strongly dependent on the geometrical setup, field size, and beam energy and is expected to be within 5 %–40 % considering the range and qualities of interventional beams (Ma *et al.* 2001, Tomic *et al.* 2010). The backscatter factor was added to the overall uncertainty analysis. For the range of energies used in interventional beams, the conversion of air kerma to absorbed dose to skin is considered to be equal to one.

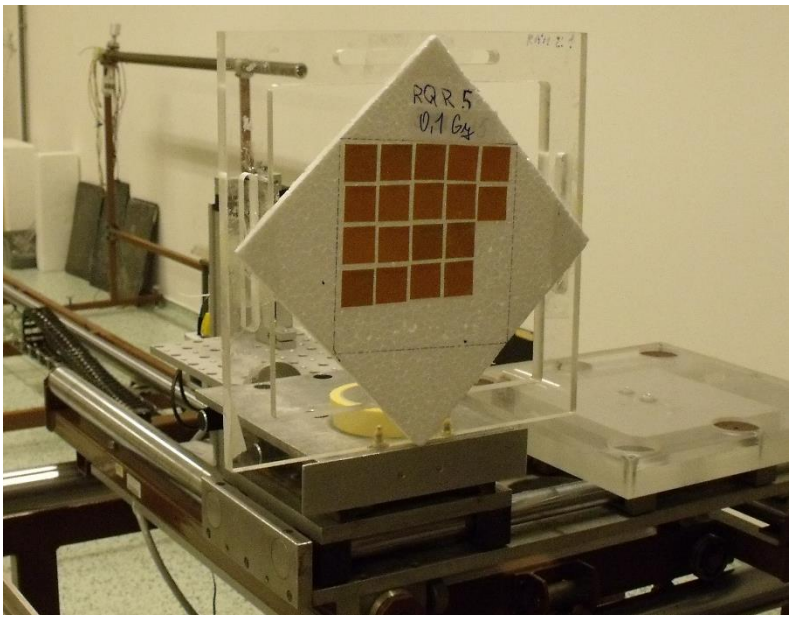

Figure 3.9. Irradiation conditions at NRPI SSDL for a free-in-air characterization of XR-RV3 Gafchromic films pieces coming from all participating centers (adopted from Farah *et al.* 2015a).

Table 3.7. X-ray equipment, dosimetry devices, radiation qualities and dose uncertainties used for film characterization in standard laboratory conditions as well as in clinical conditions (adopted from Farah *et al.* 2015a).

*Standard Laboratory**	*X-ray systems*	*Ionization chamber type and volume*	*Traceability (radiation quality)*	*Radiation quality*	*Tube voltage (kV)*	*First HVL (mm Al)*	*Air kerma rate ($mGymin^{-1}$ at 1 m)*	*Dose delivery uncertainty (k=2) (%)*
IRSN	320 kV Seifert	PTW M23361 cylindrical – 30 cc Custom-made parallel plate – 4.73 cc	N-60 – N-250	N-60	60	5.82	0.92	2.3
				H100	100	6.56	3.10	
ENEA-INMRI	160 kV Seifert Isovolt	Custom-made Spherical – 0.38 cc	RQR, RQA	RQR4	60	2.19	56.60	2.5
				RQR6	80	3.01	92.84	
				RQR9	120	5.00	104.17	
VINCA		Magna A650, Exradin, parallel plate – 3 cc	RQR, RQT	3 cc	80	3.01	30.5	2.6
				RQR8	100	4.00	44	
NRPI	160/320 kV Seifert Isovolt	Exradin A4 spherical – 30 cc	N-40 – N-100 RQR, RQT, RQA5	RQR5	70	2.58	40.30	2.8
				RQR9	120	5.09	85.7	2.8
				A2	80	4.68	24.7	3.4
				A4	120	6.64	63.5	3.4
				B2	80	6.00	14.2	3.4
				B4	120	8.17	43.6	3.4
				C2	80	8.63	3.7	3.4
				C4	120	11.2	19.2	3.4

* IRSN - Institut de Radioprotection et de Sûreté Nucléaire, France; ENEA-INMRI - Istituto Nazionale di Metrologia delle Radiazioni Ionizzanti Italy; VINCA - Vinca Institute of Nuclear Sciences, Serbia; NRPI - National Radiation Protection Institute, Czech Republic

3.2.3.2 Film response in SSDL conditions

Films irradiated to a dose of 0.5 Gy using different beam qualities (RQR5, RQR9, A, B and C series) showed lower mean pixel values when irradiated with beams of higher quality (kV or filtration). Additionally, Figure 3.10. shows that the difference on film darkening (MPV) increases with the change in radiation quality reaching up to 15 % for the C-120 beam, the farthest from the reference radiation beam quality (RQR5). From this figure, it can be seen that although the differences in pixel value are not uniform for the four sites, the general trend is consistent. While IRSN found a difference on film darkening between C-120 and RQR5 beams limited to within 6.5 %, higher values were found by the other three centers. The different effect of beam quality observed between the centers is mainly due to readout uncertainties (uniformity, stability, warm-up, software, etc.) along with a limited contribution of film batch effect (4 centers participating, each with one specific film batch) and should not be attributed to film response variability with beam quality. This is one of the key inputs of this multi-site study which provides wider uncertainty estimates through the adding of readout variability. Finally, it should be noted that uncertainties associated with signal value can induce higher uncertainties in terms of dose as the latter strongly depends both on signal uncertainty and on the calibration curve (Richlev *et al.* 2010).

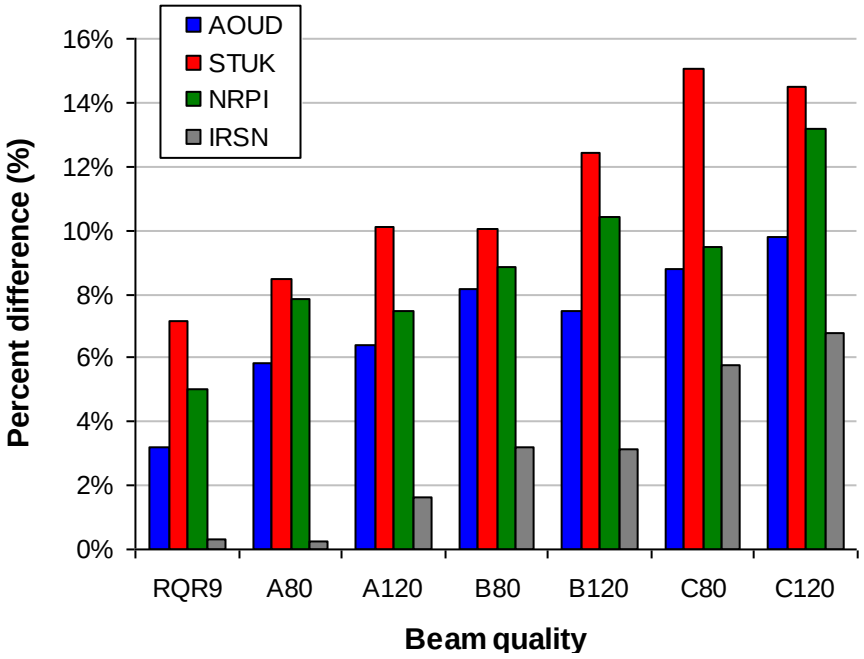

Figure 3.10. Difference to the RQR5 calibration beam of film response with RQR9, A, B and C beam qualities for films irradiated at NRPI to 0.5 Gy (adopted from Farah *et al.* 2015a).

The additional analysis conducted at IRSN showed 2.8 % difference on the mean pixel value when comparing N-60 *vs.* H-100 beam qualities and irradiations to a dose of 1 Gy. Similar results were also found at ENEA-INMRI where irradiations of films coming from three different batches were made to different dose levels (0.1 Gy to 8 Gy) and showed that radiation quality may induce substantial differences on pixel value. Namely, for yellow side irradiations, up to 4 % difference on pixel value was registered for RQR4 vs. RQR6 beams and up to 13 % for RQR4 vs. RQR9 beams. White side

irradiations showed higher values (up to 8 % for RQR4 vs. RQR6 and up to 20 % for RQR4 vs. RQR9). This result is in agreement with data by McCabe et al. (2011) who showed that the energy dependence of XR-RV3 film decreased as the air kerma level increased with larger energy dependence of white-facing exposures (with almost 25 % difference between the UW60-M and UW120-M beam qualities at 1 Gy air kerma) compared against orange-facing exposures (film darkening difference around 15 %).

3.2.4 Calibration with clinical beam qualities

3.2.4.1 Clinical beams and characterization setup

Similarly, the characterization of XR-RV3 in clinical radiation environment was carried out at AOUD (Italy) and HJV (France) using interventional x-ray equipment, clinically relevant beams qualities, and setups (Table 3.8.). In this case, free-in air irradiations were carried out but the tube-to-film distance was limited to 50 cm for practical reasons. Film pieces were again cut to 3×3 cm^2 and taped on a thin polystyrene support to reduce backscattered radiation. As in SSDL laboratory, and prior to film irradiations, the dose delivery in clinical settings was monitored using different ionization chambers properly calibrated at the same beam qualities used for the measurement. These detectors were positioned in the central uniform region of the radiation fields at the presumed position of films. During film irradiations, tube output was monitored through online dose indicators of the x-ray units. Namely, the dose area product and cumulative air kerma at reference interventional point were carefully registered and monitored to match the values obtained during the reference dosimetry step (performed using the ionization chambers).

Table 3.8. present the list of equipment used in clinical facilities for the characterization of XR-RV3 films including the type of x-ray tube, the type of ionization chamber, the considered radiation beam qualities, air kerma rates, and delivery-specific uncertainties. Backscatter factor as well as the beam uniformity were again included in the overall delivery uncertainty; this latter component was estimated to be within 5 % in clinical conditions.

Table 3.8. X-ray equipment, dosimetry devices, radiation qualities and dose uncertainties used for film characterization in clinical conditions (adopted from Farah *et al.* 2015).

Hospital	*X-ray systems*	*Ionization chamber type and volume*	*Radiat. Quality*	*Tube voltage (kV)*	*Beam current (mA)*	*First HVL - inherent filtration (mm Al)*	*Additional filtration (mm Cu)*	*Air kerma rate (μGys^{-1} at 0.5 m)*	*Dose delivery uncertainty (k=2) (%)*
AOUD- Udine University Hospital, Italy	Siemens Axiom Artis	20X6-6 General Purpose RadCal – 6 cc	Clinical	75	596	4	-	5300	5%
				120	673	6	-	17980	
HJV– Hôpital Jean Verdier, France	GE IGS 540	20X6-6 General Purpose RadCal – 6 cc	Clinical	60	100	2.45	-	205	5%
				70	100	3.09	-	268	
				80	100	3.42	-	366	
							0.1	198	
							0.2	136	
							0.3	99	
					10		-	36	
					50		-	185	
					200		-	733	
					400		-	1476	
				90	100	3.83	-	468	
				100	100	4.20	-	585	
				110	100	4.51	-	711	
							0.1	463	
							0.2	343	
							0.3	278	
					10		-	79	
					50		-	361	
					200		-	1393	
					400		-	2782	
				120	100	4.82	-	845	

3.2.4.2 Film response in clinical conditions

Figure 3.11. plots the variation of film response as a function of dose for the two clinical beams of medium (75 kV, AVL4 mm Al) and high (120 kV, 6 mm Al) energy used at AOUD. Considering the identical trend in pixel value *vs.* dose, it is possible to conclude that the observed difference on film darkening is due to variability in film response and is not determined by dose delivery and scanner-related uncertainties. In this case, a maximum 9% difference on film reading was observed for the same dose delivered by a medium or a high energy clinical beam. For the dose range examined in this study, film response appears to be dose independent as shown in Figure 3.11. Similar findings were observed for films irradiated to 0.3 Gy at HJV with tube voltage or additional copper filtration covering the entire possible clinical range. Figure 3.12. clearly shows a higher variability of film response as a function of radiation quality for white side film exposures when compared to yellow side irradiations. From this result, and considering the clinical beams regularly used on current x-ray systems (60–120 kV, HVL 2.46–7.75 mm Al), it can be concluded that film response variation with radiation quality is limited to within 6–8 %. Yellow side film exposure positively contributes in reducing this uncertainty. In agreement with this study's findings, McCabe *et al.* (2011) showed film darkening differences between UW80-M and UW120M within 10 % for yellow and 15 % for the white side with exposure to 0.5 Gy. However, in this work, the radiation quality effect is found to be dose independent while McCabe *et al.* (2011) observed different film behavior depending on the dose, with the highest errors on the lowest doses. The different findings may be due to scanner-related uncertainties (non-uniformity, stability, warm-up, readout, etc.).

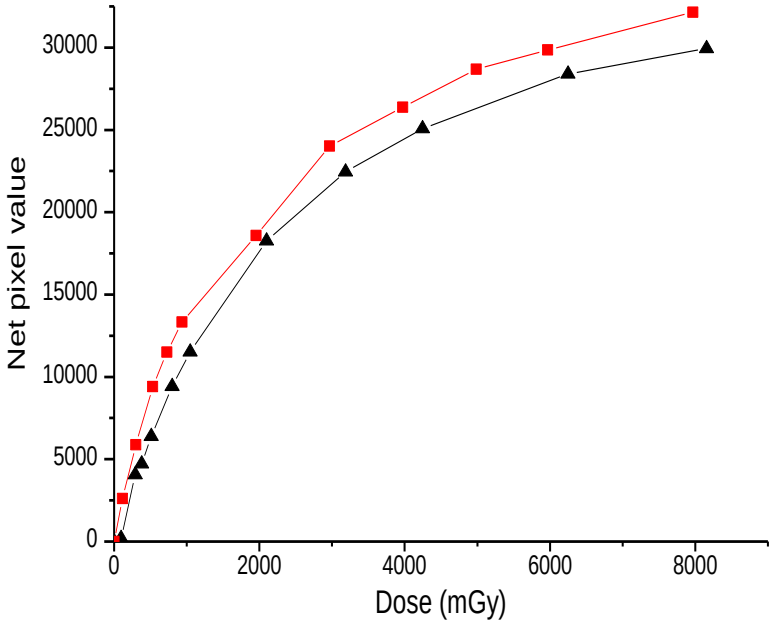

Figure 3.11. Comparison of the two calibration curves acquired with clinical beams of medium (red) and high (black) energy (adopted from Farah *et al.* 2015a).

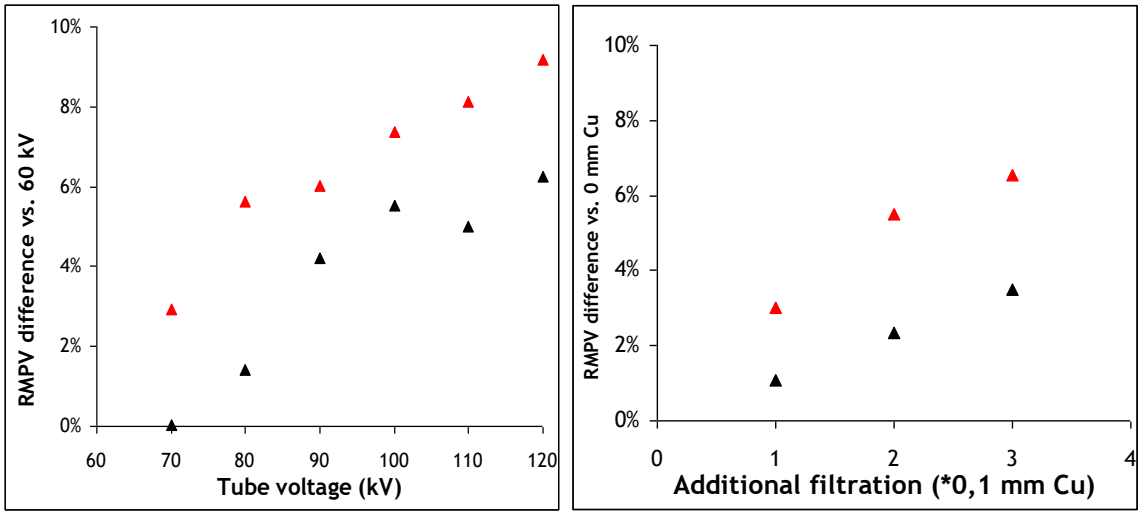

Figure 3.12. Variation of XR-RV3 films' response (in terms of Reflectance) as a function of tube voltage (left) and additional filtration (right) for clinical beams and both yellow (black) and white side film irradiations (red) (adopted from Farah *et al.* 2015).

3.2.5 Gafchromic film uncertainties

3.2.5.1 Scanner-related uncertainty

Scanner uniformity and stability

Scan uniformity was checked while using a neutral sheet of pure white (80 gmm^{-2}) matte paper covering the entire scan bed. The advantage of using a white paper with a stable behavior over time and no potential effect of temperature or repetitive UV light has been discussed elsewhere (Alnawaf *et al.* 2012). Additionally, and for the HP Scanjet G3110, the analysis was completed using a 10 x 10 cm^2 black piece of paper to investigate the impact of film darkness, i.e. variation in the signal to noise ratio, on scanner performance and uniformity. Indeed, larger variations of scan uniformity in the direction perpendicular to the lamp motion axis have been highlighted when darker films were used (Paelinck *et al.* 2007). Scan uniformity was hence checked using 2.8 x 2.8 cm^2 regions of interest (ROI) successively migrated on the entire scanner bed following the literature approach (McCabe *et al.* 2011). Comparison focused on MPV values registered at the central area of the scanner bed against peripheral areas in both parallel and perpendicular directions to the lamp motion axis. The ratio between coefficient of variation (COV = standard deviation /Mean Pixel Value) central/peripheral was hence calculated to evaluate the uniformity of the scanner bed.

The short and long term stability of the scanner were checked using the same method as for the uniformity test and considering both a white and a black piece of paper. For short term stability, scanning of the white/black piece of paper in the reflective mode was performed for 10 consecutive times. The short term stability of the scanner was calculated as the standard deviation (SD), on the 10 readings, of the average pixel value in each ROI. Similarly, long term stability was calculated as the SD of the ROI pixel value for 10 readings performed once a week for a period of 10 weeks.

Table 3.9. presents the scan uniformity and stability results, based on MPV analysis and the white piece of paper, for six scanner models showing that all of them have satisfactory performance for film dosimetry application. Using the black piece of paper and the HP Scanjet 7650 model, VINCA showed a scanner uniformity loss in both directions with respect to scanner lamp motion axis where

the uniformity coefficient was of 1.8 % in the parallel direction and 1.7 % in the perpendicular direction. In general, uniformity correction matrices could be needed as the uniformity on pixel value, in the central area and at the edges of the scanners was within 2 %; these can be developed following the literature approach (McCabe *et al.* 2011). Table 3.9. also indicates that the non-uniformity in the perpendicular direction (with respect to lamp axis) is higher than that in the parallel direction; this result was also highlighted in the literature (McCabe *et al.* 2011, Paelinck *et al.* 2007). The major contribution to scanner-related uncertainties comes from the long term stability of the scanner.

When compared to literature data, uncertainties for the EPSON Pro 1680 Expression scanner found here are lower than the 8 % overall scanner-related uncertainty of Paelinck *et al.* (2007) who highlighted the lamp warm-up as a major contributor to this uncertainty. Paelinck *et al.* (2007) Alnawaf *et al.* (2012) indicated similar uniformity values in the parallel and perpendicular direction in reflection mode for the V700 and the 10000XL models. These findings are generally larger than the overall 0.9 % (k=2) scanner-related uncertainty determined by McCabe *et al.* (2011) for the Epson 10000XL scanner. Based on this result, it is recommended to regularly check scanner performance and to correct for any scan area uniformity loss, using uniformity correction matrices, and for the long term stability drift by normalizing the readings to the scanner-specific daily reference reading of a non-irradiated film (considered as background).

Table 3.9. Scanner performance test results for the used desktop scanner models and the white piece of paper (adopted from Farah *et al.* 2015).

Institution	*Scanner model*	*Non-uniformity*		*Stability*	
		Parallel to scan direction	*Perpendicular to scan direction*	*Short term*	*Long term*
AOUD	Epson Expression 1680 Pro	2%	2%	0.5%	3%
	Epson Perfection V750 Pro	1%	1.2%	0.3%	2.7%
FBF	Epson Expression 10000XL	0.3%	0.3%	0.7%	3%
IRSN	Epson Perfection V700 Photo	0.7%	1%	0.1%	2.2%
STUK	Epson Expression 1600 Pro	1%	1.5%	0.8%	1.5%
VINCA	HP Scanjet 7650	0.4%	0.3%	0.1%	3.6%

Scanner-to-scanner variability

Finally, although a common reading protocol was defined and used by all participants to harmonize film dosimetry, several parameters such as scanner model, post-processing software and local analysis procedures may have an impact on film readings. Thus, to compare local practice and determine uncertainty on film dosimetry related to the scanner model and the readout process, films from each participating centre were read a second time by a unique operator (AOUD). Local readings were then compared against the ones made by AOUD to determine the readout variability (software and warm-up effects) from one center to another which enables better understanding of subsequent results.

Figure 3.13. compares IRSN readings of 10 film pieces, irradiated at NRPI to different dose levels (0.1–5 Gy) using the RQR5 beam quality, with the Epson Perfection V700 model against those done at AOUD with the Epson Expression 1680 Pro or with the Epson Perfection V750 Pro. The figure shows up to 17% difference on the MPV due to the scanner model itself. This could be reasonably explained by the difference in the UV wavelength of each scanner, by the different warm-up methodology as well as by the different analyzing software used. Indeed, in this particular exercise the warm-up of the scanner was not integrated into the common reading protocol and could be responsible for reading drifts of up to 4 % for the EPSON Expression 1680 Pro (Paelinck *et al.* 2007) and 3 % for the Epson Perfection V700 (Huet *et al.* 2012). However, when the reading is normalized to the scanner-specific background, using the reading of a non-exposed film (Reflectance = $\log(MPV_{unexposed}/MPV_{exposed})$, the difference on the readings of the three scanners decreases to within 5%. Additionally, scanner-to-scanner reading variability was found to show no dependence on film dose. Based on this result, it is made clear that two scanner models could only be compared if the readings are normalized to the scanner-specific background. The scanner readout uncertainty, including warm-up and software-induced errors, was hence estimated to be within 5 % at the considered dose range (0.1–5 Gy) representative of interventional radiology procedures.

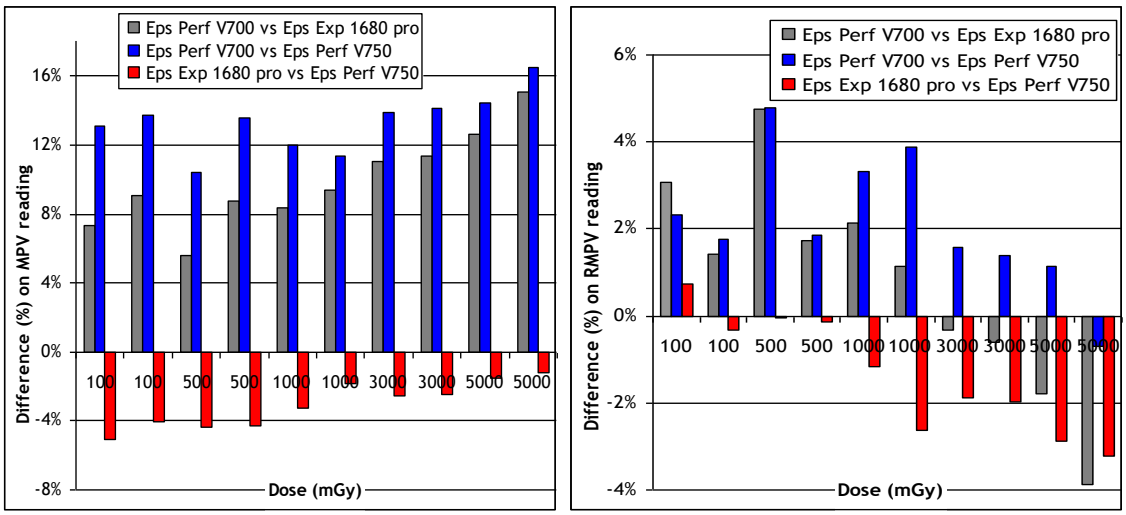

Figure 3.13. Comparison of the Epson Perfection V700, Epson Expression 1680 Pro and Epson Perfection V750 Pro scanners in terms of variation in MPV (left) and background-normalized Reflectance (right) (adopted from Farah *et al.* 2015).

3.2.5.2 Film-related uncertainty

To fully investigate the performance of XR-RV3 films in standard laboratory and clinical conditions, film pieces of different batches where irradiated with setups covering the entire dose range and beam qualities encountered in interventional radiology. The study included film-to-film uniformity, film darkening over time, dose rate dependence and radiation quality effect. In all subsequent analysis, all films pieces (3 x 3 cm^2) were read while set in the central area of each scanner to reduce non-uniformity uncertainties and avoid problems associated to edge areas.

Film-to-film uniformity

Film uniformity in one batch was studied in the PSDLs at ENEA-INMRI and VINCA and in clinical conditions using clinical x-ray tubes and beam qualities representative of fluoroscopy procedures at AOUD and HJV. At ENEA-INMRI, 6 film pieces of the same batch were irradiated using the RQR6 beam, to 0.5 Gy and 4Gy. Meanwhile, at VINCA, film pieces of a single batch were irradiated to an air kerma of 0.5, 1, 1.5, 2 and 2.5 Gy using an RQR8 beam quality (IEC 2005). At AOUD, film uniformity in one batch was studied on different pieces of films coming from the same batch irradiated to 1 Gy with a medium energy clinical beam (75 kV, HVL 4 mm Al). Similarly, at HJV, uniformity was studied for film pieces of a same batch irradiated to 0.3 Gy using a low energy clinical beam (60 kV; HVL 2.45 mm Al) and using both white and yellow side film exposure; i.e. film side facing the X-ray tube. For all film pieces and centers, single film uniformity also known as intra-sheet uniformity, was calculated using the COV value. Meanwhile, the batch-to-batch variability, i.e. inter-sheet uniformity, was determined by comparing the response of XR-RV3 film pieces of 3 different batches. These were positioned one next to the other without overlapping and simultaneously irradiated at NRPI (National Radiation Protection Institute, Czech Republic) to a dose ranging from 0.1 to 5 Gy using an RQR5 beam.

The COV was used to determine the film-to-film uniformity in one batch. Film pieces from all centers were found to have an intra-sheet uniformity within 0.5 %; better than literature findings for other film types (Richley *et al.* 2010). This can be explained by the small fragment sizes (3 x 3 cm^2), good irradiation uniformity (film pieces aligned with the center of the beams) and low scanner uncertainties (readings in the central region of the scanner). Films irradiated at ENEA-INMRI to 0.5 Gy and 4 Gy with an RQR6 beam showed a film-to-film uniformity value within 0.5 % and 0.7 %, respectively. The test at VINCA with an RQR8 beam showed a film-to-film uniformity of 1.4 %, 1.6 %, 1.3 %, 1.6 % and 1.6 % for dose level of 0.5, 1.0, 1.5, 2.0 and 2.5 Gy, respectively. Meanwhile, at AOUD, films irradiated to 1 Gy with a medium energy clinical beam (75 kV, HVL = 4 mm Al) showed a good uniformity, with a COV of 0.5%. Similarly, film uniformity was within 0.5% for both yellow and white side irradiations to 0.3 Gy at HJV and a low energy clinical beam (60 kV, HVL = 2.45 mm Al). The short term stability of the scanner, its non-uniformity as well as warm-up effects also contributes to the film uniformity figures given above which could explain the larger uncertainty value found at VINCA. Nonetheless, this result on multiple batches in both laboratory and clinical settings shows that XR-RV3 film-to-film uniformity is satisfactory and dose-independent. These findings are lower than the 2.5% (k=1) film uniformity uncertainty determined by McCabe *et al.* (2011) and confirm manufacturer's indications on film uniformity in one batch (<5%). Meanwhile, the batch-to-batch variation of XR-RV3 film was found to be within 7 % for non irradiated films and within 24 % for films irradiated at ENEA-INMRI to a dose of 4 Gy using the RQR6 beam quality. In the latter case, the readout difference is lower when comparing reflectance (within 7 %) further highlighting the need for background normalization. Nonetheless, these values are high, indicating that each new batch must be calibrated separately.

Film darkening over time and effect of scan light on early readings

Films irradiated at IRSN and VINCA to a dose of 0.5 Gy and 1 Gy using N-60 and RQR8 beams, respectively, were read between 1 hour and 7 days post exposure (ISO 1996, IEC 2005). Additional irradiations to a dose of 0.1, 0.5, 2, 4 and 8 Gy, using an RQR6 beam (IEC 2005), were carried out at ENEA-INMRI while using both white and yellow side exposures. Finally at VINCA, in addition to investigating the pixel growth, the effect of repetitive readings, i.e. exposure to U.V. scanner light, on pixel value was studied during the early stages of the polymerization process. Similarly, in clinical

conditions (75 kV, HVL = 4.3 mm Al), irradiations to different doses (0.5 Gy to 10.5 Gy) were conducted at AOUD with the same reading intervals (1, 2, 4, 24, 48 hours and 7 days).

Films from different batches were found to continue to darken with time after exposure, but generally stabilizing 24 hours post-irradiation for both laboratory and clinical beam qualities. The largest difference on reflectance between the 1 h post-irradiation reading and the 24 h reading was within 3%. In addition, film darkening analysis at FBF showed no dependence on the dose level (0–10 Gy) or on exposure side (yellow or white). Finally, analysis at VINCA showed little effect (<1.5 %) of repetitive reading, i.e. UV light, even during the early stages of the polymerization process. This null effect of scanner UV light on films was also observed for 10 successive readings of un-irradiated films at IRSN (reading value within 0.3 % - Epson Perfection V700 Photo) and VINCA (0.9 % - HP Scanjet 7650). These results are in agreement with McCabe *et al*/who noticed that the signal changes most dramatically for the first 8 hours and less noticeably thereafter. Considering the uniformity, short and long term stability specific for each scanner, it is possible to conclude that the 24 hours reading interval recommended by the manufacturer is appropriate for XR-RV3 films. The 48 h waiting period used in the common reading protocol is thus satisfactory to guarantee a stable polymerization process.

Dose rate dependence

At NRPI, 10 pieces of films, of five different batches, were irradiated free in air to 0.5 Gy with an RQR5 beam (IEC 2005) using different dose rates: 3.5, 10, 20, 40, 60 and 100 mGy/min. Two film pieces were used for each dose rate value. Reading of all films was done by one center (AOUD using the Epson Expression 1680 Pro scanner). The test was also done at AOUD using 3 clinical beams: fluoroscopy (75 kV, 96 mA, 0.9 mm Cu, 7.5 p/s), cineangiography (70 kV, 390 mA, 0.1 mm Al, 7.5 fr/s) and Digital Subtraction Angiography (70kV, 169 mA, 3.4 mm Al, 2 fr/s) and different dose rates delivered by Siemens Axiom Artis system: respectively 1.9 mGy/min, 340 mGy/min and 1080 mGy/min. In this case, films were irradiated free-in-air to a dose of 1 Gy and came from two different batches. Similar irradiations were carried out at HJV with 80 kV and HVL of 3.45 mm Al while manually setting the tube current at 10, 50, 100, 200 and 400 mA. In this case, 3 x 3 cm^2 film pieces of a single batch were simultaneously irradiated (placed next to each other) to a dose of 0.3 Gy considering white and yellow side film exposures.

Figure 3.14. presents the results of the dose rate dependence of film response studied in SSDL conditions at NRPI (dose of 0.5 Gy). When compared against irradiations with the lowest dose rate of 3.5 $mGymin^{-1}$, the figure indicates that XR-RV3 films have a response variability within 4.2% for laboratory dose rates of up to 100 $mGymin^{-1}$. This result was also confirmed for films characterized in clinical conditions at AOUD (dose of 1 Gy) where film darkening did not differ by more than 4.9% with dose rates ranging from 1.9 mGy min^{-1} to 1080 $mGymin^{-1}$ (at 0.5 m). Similarly, at HJV and in clinical conditions (dose of 0.3 Gy), the dependence also remains within 4% at dose rates ranging from 30 mGy min^{-1} to 165 $mGymin^{-1}$ (i.e. with 10 mA to 400 mA) at both 80 kV and 110 kV and yellow side exposures. Higher values were observed for white side film exposures with up to 10 % difference on film reading. This null effect of dose rate and pulse rate on film darkening may be reasonably explained by the slow polymerization process of GafChromic films. McCabe *et al.* (2011) reported that the XR-RV3 manufacturer indicates a dose rate dependence <3 % between 0.03 Gy min^{-1} and 3 $Gymin^{-1}$, in agreement with this study's findings. As a conclusion, and although the dose rate is very different in laboratory and in clinical conditions, this parameter is shown to have a small impact on the response of XR-RV3 films and to be independent from the dose delivered to the films.

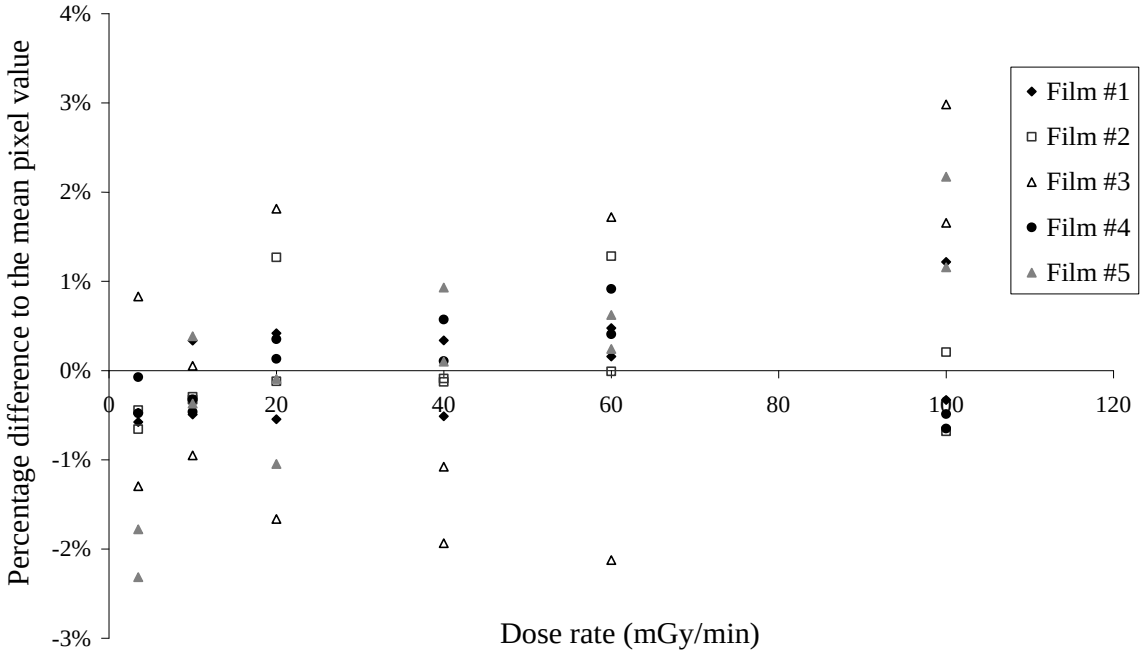

Figure 3.14. Percentage difference on background-normalized Reflectance recorded at different dose rate in standard laboratory conditions using an RQR5 beam (adopted from Farah *et al.* 2015a).

3.2.5.3 Fitting-related uncertainties

Fitting equation and algorithm

Different functions have been used in the literature to model the response of XR Type R Gafchromic films as a function of film exposure. These include exponential functions, polynomials or ratio of polynomials (Quai *et al*. 2002, Thomas *et al*. 2005, Rampado *et al*. 2006) and more simplistic equations with dose inversely proportional to pixel value (Lewis *et al*. 2012).In addition, the quality of a fit may also be affected by the fitting routine as different software and fitting algorithms can be used to determine the fit parameters. Excel Solver (Frontline Systems, Inc.) was first considered being a very common and widely available fitting tool. In this case, the linear Least Squares method (LS) was used to minimize the square of the error between the original data and the values predicted by the equation (Bjork 1996). Statistically more robust nonlinear iterative data fitting based on the Levenberg-Marquardt algorithm, was also tested using Matlab (Mathworks, Natick, MA). Finally, polynomial fitting based on reflectance was considered to limit the impact of readout process on fitting uncertainties (Devic *et al*. 2004, Devic *et al*. 2005) . Similarly, the quality of a linear fit plotting dose as a function of MPV, net(MPV), Reflectance and $MPV_{unexposed}/MPV_{exposed}$ was tested as a simple and easy to use equation.

Table 3.10. Tested fit functions for the calibration of XR-RV3 gafchromic films (adopted from Farah *et al.* 2015a).

Fit Type	*Used by*	*Original film type*	*Number of parameters*
$D = a\, e^{(-netPV/b + c)}$ where $netPV = (PV_{bkg} - PV)$	Quai et al (2002)	XR-RV1	3
$D = a\,(e^{net\Delta PV/k - 1} - 1)$ $net\Delta PV = k*PV_{unexp}/PV_{exp}$ (K = 28 000)	Rampadao et al (2006)	XR-RV1	1
D = a netPV^3 + b netPV^2 + c netPV + d where $netPV = (PV_{bkg} - PV)$	Thomas et al (2005)	XR-RV1	4
D = a*netPV /(b-netPV) where $netPV = (PV_{bkg} - PV)$	Blair and Meyer (2009)	XR-RV2	2
D = (a + PV)/(b + c*PV) + d*PV	Labattu et al. (2013)	XR-RV3	4
D = a + b/(c + PV)	Lewis et al (2012)	EBT-3	3

Among the multiple fit functions tested in this study, exponential equations (Quai *et al*. 2002), were found to be inappropriate for XR-RV3 film calibrations. Errors on the high dose values generally exceeding 40% were obtained with these functions since the film response with dose does not show exponential behavior and since the number of fit coefficients involved in both equations is insufficient (limited to 2). The other four equations introduced in the literature (Blair and Meyer 2009, Thomas *et al*. 2005, Lewis *et al*. 2012, Labattu *et al*. 2013) reproduce fairly accurately film darkening as a function of dose (Table 3.11.). However, results clearly indicate that no optimal fit function exists while fitting-related uncertainties are shown to be a major contributor to the overall XR-RV3 film dosimetry uncertainty. One should also note in Table 3.11., larger dose errors at the 2 Gy dose level; this is due to a reading outlier. In addition, fitting algorithm showed little effect on the overall fit quality as LS and Levenburg-Marquardt algorithms were found to have similar results. As such, the widely available Excel Solver tool with the least square method can be considered as a reliable and easy to use method for XR-RV3 films calibration and fitting. Finally, the two other fitting equations tested in this work showed the best performance. Indeed, polynomial fitting based on Reflectance involve errors limited to ±11 % at the entire low and high dose range (Table 3.11.). Similarly, the linear fit plotting dose *vs.* $MPV_{unexposed}/MPV_{exposed}$ involved errors limited to within 10 % at the 1-8 Gy dose range with slightly worse results at the 0-1 Gy range compared against the polynomial fitting based on Reflectance. Meanwhile, linear fitting based on MPV, net(MPV) or Reflectance did not perform well with errors >20 % at the 1-8 Gy level.

Table 3.11. Performance of the tested fitting functions considering data of the medium energy clinical beam (AOUD) and using all calibration points (11 points, entire dose range 0-8 Gy) (adopted from Farah *et al.* 2015a).

Theoretical dose (mGy)	*Tomas et al. (2005)*		*Blair and Meyer (2009)*		*Lewis et al.(2012)*		*Labattu et al. (2013)*		*Polynomial Reflectance*		*Linear ($MPV_{unexposed}/MPV_{exposed}$)*	
	Dose (mGy)	*Diff. (%)*	*Dose (mGy)*	*Diff. (%)*	*Dose (mGy)*	*Diff. (%)*	*Dose (mGy)*	*Diff. (%)*	*Dose (mGy)*	*Diff. (%)*	*Dose (mGy)*	*Diff. (%)*
7970	7711	-3	8010	1	7990	0	8076	1	7965	0	7933	0
5971	6027	1	5849	-2	5864	-2	5746	-4	5890	-1	5874	-2
4984	5290	6	5070	2	5089	2	4980	0	5114	3	5113	3
3976	4048	2	3906	-2	3924	-1	3884	-2	3932	-1	3959	0
2967	3047	3	3054	3	3064	3	3099	4	3055	3	3099	4
1955	1555	-20	1779	-9	1768	-10	1899	-3	1741	-11	1789	-9
936	881	-6	1032	10	1002	7	1125	20	983	5	1007	8
726	749	3	834	15	800	10	903	24	785	8	799	10
531	630	19	636	20	595	12	666	25	588	11	589	11
299	439	47	357	19	307	3	307	3	312	4	292	-2
116	187	61	145	25	89	-23	8	-93	105	-10	67	-42

Impact of fitting parameters

To choose the best fit equation, it is necessary to study the behavior and performance of each equation with fitting parameters. The optimal number of calibration points was studied since, for practical reasons including restricted access to interventional x-ray system, a limited number of acquisitions is usually considered. Thus, and for each equation, the number of calibration points was gradually increased (6, 8 and 11 points) while studying the impact on fit quality. These points were all sampled in the 1–8 Gy range using the interventional radiation quality. In addition, since patient skin doses in fluoroscopy-guided interventional procedures may vary from few mGy up to several Gy, the dose distribution and sampling of calibration points can be critical. Therefore, the impact on fit quality of calibration points with a restricted upper dose limit (of 4, 6 or 8 Gy) was studied. Finally, the precision of film readings (MPV) as well as that of fit coefficients may also influence the quality of the fit depending on the considered equation. The performance of polynomial fitting based on reflectance with the number and dose range of calibration points was also checked.

Figure 3.15. and Tables 3.12. present a summary of fitting related uncertainties and provide the deviation, with respect to the delivered dose, of fitting estimates for film pieces irradiated to a dose in the 1–8 Gy range. The work was exclusively focused on the high dose range where tissue reactions (deterministic effects) may occur to the skin. Figure 3.15. shows that the four fitting equations fail to fully and adequately reproduce films response at the 1–8 Gy dose range when a limited number (6 points only; namely at 0.3, 0.5, 1, 3 and 5 Gy) of experimental data points is considered. The highest dependence on the number of calibration points was observed for polynomial functions where the error on the 8 Gy value was of -17 % for the fit by Thomas *et al.* (2009) and +55 % for the one by Labattu *et al.* (2013). With 8 or more calibration points, fit quality becomes fairly satisfactory as the largest error on the 1–8 Gy range (except the 2 Gy point) was < 7 % for all four equations (Blair and Meyer 2009, Thomas *et al*. 2005, Lewis *et al*. 2012, Labattu *et al*. 2013). The precision of non-integral fit coefficients is of relevance only for polynomial functions (Blair and Meyer 2009, Labattu *et al*. 2013) and becomes fully satisfactory for the >1 Gy dose records starting from 2 digits (error <10 %). In addition, literature reports on skin burns and injuries clearly indicate high interventional doses ranging up to several tens of grays in accidental situations. For an optimal monitoring in routine conditions, it is therefore necessary to carry out film calibrations to, at least, a dose of 8 Gy. The impact of the number of calibration points is also large at the low dose range (i.e. < 1 Gy) where an error of up to 80% was registered with the fit by Thomas *et al.* (2005) (at 0.1 Gy and 8 calibration points), 20 % for the equation introduced by Blair and Meyer (2009) (at 0.3 Gy and 6 calibration points), 19 % for the fit by Lewis *et al.* (2012) (at 0.1 Gy and 6 calibration points) and 57 % for the function used by Labattu *et al.* (2013) (at 0.1 Gy and 6 calibration points). Moreover, while extrapolation of high doses is strongly proscribed, Table 3.11. shows that film calibration to a limited dose range (4 or 6 Gy for example) can induce up to a factor 2 over/under estimates of skin dose. The equation by Lewis *et al.* (2012) provides the best fitting that reproduces the response of the XR-RV3 films at the highest dose levels when a limited calibration range is used. In general, the sampling of calibration points should be equally distributed in the whole range of concern (0–8 Gy). Moreover, one should never use a polynomial equation with higher degree than absolutely necessary; in this case third order polynomials as used by Thomas *et al.* (2005) were found appropriate. Finally, it should be noted that using a calibration curve determined only from calibration points >1 Gy would limit the errors on the high dose range (1–8 Gy) to within -11 % for all fit functions but would result in errors by up to a factor 2 on the low dose estimates; the effect is highest for polynomial fits (Blair and Meyer2009, Labattu *et al*. 2013). In addition, the quality of the fit may strongly be affected by

reading outliers and uncertainties in the data to be fitted with again the highest sensitivity for polynomial functions. Finally, as shown in Figure 3.15. and Tables 3.12, polynomial fitting based on Reflectance involve lower variability with fit parameters when compared against polynomial functions based on mean pixel values (Blair and Meyer 2009, Labattu *et al.* 2013).

Table 3.12. Impact of the dose range of calibration points on the precision of tested fitting functions. Values given here represent the maximum difference on dose at the 1–8 Gy range where deterministic effects to the skin can occur (adopted from Farah *et al.* 2015a).

Dose range of calibration points	*Theoretical dose (mGy)*	*Tomas et al (2005)*		*Blair and Meyer (2009)*		*Lewis et al. (2012)*		*Labattu et al. (2013)*		*Polynomial Reflectance*	
		Dose (mGy)	*Diff. (%)*	*Dose (mGy)*	*Diff. (%)*	*Dose (mGy)*	*Diff. (%)*	*Dose (mGy)*	*Diff. (%)*	*Dose (mGy)*	*Diff. (%)*
0–4 Gy	7970	6222	-22	8732	10	8235	3	16750	110	6879	-14
	5971	5199	-13	6132	3	5966	0	7354	23	5477	-8
	4984	4728	-5	5242	5	5153	3	5740	15	4889	-2
	3976	3885	-2	3959	0	3946	-1	3983	0	3912	-2
	2967	3142	6	3051	3	3067	3	2991	1	3115	5
	1955	1816	-7	1740	-11	1759	-10	1738	-11	1793	-8
	936	968	3	996	6	996	6	1033	10	977	4
0–6 Gy	7970	7172	-10	8233	3	8235	3	9363	17	7923	-1
	5971	5761	-4	5917	-1	5966	0	5983	0	5879	-2
	4984	5132	3	5100	2	5153	3	5044	1	5111	3
	3976	4048	2	3896	-2	3946	-1	3811	-4	3937	-1
	2967	3143	6	3028	2	3067	3	2994	1	3061	3
	1955	1689	-14	1748	-11	1759	-10	1819	-7	1743	-11
	936	915	-2	1008	8	996	6	1090	16	981	5

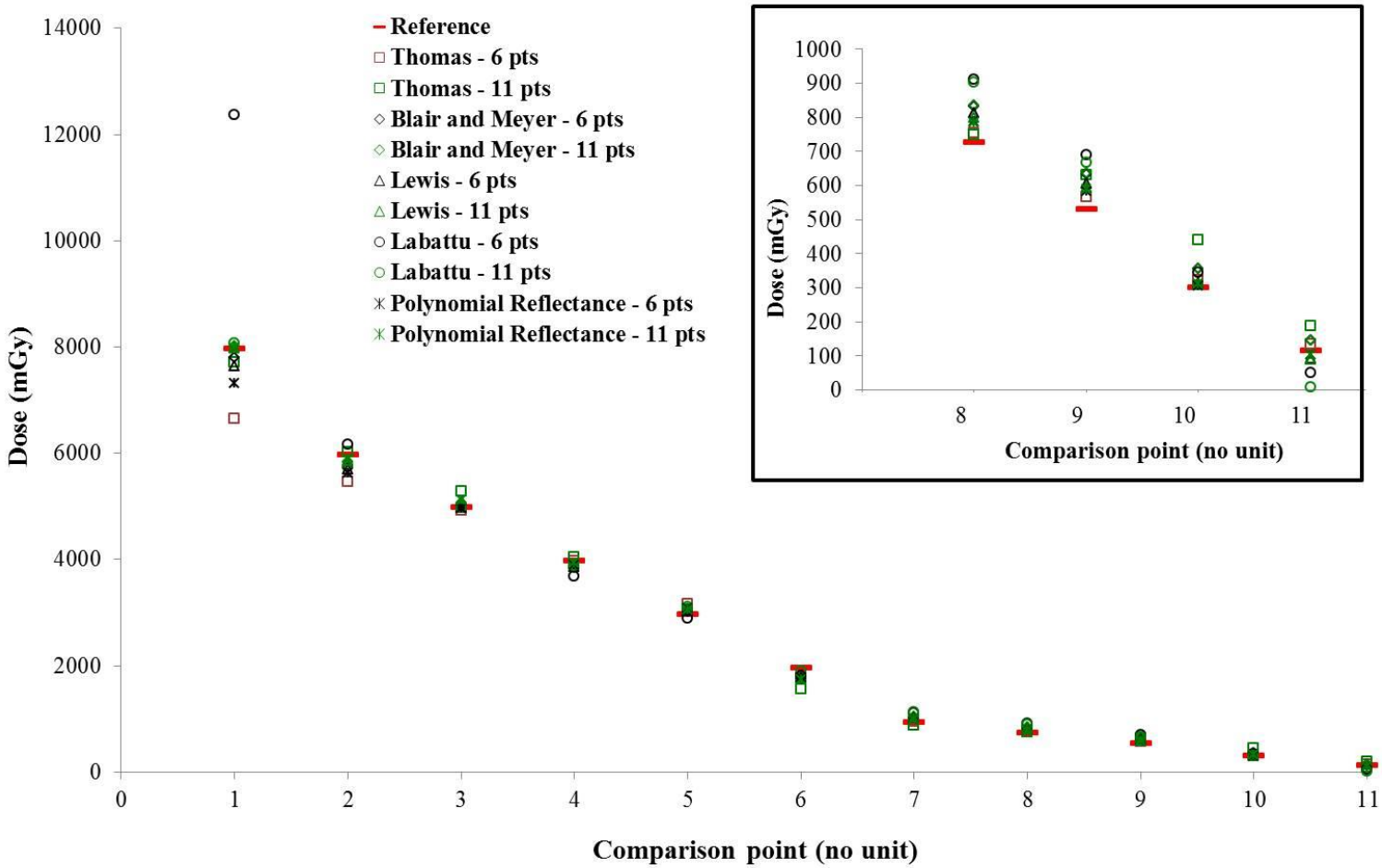

Figure 3.15. Impact of the number of calibration points (6 points – black symbols, 11 points – green symbols) on the performance of fitting equations introduced by Tomas *et al.* (2005)(rectangles), Blair and Meyer (2009) (diamonds), Lewis *et al.* (2012) (triangles), Labattu *et al.* (2013) (circles) and the polynomial fit based on Reflectance (star). Imbedded figure zooms on the low dose range (100 – 700 mGy) (adopted from Farah *et al.* 2015a).

Overall measurement uncertainties

Contrary to the strict dosimetric requirements in radiotherapy, dose assessment in diagnostic and interventional radiology is subject to considerable uncertainty. Since examinations in imaging usually involve a limited irradiation of the body, measurements accuracy of 20 % is generally required to estimate the absolute risk while higher accuracy, within 7 %, is required for cases where tissue reactions are expected (AAPM 1991). In practice, and as shown in this study, uncertainty associated with film dosimetry strongly depends on the attention given to the different influencing parameters including scanner, film and fitting-related errors. To determine the overall uncertainty associated with the use of XR-RV3 Gafchromic films to assess skin dose in interventional radiology, three different scenarios are presented in Table 3.12. for uncertainty budget calculation according to the Guide to the expression of Uncertainty in Measurements (ISO 2008).

The first scenario (Scenario A) is related to the tightly controlled measurement conditions, adequate laboratory calibrations and well defined readout protocol. In this case, avoidable yet commonly occurring errors and sources of uncertainties are minimized through the use of scanner uniformity correction matrices, long term stability correction with daily background readings, accurate polynomial fitting based on Reflectance with enough calibration points at the high dose range, etc. Scenario B also describes the case where a well-defined laboratory calibration is performed while other influencing parameters related to clinical application of dosimetry films are less controlled. In this case, the average uncertainty values obtained throughout the study (or from the literature) were considered. Finally, Scenario C describes the worst case scenario where the conditions of exposure, film handling and readout are weakly controlled and where corrections for the relevant influence quantities are not made.

As such, Table 3.13. sets the lowest possible relative combined standard deviation at about 5 % (k=1) that could only be reached if all sources of uncertainties are carefully controlled. In addition, the table clearly shows the maximum range which scanner, film and fitting uncertainties could reach (i.e. overall uncertainty of up to 39 % at k=1). Based on this multi-site approach and on the observed differences on scanner, film and fitting-related uncertainties, the authors estimate a realistic standard uncertainty of 20 % (k=1) associated with a proper use of such films to assess skin dose in the interventional environment.

Table 3.13. Summary of skin dose assessment uncertainty using XR-RV3 Gafchromic films (adopted from Farah *et al.* 2015a).

Influence quantity/parameter	*Scenario A (%)*	*Scenario B (%)*	*Scenario C (%)*	*Values taken from*
Dose delivery uncertainty				
Air kerma rate measurements	0.8	2.6	5	*Calibration certificate – QA*
Setup error and film positioning	0.1	0.5	1	*McCabe et al (2011)*
Beam uniformity	0.3	2	5	*(IAEA 2007)*
Backscatter radiation	-	5	10	*AAPM TG-61 (Ma et al. 2001)*
Scanner-related uncertainties				
Scan uniformity	0.3	0.7	2	*McCabe et al (2011)*
Short term stability	0.1	0.7	2.5	*Table 3.10.*
Long term stability	1.5	2.2	3.6	*Table 3.10.*
Scanner readout, warm-up and software effects	-	2.5	5	*Figure 3.10; Alnawaf et al. 2012; Huet et al. 2012*
Uncertainties related to a film				
Inter/intra batch uniformity	1	4	7	*Section 3.2.1.*
Darkening over time	0.5	1.5	3	*Section 3.2.2.*
Effect of scan light	0	1	1.4	*Section 3.2.2.*
Dose rate dependence	1	3	5	*Figure 3.14.*
Radiation quality dependence	2	10	15	Figures 3.11-3.12.
Film orientation	0	6	10	*Figures* 3.11-3.12*; Butson et al 2006*
Humidity and temperature during transportation and storage	0	2	5	*AAPM TG-55 (Niroomand-Rad et al. 1998)*
Uncertainties related to calibration				
Fitting equation	2	6	10	*Table 3.12.*
Dose range of calibration points	2	10	22	*Figure 3.15*
Number and distribution of data points	2	8	17	*Table 3.12.*
Reading outliers and precision of fit parameters	3	10	20	*Table 3.12.*
Relative combined standard uncertainty (k=1)	5	20	39	
Relative expanded uncertainty (k=2)	9	41	78	

3.2.6 Conclusion

In this work, a comprehensive characterization of XR-RV3 GafChromic films was carried out in standard laboratory conditions and in clinical conditions. The study included scanner-, film- and fitting-related uncertainties in order to determine the overall skin dose assessment uncertainty associated with the use of such films in the interventional environment. The key input of this multi-

site study includes characterization of films from different batches using continuous and low dose rate SDL beams as well as pulsed and high dose rate clinical beams of various qualities.

Firstly, scanner-related uncertainty analysis showed that multiple scanner models and types can be used for such dosimetry applications. However, the performance of the scanner may vary from one model to another and scan uniformity and long term stability need to be checked prior to film readings. Scanner readings were found to be mostly affected by the long term stability of the scanner with up to a 3.6 % difference between two weekly readings. To compare scanner-to-scanner readings, background normalization was shown to be mandatory. The overall scanner-related uncertainty was found to range from 2 % to 7 % at one standard deviation.

Secondly, the work showed that XR-RV3 films have good uniformity within one batch (up to 1.6 %), continue to darken with time after exposure for up to 24 hours and have a dependence on dose rate of 4.5 %. Radiation quality and film orientation were highlighted as the main sources of film-related uncertainties with up to 15 % and 10 % impact on film darkening, respectively. As such, it is mandatory to choose an appropriate calibration beam energy depending on the performance and capacities of the x-ray system used clinically prior to conducting patient skin dose measurements. If the changes in beam energy are very broad for a given procedure, and to reduce the quality effect, one could consider establishing the calibration curve at 80 kV and 4 mm Al HVL since it represents, on average, the radiation quality that could be clinically obtained (60 to 120 kV and HVL 2.45 to 7.75 mm Al). It is also recommended that films are not used with their white side facing the tube since it was found that such an exposure configuration results in a higher dependence on radiation quality. In addition, this configuration does not provide access to real time visual and qualitative information on skin exposure. The overall film-related uncertainty was estimated to range from 6% to 19 % (k=1).

Thirdly, different equations available in the literature were tested as part of the fitting-related uncertainties. The optimal function involves a balance between good fit quality and limited variability with fit parameters. Namely, results have shown that exponential fits could not correctly reproduce XR-RV3 response. Meanwhile, easy to use third order polynomials provided appropriate fitting quality but suffered from having the highest dependence on fit parameters. As such, fitting uncertainties were found to be the main source of uncertainty when determining skin dose using XR-RV3 GafChromic films. Nonetheless, practical recommendations were provided to reduce such uncertainties. Eight calibration points, uniformly sampled in the 0-8 Gy range, are optimally needed to build a satisfactory calibration curve. Besides, Excel solver with the least square method is a widely available and sufficient solution to carry out accurate fitting of the data.

Finally, being a multi-site work, non-site-specific uncertainties were assessed here providing representative estimates of errors associated with the use of XR-Type R GafChromic films in clinical routine. The overall skin dose uncertainty was found to range from 12 to 62 % highlighting the need for careful processing of film dosimetry steps.

References

AAPM 1991. American Association of Physicists in Medicine, Recommendations on Performance Characteristics of Diagnostic Exposure Meters, Report of AAPM Diagnostic X-Ray Imaging Group No. 6, Med. Phys. 19, 231–241 (1991).

Alnawaf H., Yu P, Butson M., 2012. Comparison of Epson scanner quality for radiochromic film evaluation, J. Appl. Clin. Med. Phys. 13(5), 314-321.

Alva H., Mercado-Uribe H., Rodríguez-Villafuerte M., Brandan ME., 2002. The use of reflective scanner to study radiochromic film response, Phys. Med. Biol. 47, 2925–2933.

Jörck A., 1996. Numerical Methods for Least Squares Problems ISBN 978-0-89871-360-2.

Blair A., Meyer Y., 2009. Characteristics of GafChromic® XR-RV2 radiochromic film, Med. Phys. 36(7), 3050-3058.

Butson, M., Cheung T., Yu P., 2005. XR type-R radiochromic film X-ray energy response, Phys. Med. Biol. 50, N195–199.

Butson M., Cheung T., Yu P., 2006. Scanning orientation effects on Gafchromic EBT film dosimetry, Australas Phys Eng Sci Med. 29(3): 281-284.

Devic S., Seuntjens J., Hegyi G., Podgorsak EB., Soares CG., Kirov AS., Ali I., Williamson JF., Elizondo A., 2004. Dosimetric properties of improved GafChromic films for seven different digitizers, Med. Phys. 31, 2392–2401.

Devic S., Seuntjens J., Sham E., Podgorsak EB., Schmidtlein CR., Kirov AS., Soares CG., 2005. Precise radiochromic film dosimetry using a flat-bed document scanner, Med. Phys. 32, 2245–2253.

Dini SA., Koona RA., Ashburn JR., Meigoonia AS. 2005. Dosimetric evaluation of GafChromic® XR type T and XR type R films", J. Appl. Clin. Med. Phys. 6, 114–134.

Farah J., Trianni A., Ciraj-Bjelac O., Clairand I., De Angelis C., Delle Canne S., Hadid L., Huet C., Jarvinen H., Negri A., Novák L, Pinto M., Siiskonen T., Waryn MJ., Knežević Ž. 2015a Characterization of XR-RV3 GafChromicTM films in standard laboratory and clinical conditions and means to estimate uncertainties and reduce errors, Med. Phys. 42(7) 4211-26.

Farah J., Trianni A., Carinou E., Ciraj-Bjelac O., Clairand I., Dabin J., 2015b Measurement of maximum skin dose interventional radiology and cardiology and challenges in the set-up of European alert thresholds, Rad. Prot. Dos. 164 (1-2) 138–42.

Giles ER., Murphy PH., 2002. Measuring skin dose with radiochromic dosimetry film in the cardiac catheterization laboratory, Health Phys. 82(6), 875-880.

Huet C., Dagois S., Derreumaux S., Trompier F., Chenaf C., Robbes I., 2012. Characterization and optimization of EBT2 radiochromic films dosimetry system for precise measurements of output factors in small fields used in radiotherapy, Radiat. Meas. 47, 40-49.

ISO 1996. International Organization for Standardization, "X and gamma reference radiation for calibrating dosemeters and doserate meters and for determining their response as a function of photon energy - Part 1: Radiation characteristics and production methods", ISO 4037-1 (1996).

IEC 2005. International Electrotechnical Commission, "Medical diagnostic X-ray equipment - Radiation conditions for use in the determination of characteristics", IEC 61267 (2005).

ISO 2008. ISO/IEC Guide 98-3:2008 (JCGM/WG1/100) Uncertainty of measurement -- Part 3: Guide to the expression of uncertainty in measurement (GUM:1995)

Lewis D., Micke A., Yu X., Chan MF., 2012. An efficient protocol for radiochromic film dosimetry combining calibration and measurement in a single scan, Med. Phys. 39(10), 6339-6350.

Labattu M., Guersen J., Chassin V., Cassagnes L., Magnier F., Donnarieix D., Boyer L., Chabrot P., 2013. Evaluation de la dose à la peau en radiologie interventionnelle par l'utilisation de films radiochromiques, Radioprotection 48(1), 115-126.

Ma CM., Coffey CW., DeWerd LA., Liu C., Nath R., Seltzer SM., Seuntjens JP.; 2001. American Association of Physicists in Medicine., AAPM protocol for 40-300 kV x-ray beam dosimetry in radiotherapy and radiobiology, Med Phys. 28, 868-893.

Mart C., Elson HR., Lamba MA., 2012. Measurement of low-energy backscatter factors using GAFCHROMIC film and OSLDs, J. Appl. Clin. Med. Phys. 13, 3832.

McCabe BP., Speidel MA., Pike TL., Van Lysel MS., 2011. Calibration of GafChromicTM XR-RV3 radiochromic film for skin dose measurement using standardized x-ray spectra and a commercial flatbed scanner, Med. Phys. 38(4) 1919-30.

Niroomand-Rad A., Blackwell CR., Coursey BM., Gall KP., Galvin JM., McLaughlin WL., Meigooni AS., Nath R., Rodgers JE, Soares CG., 1998. Radiochromic film dosimetry: recommendations of AAPM Radiation Therapy Committee Task Group 55. American Association of Physicists in Medicine., Med Phys. 25, 2093-2115.

Paelinck L,. De Neve W., De Wagter C., 2007. Precautions and strategies in using a commercial flatbed scanner for radiochromic film dosimetry, Phys. Med. Biol. 52, 231–242.

Quai W., Padovani R., Peterzol A., Vaño E., Guibelalde E., Toivonen M., 2002. Maximum skin dose assessment in interventional cardiology: large area detectors and calculation methods, Proceedings of 1st European IRPA Congress, Florence, Italy, 8-11 October.

Rampado O., Garelli E., Deagostini S., Ropolo R. 2006. Dose area product evaluation with GafChromic® XR-R films and a flat bed scanner, Phys. Med. Biol. 51, 403–409.

Richley L., John AC., Coomber H., Fletcher S., 2010. Evaluation and optimization of the new EBT2 radiochromic film dosimetry system for patient dose verification in radiotherapy, Phys. Med. Biol. 55, 2601-2617.

Thomas G., Chu R., Rabe E., 2003. A study of GafChromic® XR Type R film response with reflective-type densitometers and economical flatbed scanners, J. Appl. Clin. Med. Phys. 4, 307–314.

Thomas G., Li Y, Chu RY., Cheung JY., Maqbool F., Rabe F., Burns GS., 2005. Measurement of dose-area product with GafChromic® XR Type R film, J. Appl. Clin. Med. Phys. 6, 122–132.

Tomic N., Devic S., DeBlois F., Seuntjens J., 2010. Reference radiochromic film dosimetry in kilovoltage photon beams during CBCT image acquisition, Med. Phys 37, 1083-1092.

3.3 Feasibility of setting up generic alert levels for maximum skin dose in fluoroscopically guided procedures

Within the Working group 12 of EURADOS, patient skin dose measurements, along with DAP and $K_{a,r}$ recording were performed at different European hospitals for three high dose interventional procedures in radiology and cardiology. The inter-center variability of online dose indicators and their correlation with the MSD were examined. The main objectives were to investigate the feasibility of generic alert levels, compare those to published data and to assess the overall uncertainty in setting up the alert level.

3.3.1 Clinical procedures and data collection

Patient skin dose measurements were performed at different European hospitals for three typical high dose interventional procedures: chemoembolization of the liver (TACE), neuro-embolization (NE) and percutaneous coronary interventions (PCI). PCI was included because relevant data was easily available from all hospitals and because the focus of this study was to investigate the feasibility of generic alert levels, whereby data from several hospitals was needed. The results are presented and discussed in accordance with the countries involved. The total number of measurements from each country is shown in Table 3.14. For each individual procedure, the X-ray equipment used and the online dose indicators, namely fluoroscopy time, DAP or $K_{a,r}$ were recorded. Abbreviation "DAP" throughout this section means the total DAP of the procedure.

Table 3.14. Total number of measurements for all three procedures studied (TACE, PCI, NE) (adopter from Jarvinen *et al.* 2018).

Country	Method	TACE			PCI			NE			Total		
		DAP	$K_{a,r}$	FT	DAP	$K_{a,r}$	FT	DAP	$K_{a,r}$	FT	DAP	$K_{a,r}$	FT
Belgium	TLD	10	5	8	37	34	37	14	14	14	61	53	59
Croatia	Film	-	-	-	6	-	6	-	-	-	6	0	6
Finland	Film	8	8	8	7	7	7	14	14	14	29	29	29
France	Film	28	28	28	16	16	14	50	50	50	94	94	92
Greece	Film	-	-	-	-	-	-	12	12	13	12	12	13
Greece	TLD	-	-	-	-	-	-	11	11	11	11	11	11
Italy	Film	32	32	32	8	8	8	12	12	12	52	52	52
Poland	Film	-	-	-	13	13	13	14	14	14	27	27	27
Poland	TLD	-	-	-	-	-	-	12	12	12	12	12	12
Portugal	Film	13		11	-	-	-	-	-	-	13	0	11
Serbia	Film	-	-	-	12	12	12	-	-	-	12	12	12
TOTAL		91	73	87	99	90	97	139	139	140	329	302	324

Several types of fluoroscopy equipment were included in this study (Table 3.15). It has been assumed that the selection of tube voltage (kV) and field sizes for the procedures are not affected by the type of equipment and the other equipment-specific characteristics should not affect the correlation

between MSD and online dose indicators. For centers where biplane systems were used in NE procedures, participants were requested to provide separate outputs for each tube.

Table3.15. X-ray equipment used in different countries (adopter from Jarvinen *et al.* 2018).

Country	*X-ray equipment*		
	TACE	*PCI*	*NE*
Belgium	Siemens Axiom Artis Zee, Siemens Axiom Artis DTA	Philips Allura Xper FD20, Allura FD10, Integris Allura (image intensifier)	Siemens Axiom Artis Zee, Siemens Axiom Artis DTA
Croatia		Shimadzu Digitex Premier	
Finland	Siemens Polydoros A 100	Siemens Axiom Artis	Siemens Axiom Artis, Artis Zee Biplane
France	GE Innova IGS 540	Philips Allura FD10, Siemens Artis Zee floor	Siemens Axiom Artis Zee
Greece			Siemens Axiom Artis
Italy	Siemens Axiom Artis dFA	Philips Allura FD10	Siemens Axiom Artis dFA
Poland		GE	Siemens
Portugal	Philips Integris V		
Serbia		Siemens Axiom Artis dFC	

3.3.2 Maximum skin dose measurement

MSD was determined by two different dosimeters: XR-RV3 GafChromic® films or by using TL pellets and foils as described in detail by Farah et al. (2015a, 2015b). Dosimeters were directly set on the patient skin at the entrance of the patient and the TL dosimeters considered to be tissue-equivalent (Farah *et al.* 2015b). Informed consent was not requested as the patient data was treated anonymously, but patients were informed on the use of the dosimeters according to the local practices of the hospitals.

Calibrations of the dosimeters were performed considering free-in-air irradiations in standard dosimetry laboratory conditions using RQR5 beam quality (IEC 2005) or corresponding clinical beam quality according to an agreed protocol. During the calibration, the films were set with yellow side facing the X-ray tube. For on patient measurements, films were used in the same way, except in one case (by mistake) when white side was facing the X-ray tube. For the case with white side facing the X-ray tube, a correction factor was applied, estimated from the data published by McCabe (2011). For the TLD calibrations, a blind test was carried out among the participants resulting in less than 15 % differences (Kopec *et al.* 2014).

GafChromic® films were analyzed using the red channel and based on net reflectance as discussed by Soliman and Alezeti (2014). To calculate MSD from XR-RV3 scanned images, the darkest film area was identified and a region of interest (ROI) of approximately 1 cm^2 wholly encompassing this area was used. The ROI analysis was individually done by each participant using in-house Matlab® routines (Mathworks) or the ImageJ image processing software. The detailed read-out procedure is described elsewhere (Farah *et al.* 2015b).

TLD measurements were done with a uniform grid size of 140 x 40 cm^2 (86 TLDs in total and 5.7 cm inter-chip spacing). This grid spacing was selected based on results of Dabin *et al.* (2015) as a balance between spatial resolution and dosimeter preparation workload. TLDs were read according to participants own routine procedures. The MSD value was estimated from the highest chip record. In order to take into account the median underestimation of MSD due to the finite grid spacing, the MSD value was corrected based on results of Dabin *et al. (*2015). In that study, the authors used film measurements and numerical simulations of TACE, PCI and NE procedures to evaluate the MSD underestimation associated with the use of TLD grids. The uncertainty associated with the correction method was also considered in the overall uncertainty budget.

3.3.3 Determination of the alert level

The skin dose alert level for this study is defined as the value of the dose indicator above which it is likely that the MSD exceeds 2 Gy (alert level #1) or 5 Gy (alert level #2). The dose of 2 Gy is generally reported as a threshold for early transient erythema of skin appearing 2 to 24 hours after the exposure [24]. However, in interventional fluoroscopy procedures, skin damage after 2 Gy in X-ray imaging has rarely been observed, and using this level might lead to an excessive number of patients to follow-up. Therefore, the second level for the dose of 5 Gy has been proposed. The dose of 5 Gy is generally reported as a threshold for early erythema and epilation appearing 2 to 8 weeks after the exposure (ICRP 2013). Balter *et al.* (2010) have concluded that for most patients, clinically important skin and hair reactions occur only when the skin dose is higher than 5 Gy. The values of the dose indicator ≥ alert level (skin dose ≥ 2 Gy or 5 Gy) should then trigger an increased follow-up of the patient and vigilance for possible skin reactions.

The recorded dose indicator values were presented as a function of the obtained MSD values. When the data suggested a reasonable correlation between these two parameters (in practice only for DAP and $K_{a,r}$), a line was fitted to the data points, i.e. a linear least squares fit:

$$\text{DAP(or } K_{a,r}) = a + b*\text{MSD} \qquad (3.6.)$$

where a and b are fit parameters. The alert level, i.e. DAP or $K_{a,r}$ value for MSD=2 Gy or 5 Gy, was calculated from the fitted curve.

MSD values, obtained from both gafchromic film and TLD measurements, ranged from 0.1 to 6.7 Gy for TACE (max/min=67), from 0.04 to 6.9 Gy for PCI (max/min=173) and from 0.4 to 7.4 Gy for NE (max/min=19) (Table 3.16.). About 20-30 % of MSD values in all three types of procedures exceeded the studied threshold of 2 Gy and only 2-6 % of them exceeded the second threshold of 5 Gy.

Table 3.16. Range of MSD values (Gy) obtained (adopter from Jarvinen *et al.* 2018).

Country	Procedure								
	TACE			PCI			NE		
	Max	Min	Median	Max	Min	Median	Max	Min	Median
Belgium	3.2	0.1	0.9	6.9	0.04	1.9	3.0	0.4	1.0
Croatia				3.9	0.5	0.7			
Finland	4.2	0.5	1.7	5.2	0.1	0.2	2.4	0.4	1.0
France	2.8	0.2	0.7	3.0	0.3	0.8	3.6	0.4	1.0
Greece							7.4	1.2	2.6
Italy	3.9	0.3	1.2	3.2	0.6	1.5	1.3	0.4	0.7
Poland				1.3	0.1	0.6	4.0	0.6	1.5
Portugal	6.7	0.8	1.9						
Serbia				3.3	0.3	0.7			

The values obtained for the slope (b in Eq. 3.6) and the intercept (a in Eq. 3.6) of the linear fit of DAP, $K_{a,r}$ and fluoroscopy time (FT) values as a function of MSD is shown in Table 3.17., for all three procedures. Also the values of a fitting quality indicator, Pearson correlation coefficient, are given. A few examples of the DAP and $K_{a,r}$ values versus MSD for different partners are shown in Fig. 3.16. and 3.17, for both GafChromic® film and TLD measurements. In Fig. 3.18 for TACE procedures, fluoroscopy time (FT) as a function of MSD is presented. Alert levels #1, corresponding to a MSD = 2 Gy, derived from the fitted lines to DAP and $K_{a,r}$ values are compared in Fig. 3.18 for all partners and all three procedures.

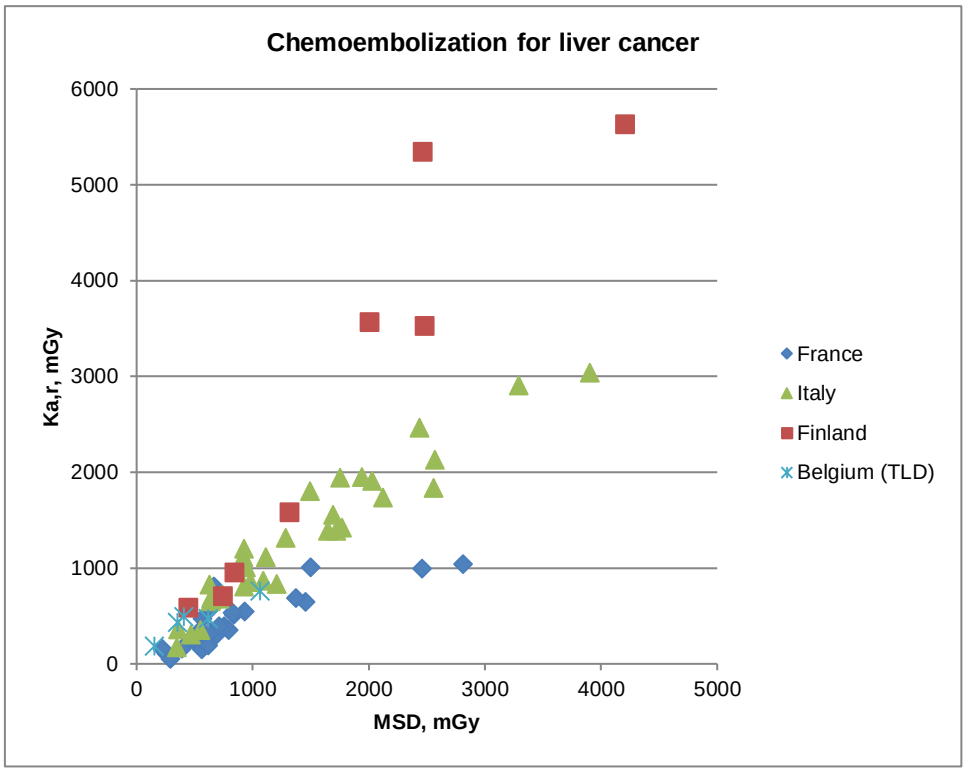

Figure 3.16. DAP values versus MSD for TACE. TLD used in Belgium, film in the other countries (adapted from Jarvinen *et al.* 2018).

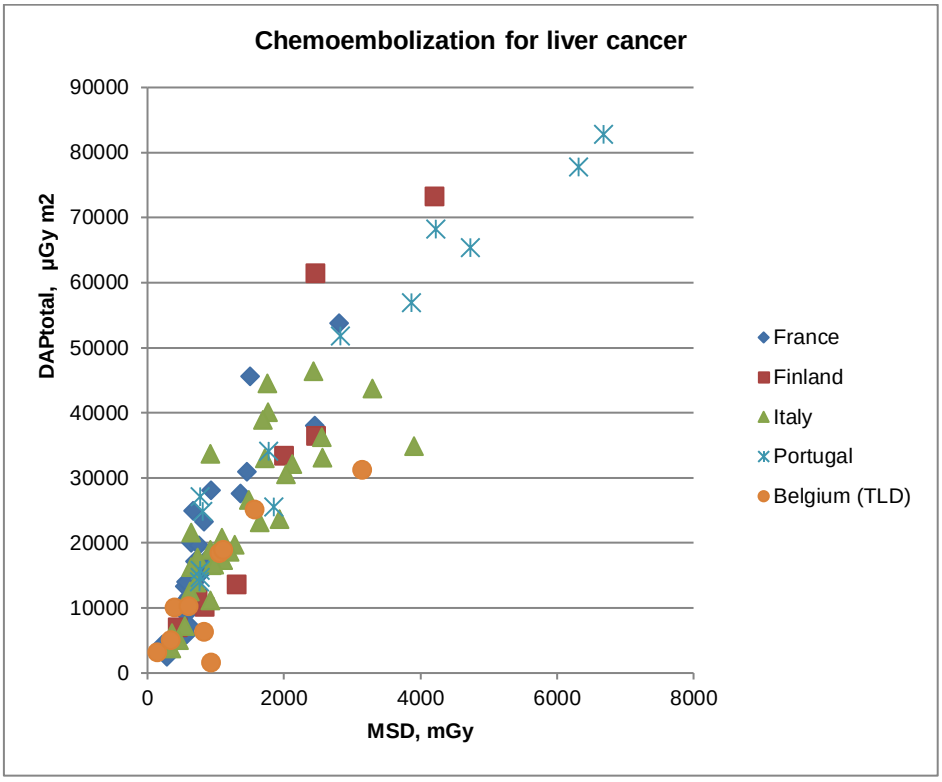

Figure 3.17. $K_{a,r}$ values versus MSD for TACE. TLD used in Belgium, film in the other countries (adapted from Jarvinen *et al.* 2018).

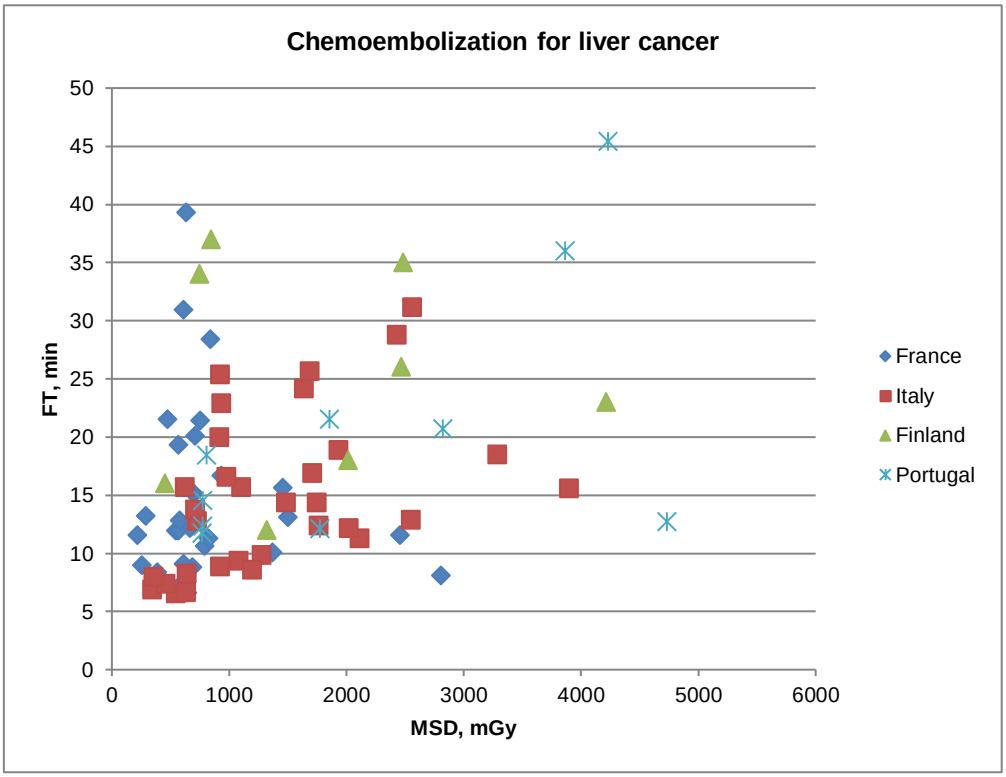

Figure 3.18. Fluoroscopy time values versus MSD for TACE. TLD used in Belgium, film in the other countries (adapted from Jarvinen *et al.* 2018).

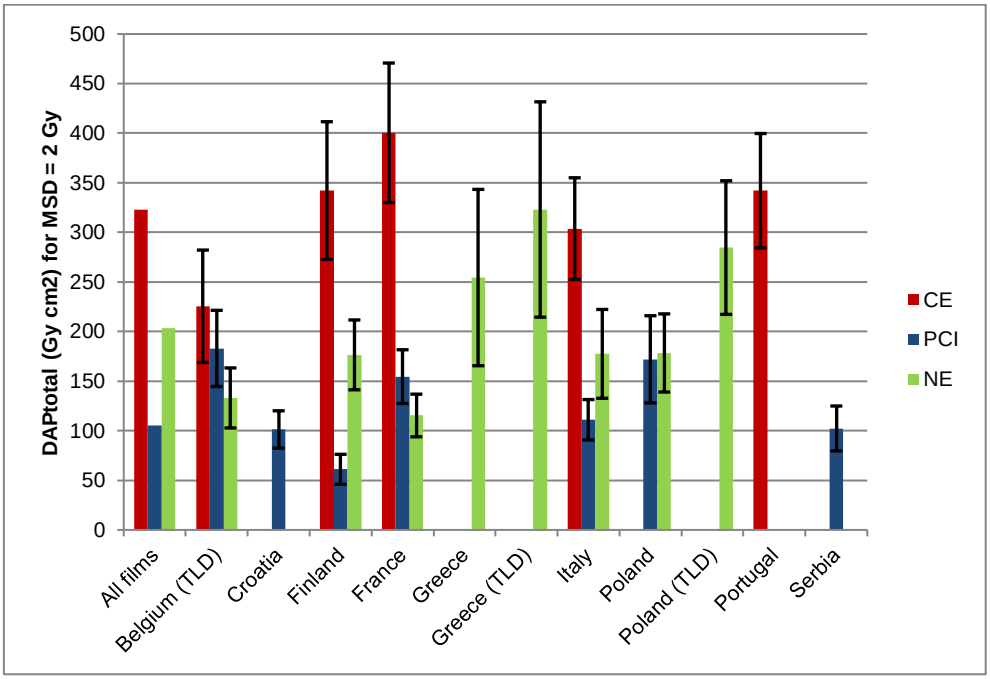

Figure 3.19. Comparison of alert levels #1 (corresponding to MSD = 2 Gy) for all three procedures (TACE, PCI and NE) obtained by different partners, given as DAP values. Error bars correspond to coverage factor k = 1

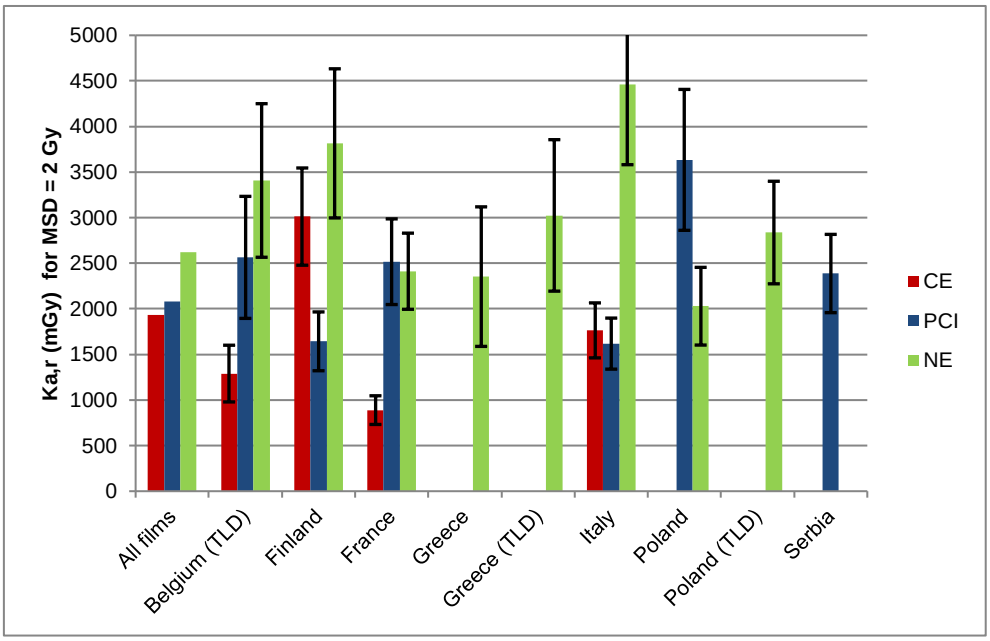

Figure 3.20. Comparison of alert levels #1 (corresponding to MSD = 2 Gy) for all three procedures (TACE, PCI and NE) obtained by different partners, given as Ka,r values. Error bars correspond to coverage factor k = 1

The results of uncertainty estimations are summarized in an section 3.3.4 and the uncertainty of alert levels (σ) is shown by error bars in Fig. 3.19. The uncertainty of the (hospital-specific) alert levels was mostly about 20-30 %.

The results indicated that there is generally a large variation in MSD values for a given procedure (max/min from 19 to 173). While no data on skin damage was recorded (it was neither obligatory nor possible to follow up the patients in this study), the results indicated that in several procedures the threshold for skin damage risks was exceeded and this supports the need for setting up alert levels.

As can be seen from Table 3.17. and graphically from the two examples in Fig. 3.16. and 3.17., there was a reasonable correlation between DAP or $K_{a,r}$ and MSD. The correlations were best for TACE, where the Pearson correlation coefficient ranged from 0.79 to 0.97 for DAP and from 0.85 to 0.96 for $K_{a,r}$. For PCI procedures, the Pearson correlation coefficient ranged from 0.49 to 0.94 for DAP and from 0.64 to 0.96 for $K_{a,r}$. The correlations for NE were the weakest, the Pearson correlation coefficient from 0.35 to 0.89 for DAP and from 0.50 to 0.91 for $K_{a,r}$. For TACE and PCI procedures, the correlations were about the same for DAP or $K_{a,r}$, while for NE procedures, correlations were a little better for $K_{a,r}$ than for DAP (as shown above by comparing the Pearson correlation coefficients factors). The results thus suggest that both DAP and $K_{a,r}$ can be used to determine skin dose alert levels.

As could be expected, the linear correlation between fluoroscopy time (FT) and MSD was much weaker (Table 3.17. and Fig. 3.18.), the Pearson correlation coefficient being mostly below 0.6. FT is thus not suitable for setting up alert levels.

Looking at the images on the films irradiated in clinical conditions revealed that in TACE procedures there tended to be only one (large) irradiated area, so all the different fields overlap at some point. For PCI and NE procedures there tended to be more variety and spread in the irradiated areas; field size seems relatively constant (only a few different field sizes), but the position of irradiation (i.e. tube projection) could change a lot during each procedure. These differences in the irradiation patterns (field sizes and beam orientations) can partly explain why the correlation between DAP and MSD is better for TACE than for NE or PCI.

Linear fitting with the intercept (Eq.3.6.) was applied because it was assumed that the calibration of the DAP or $K_{a,r}$ meter could have an off-set. However, also fitting through the origin was tested; the fitting in this case was slightly worse while the effect on the alert levels was typically less than 10 %.

As could be expected, the linear correlation between fluoroscopy time (FT) and MSD was much weaker (Table 3.17. and Fig. 3.18.), the Pearson correlation coefficient being mostly below 0.6. FT is thus not suitable for setting up alert levels.

Looking at the images on the films irradiated in clinical conditions revealed that in TACE procedures there tended to be only one (large) irradiated area, so all the different fields overlap at some point. For PCI and NE procedures there tended to be more variety and spread in the irradiated areas; field size seems relatively constant (only a few different field sizes), but the position of irradiation (i.e. tube projection) could change a lot during each procedure. These differences in the irradiation patterns (field sizes and beam orientations) can partly explain why the correlation between DAP and MSD is better for TACE than for NE or PCI.

Table 3.17. The values of slope (b in Eq.3.6) and the intercept (a in Eq. 3.6), and Pearson correlation coefficient p for linear fitting of DAP, $K_{a,r}$ and FT versus MSD (adopter from Jarvinen *et al.* 2018).

Country	DAP			$K_{a,r}$			FT		
	Slope Gy cm²/Gy	Intercept Gy cm²	p	Slope Gy/Gy	Intercept mGy	p	Slope, min/Gy	Intercept min	p
				TACE					
Belgium TLD	129	28.8	0.85	0.55	184	0.94			
Finland	192	-40.9	0.95	1.54	-77	0.93	-0.0001	25.4	0.02
France	192	16.3	0.90	0.39	103	0.85	-0.0018	16.3	0.14
Italy	111	81.0	0.79	0.81	144	0.96	0.0034	10.1	0.44
Portugal	112	117.4	0.97				0.0028	13.6	0.51
				PCI					
Belgium TLD	52	81.1	0.65	1.01	543	0.64	0.0067	21.7	0.51
Croatia	38	25.2	0.94						
Finland	25	11.0	0.94	0.69	263	0.96	0.0047	8.8	0.76
France	64	26.5	0.88	1.00	509	0.80	0.0037	11.8	0.43
Italy	47	16.5	0,91	0.60	418	0.92	0.0098	1.3	0.82
Poland	86	0.23	0.70	1.87	-112	0.83	0.0079	12.4	0,54
Serbia	22	58.2	0.49	0.50	1390	0.67	0.0028	190.8	0.52
				NE					
Belgium TLD	31	-8.6	0.47	1.02	1367	0.56	0.0103	33.1	0.37
Finland	64	49.1	0.70	2.10	-386	0.83	0.0268	8.1	0.87
France	45	26.1	0.53	1.15	107	0.83	0.0129	6.8	0.70
Greece	167	-79.5	0.75	1.52	-690	0.78	0.0039	28.1	0.39
Greece TLD	105	112.4	0.77	0.98	1074	0.81	0.0019	28.1	0.26
Italy	66	46.3	0.62	2.25	-35	0.91	0.0107	11.9	0.56
Poland	31	115.6	0.35	0.55	922	0.50	0.0013	23.6	0.12
Poland TLD	102	80.0	0.89	0.57	1696	0.58	0.0029	26.4	0.21

Linear fitting with the intercept (Eq.3.6.) was applied because it was assumed that the calibration of the DAP or $K_{a,r}$ meter could have an off-set. However, also fitting through the origin was tested; the fitting in this case was slightly worse while the effect on the alert levels was typically less than 10 %.

Alert levels based on DAP showed lowest variability among different countries for TACE procedures while the widest alert level dispersion was for NE procedures (Fig. 3.19); this is in total agreement with previous observations on the fitting quality. For TACE, the consistency of the alert levels between different countries was better for DAP than for $K_{a,r}$: standard deviation of the values was 20 % for DAP and 50 % for $K_{a,r}$. For PCI and NE, the consistency of alert levels for DAP and $K_{a,r}$ were about the same (standard deviations of alert values about 30 % in both cases). The different irradiation patterns (as discussed above) could be the reason for these different conclusions on the consistencies (TACE vs. PCI and NE).

Alert levels based on DAP or $K_{a,r}$ values roughly coincided between most countries taking into account the estimated uncertainties (Appendix). A one sample *t* test was used to analyze more precisely if the alert levels obtained in different countries deviated significantly from the mean alert level for all countries. The country-specific alert level deviated significantly ($p < 0.01$) from the mean value in one case for TACE (Serbia, for alert levels 2 Gy and 5 Gy), in two cases for PCI (Finland for 2 Gy and Poland for 5 Gy) and in two cases for NE (Greece TLD for 2 Gy and Greece film for 5 Gy).

The results of the one sample *t* test were used to select countries whose data were used to calculate the new mean alert level. The above countries with $p<0.01$ were excluded from this calculation. The resulting mean alert levels and the generic alert levels based on them are suggested in Table 3.18., for MSD of both 2 Gy and 5 Gy. The generic alert levels are the rounded mean values of the data accepted for calculation.

One should note that the X-ray field dimensions in TACE procedures are typically larger than in PCI or NE procedures leading to high DAP/MSD value (see the slope values in Table 3.17) and, accordingly, higher alert level.

Table 3.18. Suggested generic alert levels for MSD of 2 Gy and 5 Gy, based on mean alert levels of selected countries (countries which had roughly consistent alert levels) (adopter from Jarvinen *et al.* 2018).

Procedure	Suggested alert level DAP(Gy cm^2)		Mean alert level DAP (Gy cm^2)		Number of countries included
	for MSD = 2 Gy	for MSD = 5 Gy	for MSD = 2 Gy	for MSD = 5 Gy	
TACE	300	750	323	746	5
PCI	150	250	138	235	6
NE	200	400	189	389	7

Table 3.19. Comparison of alert levels in terms of DAP for MSD=2 Gy suggested in this work with similar levels published earlier (adopter from Jarvinen *et al.* 2018).

Procedure	Publication	Alert level, DAP Gy cm^2	Number of procedures	MSD measurement device
TACE	*This work*	*300*	*91*	*RC film*
	SAFRAD (2016)	500		
	Struelens *et al.* (2014)	330	30	TLD
	D'Alessio *et al.* (2013)	530	15	RC film and micro MOSFET
	Miller *et al.* (2003) Stecker *et al.* (2009)	350	709	
PCI	*This work*	*150*	*49*	*RC film*
	SAFRAD (2016)	300		
	ICRP (2013)	150-250		
	NCRP (2010	300		
	Bogaert *et al.* (2009)	125-250	318	TLD
	Domienik *et al.* (2008)	345-415	27-54	RC film
	Trianni *et al.* (2006)	140	33	RC film
NE	*This work*	*200*	*104*	*RC film and TLD*
	Struelens *et al.* (2014)	240	30	TLD
	Sandborg *et al.* (2012)	300	50	TLD
	Sandborg *et al.* (2010)	430	71	TLD
	Moritake *et al.* (2011)	185	35	PLD
	Moritake *et al.* (2008)	300	28	PLD
	D'Ercole *et al.* (2007)	700	21	RC film

Table 3.19. compares the suggested alert levels for MSD=2 Gy with a few similar values published in recent years. For all three procedures, the results of this work are lower than, or close to the lowest values, in the earlier publications. The best agreement with the published alert levels is for TACE (standard deviation of different values 26 %, compared with 40 % for PCI and 54 % for NE), as could be expected from the above-mentioned considerations of the best correlation between DAP and MSD. Some of the observed differences can be related to the roughness of this comparison, because some of the other values in Table 3.19 are either extrapolated from the published data, or can be associated with different procedure patterns (field sizes, C-arm angulation, etc.) and higher uncertainties in the MSD determination.

Due to the observed variation of the results of alert levels between countries in this work, and also due to the variation with and within the results published earlier, it is considered important for the interventional radiology and cardiology facilities to study the correlations and establish alert levels locally. The generic alert levels suggested in Table 3.18. should only be used as the first approximation until verified by local measurements. For such local studies, it would be useful to examine at least the following procedural factors which can have a major impact on both the MSD values and the alert levels:

- Beam orientations (tube angulations)
- Field sizes and the use of magnification (in magnification, field size is decreased while beam output is increased, to maintain image quality, leading to higher skin dose)
- Beam limiting (collimation; DAP value decreases while skin dose per unit area remains the same)
- Distances of x-ray tube and image detector from patient skin (effects by table height, size of patient, operator height)
- User's skill level
- Complexity of procedure

The software-based dose mapping tools provide real-time information on the patient skin doses during the procedure (Boujan *et al.* 2014, den Boer *et al.* 2001). Such tools should take into account the impact of the above parameters of the patient exposure geometry. Therefore, the validation of these tools by direct measurements of skin doses is of high importance and should be a goal of future studies for skin dose alert levels.

There are few published alert levels at 5 Gy although these are clinically more relevant, and less of a burden in terms of the number of recall and follow up of patients. However, a general alert level of DAP= 500 Gy cm^2 at 3 Gy MSD has been suggested (Stecker *et al.* 2009).

3.3.4 Uncertainty estimation

Uncertainties on the alert levels (hospital-specific alert levels) given in terms of DAP and $K_{a,r}$ were estimated by combining in quadrature the following uncertainty components:

$$\sigma^2 = \sigma_{\mathrm{DAP}}^2 + \sigma_{\mathrm{DISPL}}^2 + \sigma_{\mathrm{LSQ}}^2 \qquad (3.7.)$$

where σ_{DAP} is the uncertainty (one standard deviation) of the calculated DAP value (similarly for $K_{a,r}$ value), σ_{DISPL} is the uncertainty of the recorded (indicated) DAP value (similarly for $K_{a,r}$ value), and σ_{LSQ} is the uncertainty due to the quality of the linear fit (Eq. 3.6).

The uncertainty σ_{DAP} of the calculated DAP value at 2 Gy was estimated by:

$$\sigma_{\mathrm{DAP}} = \frac{\partial(\mathrm{DAP})}{\partial(\mathrm{MSD})}\sigma_{\mathrm{MSD}} \qquad (3.8.)$$

where σ_{MSD} is the uncertainty of assessed MSD. The values of σ_{MSD}were estimated by each partner for the local clinical conditions and procedures, based on the general uncertainty estimates given by Farah *et al.* (Farah *et al.* 2015a). For this estimation, all relevant influencing parameters were analyzed in detail.

In addition to the uncertainty of calculated DAP and $K_{a,r}$ values, the console values (recorded DAP and $K_{a,r}$ values) have an inherent uncertainty (σ_{DISPL}), the magnitude of which is related to the acceptability criteria for the x-ray equipment and displayed dose indicators. The values for these uncertainties were taken consistently by assuming the maximum error of 25 %, which is the acceptability criteria for DAP indication (IEC 2000, EC 2012), leading to one standard deviation of 14.4 % for normal distribution.

Additional uncertainty comes from the quality of the linear least squares fit to the clinical DAP and $K_{a,r}$ values (Eq. 3.6.). The standard deviation of the DAP (and similarly for $K_{a,r}$) estimate, resulting from the standard deviation of the fitted slope and intercept, is estimated from (EC 2012):

$$\sigma_{\mathrm{LSQ}}^2 = \frac{1}{n-2}\sum_{i=1}^{n}(\mathrm{DAP}_i - \widehat{\mathrm{DAP}_i})^2\left[\frac{1}{n} + \frac{(x_p - \overline{\mathrm{MSD}})^2}{\sum(\mathrm{MSD}_i - \overline{\mathrm{MSD}})^2}\right] = \sigma_{\mathrm{data}}^2\left[\frac{1}{n} + \frac{(x_p - \overline{\mathrm{MSD}})^2}{\sum(\mathrm{MSD}_i - \overline{\mathrm{MSD}})^2}\right] \quad (3.9.)$$

where n is the number of data points (DAP values), DAP_i are the console DAP values with a predicted value $\widehat{\mathrm{DAP}_i}$ from the linear fit, x_p is the alert level (here, 2 Gy or 5 Gy), MSD_i are the measured skin doses and $\overline{\mathrm{MSD}}$ is their mean value.

The fit quality can also be assessed with (similarly for $K_{a,r}$):

$$R^2 = 1 - \frac{\sum_{i=1}^{n}(\mathrm{DAP}_i - \widehat{\mathrm{DAP}_i})^2}{\sum_{i=1}^{n}(\mathrm{DAP}_i - \overline{\mathrm{DAP}})^2} \quad (3.10.)$$

where $\overline{\mathrm{DAP}}$ is the mean of the recorded console DAP values. $R^2 = 1$ indicates a perfect fit. The range of the square root of R^2 (Pearson correlation coefficient) were given in Table 3.17.

The results of the uncertainty estimations for alert level #1 (MSD= 2 Gy) are summarized in Table 3.20. for evaluations in terms of DAP; σ is the uncertainty of alert level. The uncertainties σ for alert level #2 would be about the same. Similar estimations were carried out for evaluations in terms of $K_{a,r}$, yielding about the same level of uncertainties for alert level.

Table 3.20. Estimated uncertainties (%) for evaluations in terms of DAP. σ is the uncertainty of alert level #1 (MSD= 2 Gy, coverage factor k=1). σ_{DISPL}: uncertainty of indicated DAP (console value), σ_{MSD}: uncertainty of assessed MSD, σ_{DAP}: uncertainty of calculated DAP at MSD=2 Gy, σ_{LSQ}: uncertainty of the linear fit (DAP vs MSD) (adopter from Jarvinen *et al.* 2018).

Country:		Belgium	Croatia	Finland	France	Greece		Italy	Poland		Portugal	Serbia
Method:		TLD	Film	Film	Film	Film	TLD	Film	Film	TLD	Film	Film
All	σ_{DISPL}	14.4	14.4	14.4	14.4	14.4	14.4	14.4	14.4	14.4	14.4	14.4
TACE	σ_{MSD}	18.9		9.8	8.4			9.6			10.6	
	σ_{DAP}	17.9		10.2	8.3			8.4			8.8	
	σ_{LSQ}	12.3		9.2	5.9			5.3			5.2	
	σ	26.0		19.9	17.7			17.5			17.7	
PCI	σ_{MSD}	25.3	10.5	9.8	8.4			9.6	10.5			10.9
	σ_{DAP}	19.3	9.3	12.4	7.8			8.9	10.5			7.1
	σ_{LSQ}	10.4	8.6	13.6	7.1			7.9	18.3			16.1
	σ	26.3	19.2	23.4	17.9			18.7	25.6			22.8
NE	σ_{MSD}	24.7		9.8	8.4	10.5	24.7	9.6	10.5	24.7		
	σ_{DAP}	16.8		8.4	7.5	11.6	20.4	8.4	6.1	21.4		
	σ_{LSQ}	13.4		11.8	9.8	28.7	25.7	19.4	16.3	6.0		
	σ	25.9		20.5	19.0	34.1	35.8	25.6	22.6	26.5		

3.3.5 Conclusions

Ideally, the skin dose alert levels could be set internationally as a function of an online dose indicator to prevent skin injuries and to identify which patients require follow-up. However, variation in procedure's complexity, level of optimization, user's skill level and techniques in performing the procedure result in large dispersion of dose indicators corresponding to a pre-determined skin dose. The results of this study indicate that generic, hospital-independent alert levels are feasible in some interventional procedures (like chemoembolization of the liver) but should be used cautiously, only as the first approximation; hospital-specific alert levels are preferred as the final approach and should be set to reflect the clinic's specific working procedures. The uncertainty of MSD measurements with GafChromic® films and TLDs is typically 10-20 % (k=1) and provides reasonably accurate determination of the skin dose alert levels but the measurements are time consuming. In the future, software-based dose mapping tools may provide a more user-friendly approach to follow-up patient skin dose in real time during the procedure provided they are well validated and benchmarked against measurements.

References

Balter S., Hopewell J.W., Miller D.L., Wagner L.K and Zelefsky M.J. 2010. Fluoroscopically guided interventional procedures: A review of radiation effects on patients' skin and hair, Radiology 254 (2), 326-341.

Bogaert E., Bacher K., Lemmens K., Carlier M., Desmet W., De Wagter X. 2009. A large-scale mutlicentre study of patient skin doses in interventional cardiology: dose-area product action levels and dose reference level, Br. J. Radiol. 82303-12.

Boujan F., Clauss N., Santos E., Boon S., Schouten G., Mertz L., 2014. Dietemann JL, A new method of real-time skin dose visualization. Clinical evaluation of fluoroscopically guided interventions, Neuroradiology 56:971-6.

D'Alessio D., Giliberti C., Soriani A., Carpanese L., Pizzi G., Vallati GE., Strigari L., 2013. Dose evaluation for skin and organ in hepatocellular carcinoma during angiographic procedure, J. Exp. Clin. Cancer Res. 32 (1) 81.

Dabin J., Negri A., Farah J., Ciraj-Bjelac O., Clairand I., De Angelis C., Domienik J., Jarvinen H., Kopec R., Majer M., Malchair F., Novák L., Siiskonen T., Vanhavere F., Trianni A., Knežević Ž., 2015. Characterization of grids of point detectors in maximum skin dose measurement in fluoroscopically-guided interventional procedures, Phys. Med. 31(8): 1112–17.

den Boer A., P. de Feijter J, Serruys PW., Roelandt JRTC., 2001. Real-time quantification and display of skin radiation during coronary angiography and intervention, Circulation, 104: 1779-84.

D'Ercole L., Mantovani L., Thyrion FZ., Bocchiola M., Azzaretti A., Di Maria F., Saluzzo CM., Quaretti P., Rodolico G., Scagnelli P., Andreucci L., 2007. A study on maximum skin dose in cerebral embolization procedures, Am. J. Neurorad. 28;503-7.

Domienik J., Papierz S., Jankowski J., Peruga J., Werduch A., Religa W., 2008. Correlation of patient maximum skin doses in cardiac procedures with various dose indicators, Rad. Prot. Dos. 132;18-24.

EC 2012. European Commission (EC), Criteria for acceptability of medical radiological equipment used in diagnostic radiology, nuclear medicine and radiotherapy, Radiation Protection No 162, European Union, 2012.

Farah J., Trianni A., Ciraj-Bjelac O., Clairand I., De Angelis C., Delle Canne S., Hadid L., Huet C., Jarvinen H., Negri A., Novák L., Pinto M., Siiskonen T., Waryn MJ., Knežević Ž. 2015a. Characterization of XR-RV3 GafChromicTM films in standard laboratory and clinical conditions and means to estimate uncertainties and reduce errors, Med. Phys. 42(7) 4211-26.

Farah J., Trianni A., Carinou E., Ciraj-Bjelac O, Clairand I., Dabin J., 2015b Measurement of maximum skin dose interventional radiology and cardiology and challenges in the set-up of European alert thresholds, Rad. Prot. Dos. 164 (1-2);138–42.

ICRP 2013. International Commission on Radiological Protection (ICRP), Radiological protection in cardiology, ICRP Publication 120, Ann. ICRP 42 (1) (2013).

IEC 2000. International Electrotechnical Commission (IEC). IEC 60580 Ed 2.0: Medical electrical equipment - Dose area product meters, Geneva, 2000.

IEC 2005. International Electrotechnical Commission (IEC), Medical diagnostic X-ray equipment - Radiation conditions for use in the determination of characteristics, IEC 61267, 2005.

Jarvinen H., Farah J., Siiskonen T., Ciraj-Bjelac O., Dabin J., Carinou E., Domienik J., Kluszczynski D., Knezevic Z., Kopec R., Majer M., Malchair F., Negri A., Pankowski P., Sarmento S., and Trianni A., 2018. Feasibility of setting up generic alert levels for maximum skin dose in fluoroscopically guided procedures, Phys Med.; 46:67-74.

Kopec R., Novák L., Carinou E., Clairand I., Dabin J., Datz H., De Angelis C., Farah., Huet C., Knežević Z., Järvinen H., Majer M., Malchair F., Negri A., Waschitz Haruz S., Siiskonen T., Szumska A. , 2014. Intercomparison of Gafchromic films, TL chips and TL foils for the measurements of skin dose in interventional radiology. Radiat. Meas. 71: 282–6.

McCabe BP., Speidel MA., Pike TL., Van Lysel MS., 2011. Calibration of GafChromicTM XR-RV3 radiochromic film for skin dose measurement using standardized x-ray spectra and a commercial flatbed scanner, Med. Phys. 38(4), 1919-30.

Miller D., Balter S., Cole PE., Lu HT., Berenstein A., 2003. Radiation doses in interventional radiology procedures: The RAD-IR study. Part II: Skin dose, J. Vasc. Interv. Radiol. 14;977-90.

Moritake T., Matsumaru Y., Takigawa T., Nishizawa K., Matsumura A., Tsuboi K., 2008. Dose measurement on both patients and operators during neurointerventional procedures using photoluminescence glass dosimeters, Am. J. Neurorad. 29; 1910-17.

Moritake T., Hayakawa M., Matsumaru Y., Takigawa T., Koguchi C., Miyamoto Y., 2011. Precise mapping system of entrance skin dose during endovascular embolization for cerebral aneurysm, Rad. Meas. 46 (12);2103-6.

NCRP 2010. National Council on Radiation Protection and Measurements (NCRP), Radiation dose management for fluoroscopically guided interventional medical procedures, NCRP Report 168. Bethesda, MD, 2010.

SAFRAD 2016. https://rpop.iaea.org/RPOP/RPoP/Modules/login/safrad-introduction.htm, 2016.

Sandborg M., Rossitti S., Pettersson H., 2010. Local skin and eye lens equivalent doses in interventional neuroradiology, Eur. Radiol. 20(3);725-33.

Sandborg M., Nilsson Althén J., Pettersson H., Rossitti S., 2012. Patient organ radiation doses during treatment for aneurysmal subarachnoid hemorrhage, Clin. Neuroradiol. 22(4);315-25.

Soliman K., Alenezi A., 2014. Patient entrance surface dose measurements using XR-QA2 Gafchromic films during micturating cystourethrography procedures, Rad. Prot. Dos. 158 (2),170-4.

Stecker MS., Balter S., Towbin RB., Miller D., Vano E., Bartal G., 2009. Guidelines for patient radiation dose management, J. Vasc. Interv. Radiol. 20, S263-73.

Struelens L., Bacher K., Bosmans H., Bleeser F., Hoornaert MT., Malchair F., Balter S., 2014. Establishment of trigger levels to steer the follow-up of radiation effects in patients undergoing fluoroscopically-guided interventional procedures in Belgium, Physica Medica 30; 934-40.

Trianni A., Chizzola G., Toh H., Quai E., Cragnolini E., Bernardi G., Proclemer A., Padovani R., 2006. Patient skin dosimetry in haemodynamic and electrophysiology interventional cardiology Rad. Prot. Dos. 117(1-3);241-6.

4. Conclusion

Despite their low invasiveness, fluoroscopically-guided interventional procedures are not without risk, particularly for patients who undergo staged or repeated intervention. The patents with maximum skin dose (MSD) above certain level should be followed-up.

This report presents the EURADOS Working group 12 activities in the area of dosimetry for interventional procedures in cardiology and radiology. The results of characterization of different dosimetric methods for skin dose assessment in interventional procedures, their application for skin doses measurement in clinical practice and establishment of trigger levels in order to evaluate the feasibility of identifying a common dosimetric indicator that correlates with the maximum skin dose are presented.

Several types of dosimeters have been used to estimate patient's skin dose distribution. Luminescence detectors usually show good energy and dose response in clinical beam qualities. However the poor spatial resolution of such point-like dosimeters may far outweigh their good dosimetric properties. The uncertainty from the sampling procedure should be estimated when point detectors are to be used in interventional procedures because it may lead to strong underestimation of the MSD.

Nowadays, Gafchromic® films are probably the most convenient and affordable solution for clinical routine. The overall uncertainty associated with the use of XR-RV3 Gafchromic® films to determine skin dose in the interventional environment can realistically be estimated to be around 20 % (k=1). This uncertainty can be reduced to within 5 % if carefully monitoring scanner, film and fitting-related errors or it can easily increase to over 40 % if minimal care is not taken. It has been demonstrated that appropriate calibration, reading, fitting and other film-related and scan-related processes, contribute to the accuracy of skin dose measurements in interventional procedures.

Ideally, the skin dose alert levels could be set internationally as a function of an online dose indicator to prevent skin injuries and to identify which patients require follow-up. However, variation in procedure's complexity, level of optimization, user's skill level and techniques in performing the procedure result in large dispersion of dose indicators corresponding to a pre-determined skin dose. The generic alert levels are feasible for some cases but should be used with caution, only as the first approximation, while hospital-specific alert levels are preferred as the final approach.

Both skin dose measurements using GafChromic® films and TLDs is provides reasonably accurate determination of the skin dose alert levels but the measurements are time consuming. In the future, software-based dose mapping tools may provide a more user-friendly approach to follow-up patient skin dose in real time during the procedure provided they are well validated and benchmarked against measurements.